F 3132

BULETINUL INSTITUTULUI POLITEHNIC DIN IAȘI

Tomul XXXI (XXXV)

Fasc. 1–4

061114.

Secția IV

CONSTRUCȚII DE MAȘINI

1985

MAGYAR TUDOMÁNYOS AKADÉMIA KÖNYVTÁRA 1831

BULETINUL INSTITUTULUI POLITEHNIC DIN IAŞI

Tomul XXXI (XXXV)

Fasc. 1–4

Secţia IV

CONSTRUCŢII DE MAŞINI

1985

COLEGIUL DE REDACȚIE

Prof. dr. chim. **CAMELUȚA BELDIE** (președinte)
Prof. dr. doc. ing. **VALERIU BLIDARU**
Prof. dr. doc. ing. **GH. CHIRIȚĂ**
Prof. dr. ing. **M. GAFIȚANU**
Conf. dr. ing. **D. LIUȚE**
Prof. dr. doc. **D. I. MANGERON**
Prof. dr. ing. **GH. MAXIM**
Prof. dr. ing. **ADRIAN RADU**
Acad. prof. dr. doc. ing. **CR. SIMIONESCU**

Această fascicolă a apărut și cu sprijinul material al Comitetului sindicatului și Consiliului U.A.S.C. al Institutului politehnic din Iași

COMITETUL DE REDACȚIE AL SECȚIEI

IV. Construcții de mașini

Prof. dr. ing. **VITALIE BELOUSOV**
Conf. dr. ing. **D. ZETU**
Conf. dr. ing. **OCTAVIAN PRUTEANU**
Conf. dr. ing. **IUSTIN BENDESCU**

REDACȚIA

Prof. dr. doc. **D. I. MANGERON**
(redactor responsabil)
Prof. dr. doc. ing. **ALFRED BRAIER**
(secretar de redacție)
Conf. dr. ing. **SPIRIDON CREȚU**
(redactor)
Asist. ing. **ANETA BRAIER**
(redactor)

BULETINUL INSTITUTULUI POLITEHNIC DIN IAŞI
BULLETIN OF THE POLYTECHNIC INSTITUTE OF JASSY
ИЗВЕСТИЯ ЯССКОГО ПОЛИТЕХНИЧЕСКОГО ИНСТИТУТА

Tomul XXXI (XXXV), Fasc. 1–4 1985

Secţia IV

CONSTRUCŢII DE MAŞINI

SUMAR

Pag.

V. MERTICARU şi P. TIVLEA, Amplificatoare de cuplu pentru roboţi industriali. Mecanisme cu roţi dinţate cu număr foarte mic de dinţi (engl., rez. rom.). 7

M. GAFIŢANU şi BARBU DRĂGAN, Analiza CEPSTRUM a influenţei defectelor asupra zgomotului roţilor dinţate (engl., rez. rom.) 15

SPIRIDON CREŢU şi VICTOR HATMANU, Analiza numerică a deformaţiei plastice la contactul liniar elasto-plastic (engl., rez. rom.) 19

CEZAR DUCA şi ADRIAN POPOVICI, Metodă analitică pentru determinarea razei de curbură a profilului în cazul camelor plane (engl., rez. rom.) 27

V. MERTICARU şi DĂNUŢ RECEANU, Criterii de selecţionare a tuburilor manometrice din componenţa manometrelor industriale (engl., rez. rom.) 35

SPIRIDON CREŢU şi CEZAR RACOCEA, Proiectarea optimă a geometriei de contact pentru rulmenţi cu role cilindrice (engl.,rez. rom.) 43

DAN URSESCU, VIRGIL GIURCĂ, I. RACOVIŢĂ şi I. ŢÂRDEA, Model matematic pentru regimurile de start ale turbomotoarelor cu gaze (engl., rez. rom.) 49

BOGDAN HORBANIUC şi EMIL LUCA, Optimizarea geometrică a tuburilor termice cu aripioare în scopul obţinerii unui flux termic maxim pe unitatea de greutate (engl., rez. rom.) 55

C. CIOCHINĂ, EMIL ANDREI, AURELIAN SIMIONESCU, OVIDIU CALANCIA, RADU DĂNILĂ, LEONACHE DRĂGOI şi FLORIN ANDREI, Cercetări experimentale privind reducerea cantităţilor de lianţi organici din componenţa amestecurilor de formare autoîntăritoare la rece (germ., rez. rom.) 63

I. HOPULELE, CARMEN NEJNERU şi M. ŞTEFAN, Stabilizarea dimensională la redresarea pieselor deformate prin tratament termic (engl., rez. rom.) 69

DRAGOŞ PARASCHIV, OCTAVIAN PRUTEANU, V. BRAHA şi GH. TEŞU, Consideraţii privind corelaţia dintre rugozitatea de suprafaţă Ra şi parametrii de lucru la frezarea frontală (franc., rez. rom.) 75

STAN PANAIT, MIRCEA COZMÎNCĂ şi I. ROMANESCU, Natura vibraţiilor torsionale din maşina de frezat dantura (franc., rez. rom.) 81

V. BRAHA, OCTAVIAN PRUTEANU, DRAGOŞ PARASCHIV, ROMEO CUDRIC şi GAVRIL MUSCĂ, Contribuţii privind influenţa forţei centrifuge în dezechilibru asupra rugozităţii de suprafaţă la strunjirea de finisare a arborilor cu rigiditate redusă (germ., rez. rom.) 87

DRAGOŞ PARASCHIV, OCTAVIAN PRUTEANU, GH. TEŞU şi NINA AFRĂSINEI, Consideraţii privind influenţa regimurilor de aşchiere asupra rugozităţii de suprafaţă Ra la rectificarea frontală (franc., rez. rom.) 93

N. GHERGHEL, Consideraţii privind legătura dintre condiţiile de precizie determinante şi gradele de libertate ce trebuie înlăturate pieselor prin orientare (germ., rez. rom.) 97

BULETINUL INSTITUTULUI POLITEHNIC DIN IAŞI
BULLETIN OF THE POLYTECHNIC INSTITUTE OF JASSY
ИЗВЕСТИЯ ЯССКОГО ПОЛИТЕХНИЧЕСКОГО ИНСТИТУТА
Tome XXXI (XXXV), Fasc. 1–4 1985

Section IV

MACHINE CONSTRUCTION

CONTENTS

Pp.

V. MERTICARU and P. TIVLEA, Torque Amplifiers for Industrial Robots. Mechanisms with Gears with Small Number of Teeth (English, Romanian summary) 7

M. GAFIŢANU and BARBU DRĂGAN, CEPSTRUM Analysis of the Total Run-out Influence on the Gear Noise (English, Romanian summary) . . . 15

SPIRIDON CREŢU and VICTOR HATMANU, A Numerical Analysis of Permanent Deformation in Elasto-Plastic Line Contact (English, Romanian summary) 19

CEZAR DUCA and ADRIAN POPOVICI, Analytical Method for the Determination of Radius of Curvature in the Case of Plane Cams (English, Romanian summary) 27

V. MERTICARU and DĂNUŢ RECEANU, Criteria of Bourdon Tube Selection for the Industrial Manometers (English, Romanian summary) 35

SPIRIDON CREŢU and CEZAR RACOCEA, The Optimum Design of the Contact Geometry for Cylindrical Roller Bearings (English, Romanian summary) 43

DAN URSESCU, VIRGIL GIURCĂ, I. RACOVIŢĂ and I. ŢÂRDEA, Mathematical Model for the Starting Condition of the Gas Turbo-Engines (English, Romanian summary) 49

BOGDAN HORBANIUC and EMIL LUCA, Optimal Geometry of Finned Heat Pipes to Achieve a Maximum Heat Flow per Unit Weight (English, Romanian summary) 55

C. CIOCHINĂ, EMIL ANDREI, AURELIAN SIMIONESCU, OVIDIU CALANCIA, RADU DĂNILĂ, LEONACHE DRĂGOI und FLORIN ANDREI, Untersuchungen zur Reduzierung der Masse von Kunstharzbindern in den kaltselbsterstarrenden Formmischungen (German, Romanian summary) . 63

I. HOPULELE, CARMEN NEJNERU and M. ŞTEFAN, The Dimensional Stabilization of pieces Deformed under Thermic Treatment (English, Romanian summary) 69

DRAGOŞ PARASCHIV, OCTAVIAN PRUTEANU, V. BRAHA et GH. TEŞU, Considérations sur la corrélation entre la rugosité de surface Ra et les paramètres de travail au fraisage frontal (French, Romanian summary) 75

STAN PANAIT, MIRCEA COZMÎNCA et I. ROMANESCU, Les sources des vibrations de torsion de la machine à fraiser les engrenages (French, Romanian Summary) 81

V. BRAHA, OCTAVIAN PRUTEANU, DRAGOŞ PARASCHIV, ROMEO CUDRIC und GAVRIL MUSCĂ, Beiträge zum Einfluss der Zentrifugalkraft bei Umwucht auf die Oberflächenrauhigkeit während des Feindrehens von nichtstarren Wellen (German, Romanian summary) 87

DRAGOŞ PARASCHIV, OCTAVIAN PRUTEANU, GH. TEŞU et NINA AFRĂSINEI, Considérations sur l'influence des régimes de coupe sur la rugosité de surface Ra pendant la rectification frontale (French, Romanian summary) 93

N. GHERGHEL, Betrachtungen hinsichtlich der Verbindung zwischen den Präzisionsbedingungen für zu bearbeitende Werkstücke und den Freiheitsgraden, die durch Ausrichtung der Werkstücke beseitigt werden müssen (German, Romanian summary) 97

BULETINUL INSTITUTULUI POLITEHNIC DIN IAŞI
BULLETIN OF THE POLYTECHNIC INSTITUTE OF JASSY
ИЗВЕСТИЯ ЯССКОГО ПОЛИТЕХНИЧЕСКОГО ИНСТИТУТА
Том XXXI (XXXV), Вып. 1 — 4 1985

Секция IV

МАШИНОСТРОЕНИЕ

Стр.

В. МЕРТИКАРУ и П. ТИВЛЯ, Множители момента для промышленых роботов. Механизмы с зубчатыми колёсами с малым числом зубьев (англ., рез. рум.) 7

М. ГАФИЦАНУ и БАРБУ ДРЭГАН, Исследование вляния радиального биения на щуму зубчатых колес с помощю CEPSTRUM-анализу (англ., рез. рум.) 15

СПИРИДОН КРЕЦУ и ВИКТОР ХАТМАНУ, Численный анализ пластический деформаций для линейного контакта (англ., рез. рум.) 19

ЧЕЗАР ДУКА и АДРИАН ПОПОВИЧ, Аналитический метод для определения радиусы кривизны плоских кулачков (анлг., рез. рум.) 27

В. МЕРТИКАРУ и ДЭНУЦ РЕЧЯНУ, Критерии выбора трубок Бурдон для промышленных манометров (англ., рез. рум.) 35

СПИРИДОН КРЕЦУ и ЧЕЗАР РАКОЧЯ, Оптималное проектирование геометрии контакта для цилиндрических подшипников качения (англ., рез. рум.) 43

ДАН УРСЕСКУ, ВИРДЖИЛ ДЖЮРКЭ, Математичиский модель для пусковых режимов газотурбинных двигателеи (англ., рез. рум.) 49

БОГДАН ХОРБАНЮК и ЭМИЛ ЛУКА, Геометрическая оптимизация термических труб с ребрами для термического максимального потока на эдиницу веса (англ., рез. рум.) 55

К. ЧИОКИНЭ, ЭМИЛ АНДРЕИ, АУРЕЛИАН СИМИОНЕСКУ, РАДУ ДЭНИЛЭ, ЛЕОНАКЕ ДРЭГОИ и ФЛОРИН АНДРЕИ, Экспериментальные исследования для снижения количества огранических связок из содержания автоупрочнённых формовочных смесей на холоде (нем., рез. рум.) 63

И. ХОПУЛЕЛЕ, КАРМЕН НЕЖНЕРУ и М. ШТЕФАН, Стабилизация определения размеров во выпрямлении безформенных деталей термической обработкой (англ., рез. рум.) 69

ДРАГОШ ПАРАСКИВ, ОКТАВИАН ПРУТЯНУ, В. БРАХА и Г. ТЕШУ, Об отношении между шероховатостю поверхносом Ra и параметрами работы при фронтальном фрезеровании (франц., рез. рум.) 75

СТАН ПАНАИТ, МИРЧЯ КОЗМЫНКЭ и И. РОМАНЕСКУ, Виды крутильных колебаний в зубообрабатывающих фрезерных станках (франц., рез. рум.) 81

В. БРАХА, ОКТАВИАН ПРУТЯНУ, ДРАГОШ ПАРАСКИВ, РОМЕО КУДРИК и ГАВРИЛ МУСКЭ, Влияние неуравновешенных центробежных сил на шероховатость поверхности при чистовои обточке нежестких валов (нем., рез. рум.) 87

ДРАГОШ ПАРАСКИВ, ОКТАВИАН ПРУТЯНУ, Г. ТЕШУ и НИНА АФРЭСИНЕЛ, О влнянии режимов резания на шероховатость поверхность Ra при фронтальном шлифовании (франц., рез. рум.) 93

Н. ГЕРГЕЛ, О связи между условиями точности определителями и степеньями свободы которые нужно удалять ориентированием (нем., рез. рум.) 97

BULETINUL INSTITUTULUI POLITEHNIC DIN IAŞI
Tomul XXXI (XXXV), Fasc. 1—4, 1985
Secția IV
CONSTRUCȚII DE MAȘINI

D.C. 521 ; 621.833

TORQUE AMPLIFIERS FOR INDUSTRIAL ROBOTS. MECHANISM WITH GEARS WITH SMALL NUMBER OF TEETH

BY

V. MERTICARU and P. TIVLEA

1. **General Considerations.** The industrial robots work on pneumatic, hydraulic and electric motors (or combinations).

The working elements of the industrial robots must meet the following important conditions:

i) their movements must be very precise ;

ii) one can easily alter their speed and position ;

iii) the running torque must be greater than the torque of the motor.

Some of the requirements imposed to the working elements of the industrial robots are met by motors (disk rotor ans axial air gap direct/ continuous current motors and step by step motors).

The utilization of the step by step motors for working the industrial robots has good results if they are associated with torque amplifiers [8].

2. **Important Conditions for Designing Gears with a Small Number of Teeth.** For reaching a high transmission ratio in a small clearance gauge it is necessary to use gears with a small number of teeth.

In designing toothed-wheels with a small number of teeth, it is necessary to remove the negative effects which occur both in their manufacturing and in their working [3], [6]:

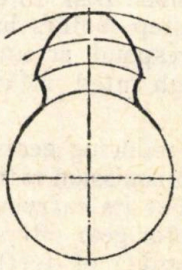

Fig. 1

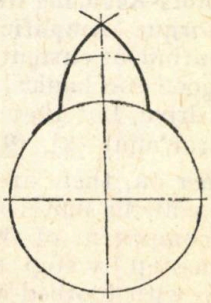

Fig. 2

i) the thinning-out of the tooth at its foot (Fig. 1) ;

ii) the sharpening of the tooth head (Fig. 2);

iii) an inadequate covering degree.

In order to avoid the thinning-out of tooth at its foot we must calculate the minimum coefficient of the profile displacement

$$x_{\min}=1-\frac{z\sin\alpha_{0t}}{2\cos\beta}. \tag{1}$$

For avoiding the sharpening of the tooth head we must calculate the maximum coefficient of the tooth head with

$$h_a^*\leqslant\frac{z}{2\cos\beta}\left(\frac{\cos\alpha_{0t}}{\cos\alpha_{at}}-1\right)-x_{\min}-0.167. \tag{2}$$

The tooth top sharpening determines its strenght diminution.
For hardened teeth it is recomanded

$$s_a\geqslant 0.5m_n. \tag{3}$$

For normalized or improved teeth

$$s_a\geqslant 0.3m_n. \tag{4}$$

In designing the toothed-wheels with a small number of teeth, we have used the logical diagram as shown in Fig. 3 [4]... [6].

3. The Manufacturing of the Toothed-Wheels with a Small Number of Teeth. The teething of the toothed-wheels with a small number of teeth has been common teething-machines, by using the rolling method.

For $z=4$, $z=3$ and $z=2$ we have used the common rolling procedure between the worm gear modulus and the semi-finished material [1], [2].

For $z=1$ we have used the rolling procedure between the wheel-cutter and the semi-finished material, a procedure that is used in manufacturing involute worm gears [1].

In Figs. 4, 5, 6 and 7 there are presented some toothed-wheels with a small number of teeth that have been made ($z=1...4$).

4. Motors-Reducing Gears with Toothed Wheels with Very Small Number of Teeth.Torque Amplifiers for Industrial Robots. Disk rotor and axial air gap continuous current motors and step by step motors have a small gauge, a good-mechanical characteristic and respond accurately to the automatic drive, but they work at relatively high rated rotation speeds ($n\simeq 3\,000$ rot/min) [8], [9].

Further on, there are presented two motor reducing gears. In Fig. 8 there is presented a motor-reducing gear with a transmission ratio of $i=200$, used as a component of the industrial robots. For its carrying out there have used a step by step motor and reducing-motor gear (step-down gear) in two step with toothed-wheels with a small number of teeth.

The pinion of the first step has been made on the motor axle, with $z=3$ (Fig. 9). This motor-reducing gear has two gaings out.

In Fig. 10 there is presented a servo-motor speed variating device with a disk rotor and axial air gap direct/continuous motor and a motor-reducing gear (step-down gear) in two steps with toothed-wheels with a small number

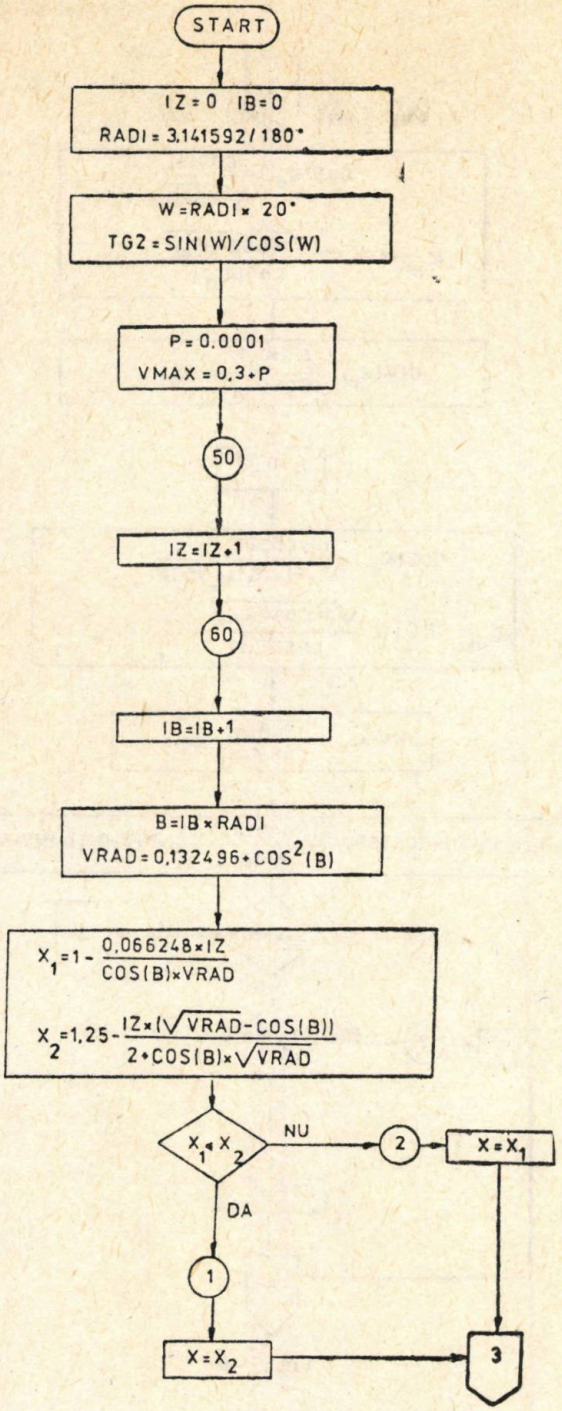
START
IZ = 0 IB = 0
RADI = 3,141592 / 180°
W = RADI × 20°
TG2 = SIN(W) / COS(W)
P = 0,0001
VMAX = 0,3 • P
50
IZ = IZ • 1
60
IB = IB • 1
B = IB × RADI
VRAD = 0,132496 • COS²(B)
X1 = 1 - 0,066248 × IZ / COS(B) × VRAD
X2 = 1,25 - IZ × (√VRAD - COS(B)) / 2 • COS(B) × √VRAD
X1 < X2
NU
2
X = X1
DA
1
X = X2
3

Fig. 3—*a*

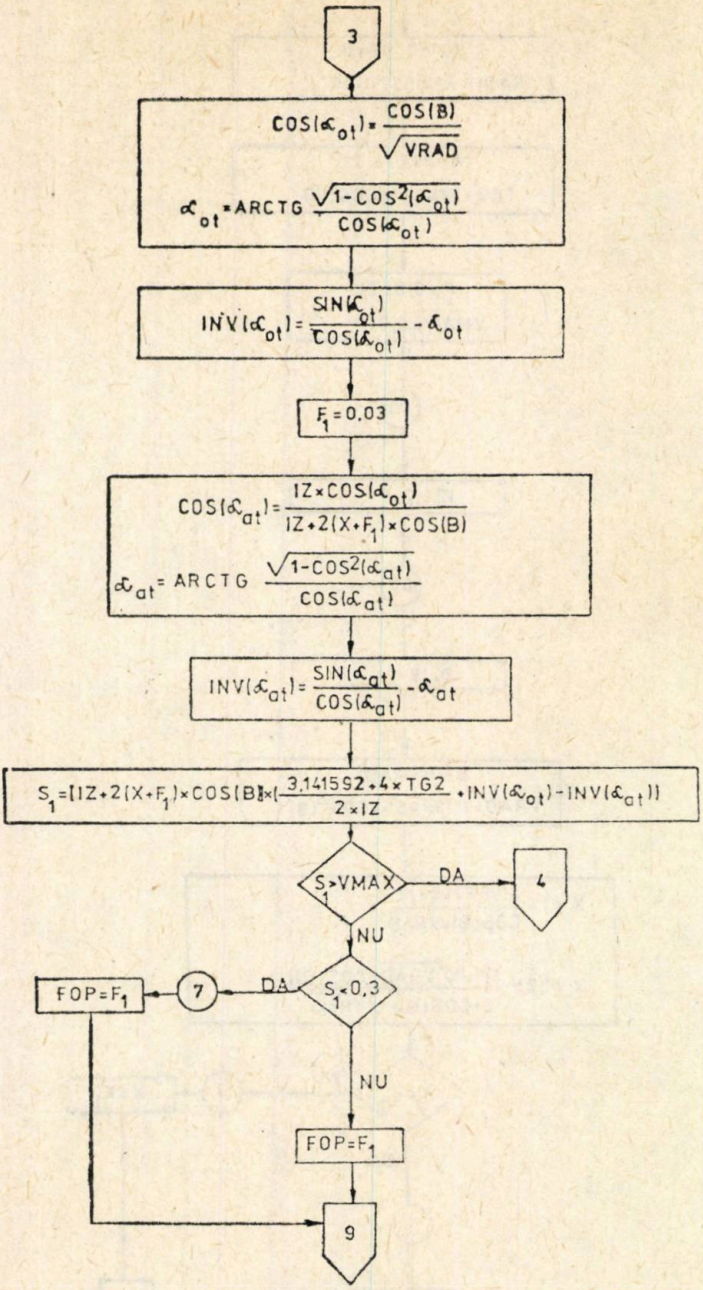
3
$COS(\alpha_{ot}) = \frac{COS(B)}{\sqrt{VRAD}}$
$\alpha_{ot} = ARCTG \frac{\sqrt{1-COS^2(\alpha_{ot})}}{COS(\alpha_{ot})}$
$INV(\alpha_{ot}) = \frac{SIN(\alpha_{ot})}{COS(\alpha_{ot})} - \alpha_{ot}$
$F_1 = 0.03$
$COS(\alpha_{at}) = \frac{IZ \times COS(\alpha_{ot})}{IZ + 2(X+F_1) \times COS(B)}$
$\alpha_{at} = ARCTG \frac{\sqrt{1-COS^2(\alpha_{at})}}{COS(\alpha_{at})}$
$INV(\alpha_{at}) = \frac{SIN(\alpha_{at})}{COS(\alpha_{at})} - \alpha_{at}$
$S_1 = [IZ + 2(X+F_1) \times COS(B)] \times (\frac{3.14159 \cdot 2 + 4 \times TG2}{2 \times IZ} + INV(\alpha_{ot}) - INV(\alpha_{at}))$
$S_1 > VMAX$
DA
4
NU
$S_1 < 0,3$
DA
7
$FOP = F_1$
NU
$FOP = F_1$
9

Fig. 3—*b*

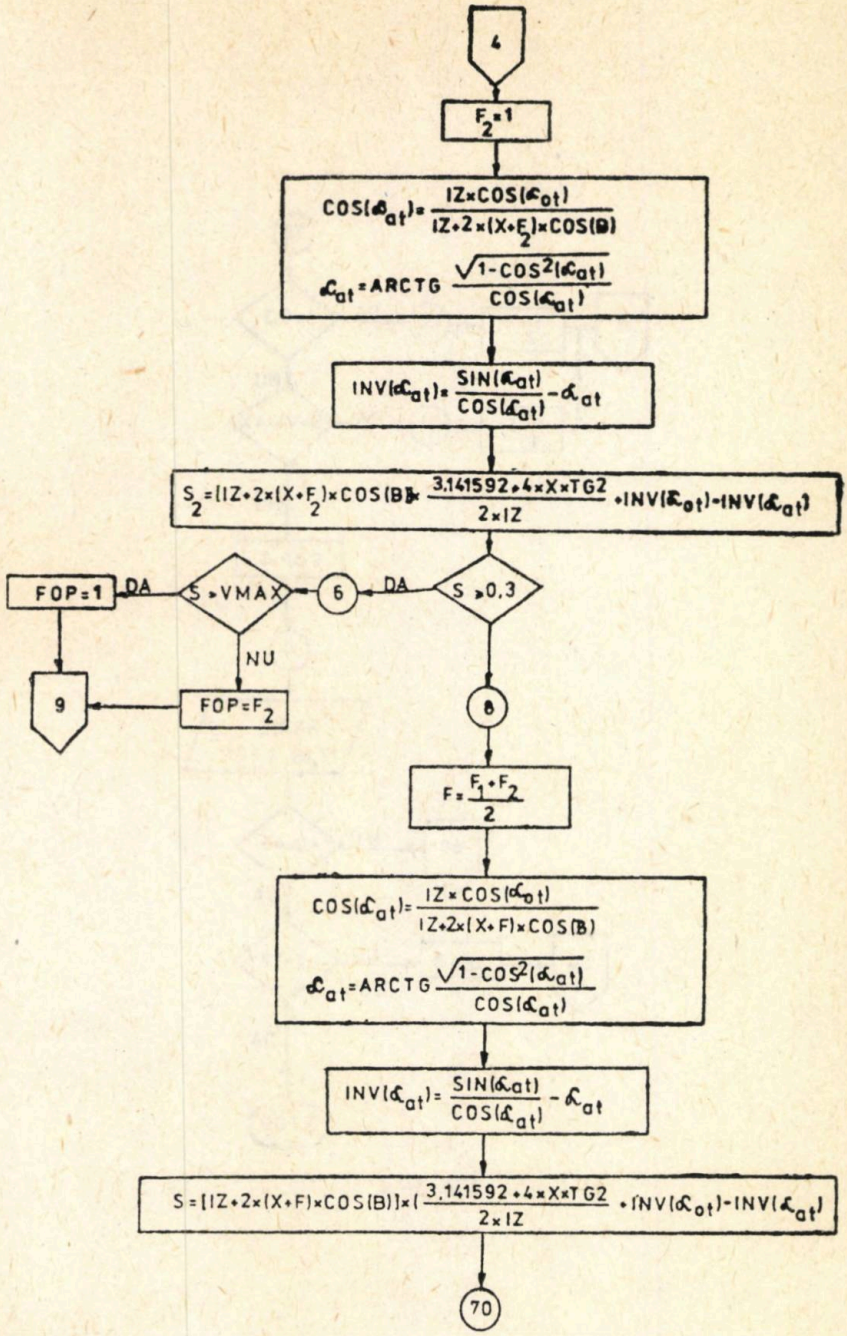
4
$F_2=1$
$\cos(\alpha_{at})=\frac{IZ\times\cos(\alpha_{ot})}{IZ+2\times(X+F_2)\times\cos(B)}$
$\alpha_{at}=\mathrm{ARCTG}\frac{\sqrt{1-\cos^2(\alpha_{at})}}{\cos(\alpha_{at})}$
$INV(\alpha_{at})=\frac{\sin(\alpha_{at})}{\cos(\alpha_{at})}-\alpha_{at}$
$S_2=[IZ+2\times(X+F_2)\times\cos(B)]\times\frac{3.141592+4\times X\times TG2}{2\times IZ}+INV(\alpha_{ot})-INV(\alpha_{at})$
$S>0.3$
DA
6
$S>VMAX$
DA
FOP=1
NU
$FOP=F_2$
9
8
$F=\frac{F_1+F_2}{2}$
$\cos(\alpha_{at})=\frac{IZ\times\cos(\alpha_{ot})}{IZ+2\times(X+F)\times\cos(B)}$
$\alpha_{at}=\mathrm{ARCTG}\frac{\sqrt{1-\cos^2(\alpha_{at})}}{\cos(\alpha_{at})}$
$INV(\alpha_{at})=\frac{\sin(\alpha_{at})}{\cos(\alpha_{at})}-\alpha_{at}$
$S=[IZ+2\times(X+F)\times\cos(B)]\times(\frac{3.141592+4\times X\times TG2}{2\times IZ}+INV(\alpha_{ot})-INV(\alpha_{at})$
70

Fig. 3—*c*

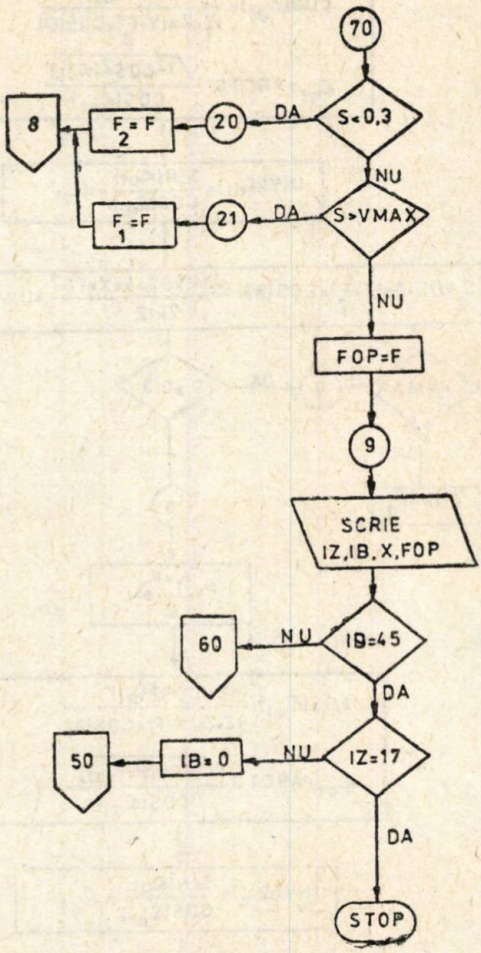
70
S<0,3
DA
20
F2=F
8
NU
S>VMAX
DA
21
F1=F
NU
FOP=F
9
SCRIE
IZ,IB,X,FOP
IB=45
NU
60
DA
IZ=17
NU
IB=0
50
DA
STOP

Fig, 3—*d*

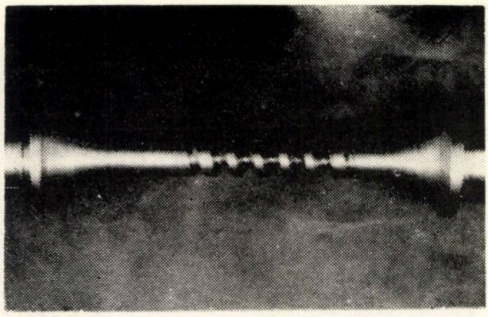

Fig. 4

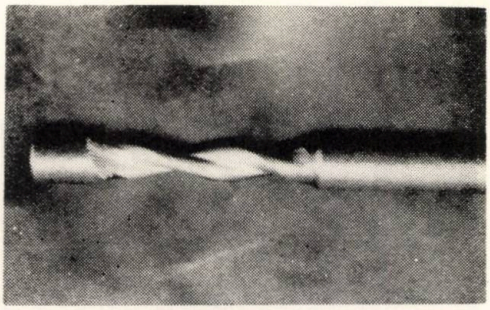

Fig. 5

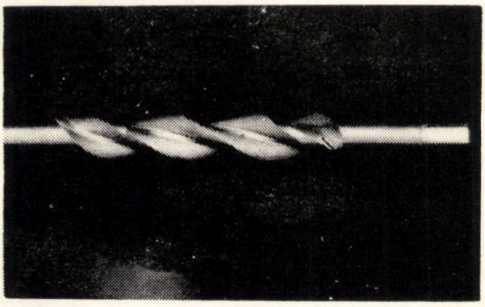

Fig. 6

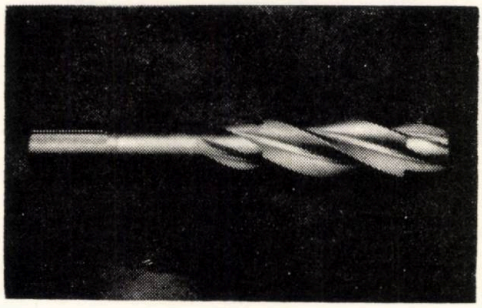

Fig. 7

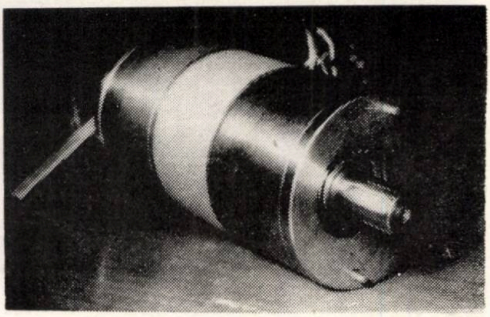

Fig. 8

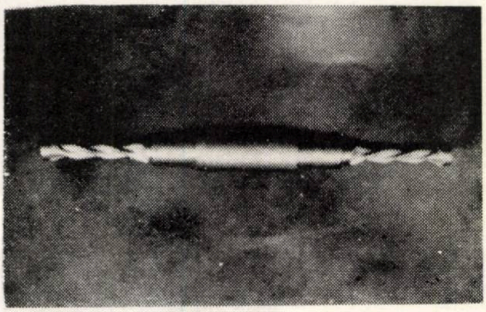

Fig. 9

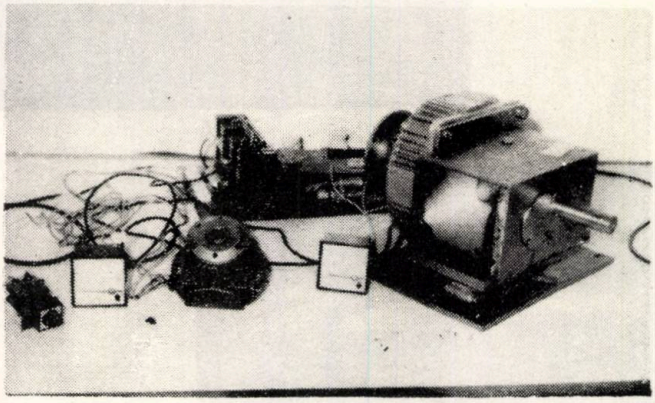

Fig. 10

of teeth having a transmission ratio of $i=150$. The pinion of the first step has been made at the axle of the rotor.

5. Conclusions. 1. Step by step motors and direct/continuous motors cannot be rationally used at low speeds.

2. Torque amplifiers made up of toothed wheels with a small number of teeth have a reduced gauge, have simple mechanism and have a high efficiency. The drive of these torque amplifiers are the same as the ones of the motor.

Notation

x — profile displacement coefficient
α_{0t} — engendering normal pressure angle in the frontal plane
h_a^* — reference coefficient of the addendum
z — number of teeth
β — helix angle
s_a — tooth top sharpening
m_n — module in the normal plane

Received May 25, 1985

Polytechnic Institute, Jassy,
Department of Machine Design

REFERENCES

1. Drăghici G., *Tehnologia tip a pieselor plane, cu axe încrucișate, cu profil complex și elicoidale*. Ed. tehn., Buc., 1977, p. 185.
2. Lungu Gh., Tureac I., Pană C., *Mașini unelte pentru mecanică fină*. Ed. did. și ped., Buc., 1981.
3. Merticaru V., Atanasiu V., *Mechanisms with Cylindrical Gear Wheels with Small Number of Teeth and Involute Profile*. Bul. Inst. polit. Iași, **XXVI (XXX)**, *3—4*, s. IV, 53—62 (1980).
4. Merticaru V., Atanasiu V., *Computation Algoritm Programed in FORTRAN to Avoid Negative Phenomena at Generation of the Cylindrical Gears with Small Number of Teeth*. Simpozion de mecanisme și organe de mașini, Univ. din Brașov, 1978, Vol. I, pp. 197—203.
5. Merticaru V., Atanasiu V., *Mathematical Model and Computer Program in FORTRAN for Helical Gearing Noise*. Papers of the Fifth World Congress on the Theory of Machines and Mechanisms, Montreal, Canada, July 8—13, 1979, Vol. 2, pp. 1144—1147.
6. Merticaru V., Atanasiu V., *Optimum Desing of Mechanisms with Spuur and Helical Gears and Involute Profils*. Papers of the Fifth World Congress on the Theory of Machines and Mechanisms, Montreal, Canada, July 8—13, 1979, Vol. 2, pp. 1140—1143.
7. Merticaru V., Tivlea P., *Servomotoreductor — sistem de acționare în structura roboților industriali*. Al 3-lea Simpozion național de roboți industriali, București, 27—29 oct. 1983, Vol. 2, pp. 367—372.
8. Pal C., Târnoveanu G., *Asupra posibilităților de utilizare a motoarelor pas cu pas (MPP) la roboți industriali*. Al 3-lea Simpozion național de roboți industriali, București, 27—29 oct. 1983, Vol. 2, pp. 381—388.
9. * * * Prospecte, I.C.P.E., București.

AMPLIFICATOARE DE CUPLU PENTRU ROBOȚI INDUSTRIALI. MECANISME CU ROȚI DINȚATE CU NUMĂR FOARTE MIC DE DINȚI

(Rezumat)

Se expune metodologia de proiectare, asistată de calculator, a roților dințate cu număr foarte mic de dinți ($z = 1 \ldots 4$), precum și modul de realizare al acestora. Se prezintă realizări de motoreductoare cu roți dințate cu număr foarte mic de dinți, folosite ca amplificatoare de cuplu pentru roboți industriali.

BULETINUL INSTITUTULUI POLITEHNIC DIN IAŞI
Tomul XXXI (XXXV), Fasc. 1—4, 1985
Secţia IV
CONSTRUCŢII DE MAŞINI

D.C. 621.833 ; 534.4

CEPSTRUM ANALYSIS OF THE TOTAL RUNOUT INFLUENCE ON THE GEAR NOISE

BY

M. GAFIŢANU and BARBU DRĂGAN

1. Generalities. The total runout is a widespread fault, causing the dividing circles of the two engaged gears not to be tangent during the whole rotation.

The relatively high frequency vibration corresponding to the engaging frequency and the low frequency corresponding to the rotation frequency of the gear are considered together, resulting a modulated vibration in magnitude, generating frequency lateral stripes in the spectrum, placed around the engaging frequencies and their harmonics.

For the determination of these modulating frequencies, the CEPSTRUM analysis is used.

For this purpose controlled total runout gears were introduced in the cinematic chain of the gear box.

2. CEPSTRUM Analysis. Fig. 1 shows the analogous scheme with compressing facilities and ZOOM analysis which realizes CEPSTRUM analysis.

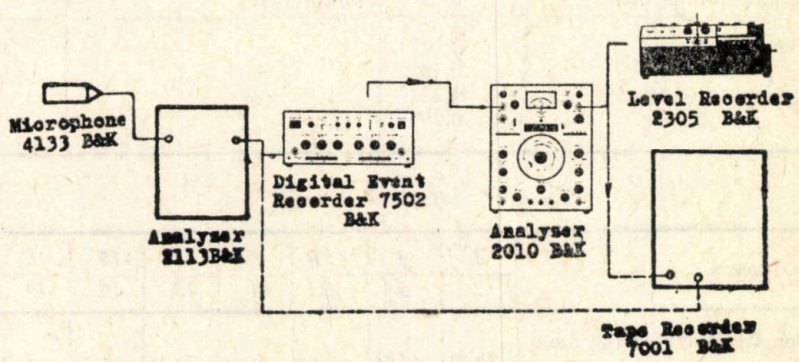

Fig. 1

3. Defective Gears Identification in Gear Transmission via CEPSTRUM Analysis. In order to study the diagnosing capabilities given by the CEPSTRUM analysis, defective gears were introduced in position *4* of the gear box of the AF 85 milling machine, the scheme of which is presented in Fig. 2.

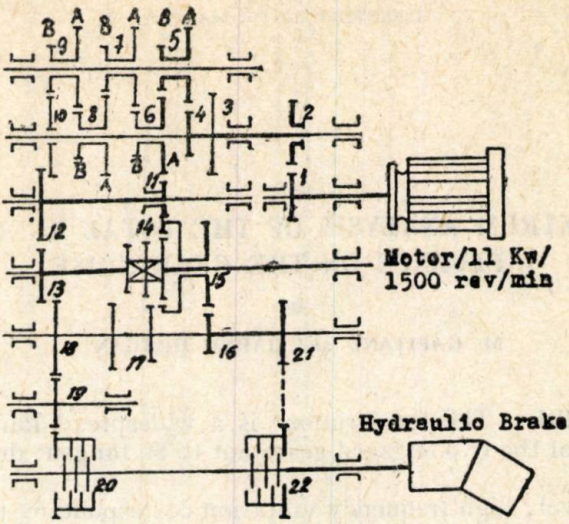

Fig. 2

Table 1 shows the constructive and functional parameters of the defective gear.

Table 1

Teeth no.	24	Material (enrich)	OLC 45
Module	2	Rotation (rev/min)	633
The specific profile drift	0	Power (kW)	2.2
Total runout	0.027 0.12 0.21 0.29		

Table 2

Engaged gears	1/2	4/5A	5B/6A	6B/11	12/13	15/16	18/19	21/22
Rotation frequency of the main gear	23.75	10.55	2.63	2.94	3.16	4.75	4.75	4.75
Engaging frequency	380	253.3	126.6	126	133	209	247	209

The defective gear gave modifications both in the frequency spectrum range and the CEPSTRUM analysis relatively to the concerned gear box (Fig. 3).

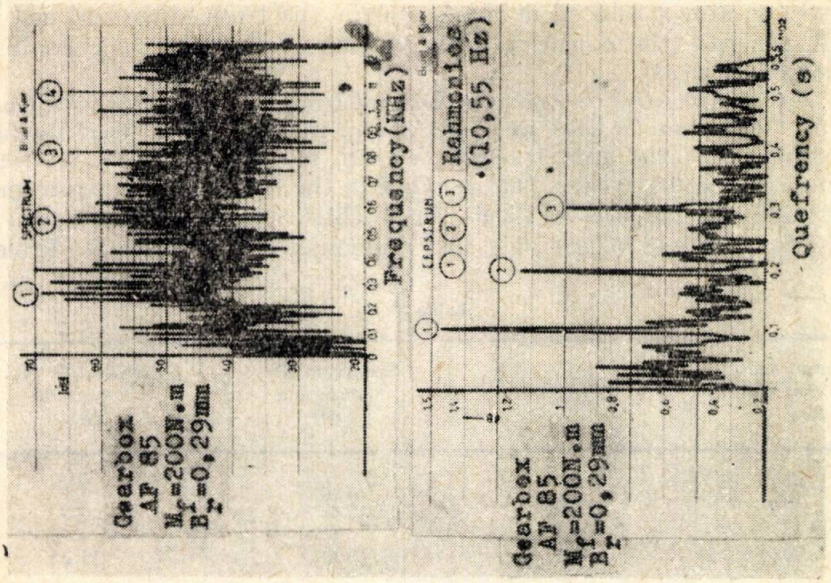
Gearbox
AF 85
Mf=200N.m
Br=0,29mm
Frequency(KHz)
Rahmonics
(10,55 Hz)
Quefrency (s)

Fig. 4

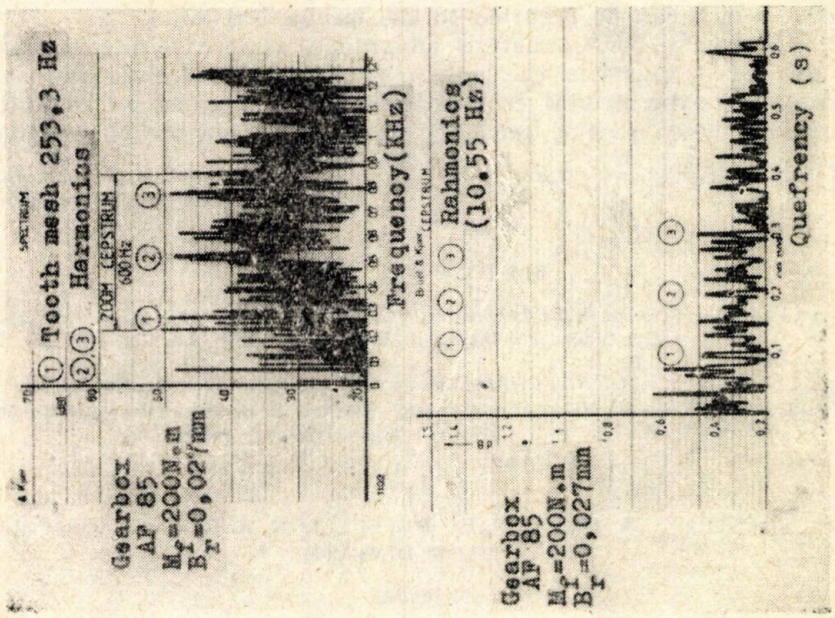
Tooth mesh 253,3 Hz
Harmonics
Gearbox
AF 85
Mf=200N.m
Br=0,027mm
Frequency(KHz)
Rahmonics
(10,55 Hz)
Quefrency (s)

Fig. 3

Comparing the calculated frequencies (Table 2) and those at which modifications were produced in the frequency spectrum range and in CEPSTRUM analysis, the defective gear position in the gear box could be identificated (Fig. 4).

The defective gear in the gear box modifies the overall level of noise with only 3 dB, from 79 dBA to 82 dBA. This increase shows that the function conditions of the gear transmission are modified, but without significant indication on the cause; mean while in the frequency spectrum range and especially in the CEPSTRUM, the modifications are evidently to the engaging frequencies ; to harmonics and rahmonics are also obvious (Table 3).

Table 3

Runout the defective gear mm	Overall noise level dB	Spectrum No. 1 harmonic dB	CEPSTRUM No. 1 rahmonic dB
0.027	79	49.5	0.44
0.12	79.5	52.5	0.8
0.21	81	62	0.94
0.29	82	69	1.25

4. Conclusion. 1. CEPSTRUM analysis allows the periodicity detection of the frequency (spectrum) giving information on the modulating frecquency which can be reported to the mechanical fauts.

2. The CEPSTRUM analysis advantage relative to the usual frequency analysis consists in the high sensibility of the former and in the simplification of experimental results interpretations, because in CEPSTRUM the periodical peaks of the frequency range spectrum are cumulative.

Received December 19, 1985

Polytechnic Institute, Jassy,
Department of Machine Design

REFERENCES

1. Randall R. B., *Advances in the Application of CEPSTRUM Analysis to Gearbox Diagnosis.* „Vibr. Rotating Mach., 2nd Int. Conf., Cambridge, 1980", London, 1980, pp. 163—168.
2. Randall R. B. e. a., *CEPSTRUM Analysis.* Brüel & Kjaer Technical Review, 3 (1981).
3. Taylor J. I., *Fault Diagnosis of Gears using Spectrum Analysis.* „Vibr. Rotating Mach.; 2nd Int. Conf., Cambridge, 1980", London, 1980, pp. 168—174.

ANALIZA CEPSTRUM A INFLUENŢEI DEFECTELOR ASUPRA ZGOMOTULUI ROŢILOR DINŢATE

(Rezumat)

Se studiază posibilităţile de diagnosticare a defectelor roţilor dinţate cu ajutorul analizei CEPSTRUM. În acest scop au fost introduse roţi dinţate cu bătaie radială controlată în lanţul cinematic al cutiei de viteze de la maşina de alezat şi frezat AF 85.

BULETINUL INSTITUTULUI POLITEHNIC DIN IAȘI
Tomul XXXI (XXXV), Fasc. 1—4, 1985
Secția IV
CONSTRUCȚII DE MAȘINI

D.C. 624.078 ; 539.388

A NUMERICAL ANALYSIS OF PERMANENT DEFORMATION IN ELASTIC-PLASTIC LINE CONTACT

BY

SPIRIDON CREȚU and VICTOR HATMANU

1. Introduction. When a rolling element is pressed with a sufficiently high load on a bearing raceway a plastic indentation may remain in the raceway. These permanent deformations, if they are too large can cause excessive vibration and possibly stress concentrations [5], [8].

În the first part of the paper process of plastic deformation at rolling contact is treated analitically. The study is based on both the Prandtl-Reuss equations and the von Mises yield criterion. Ramberg-Osgood's equation was employed to consider the yielding process of the hardened bearing steel.

In the second part of the paper the correlation with the experimental measurements are discussed. There are used some of authors' measurements [1] carried out on point contact, but also the W i c k s t r a n d's measurement [4] carried out on line contact. There is a close agreement between displacements obtained from theory and those obtained experimentally.

2. Theory. The total state of strain existing at a point in a material can be explained by the deformation tensor ε_{ij} which can be written as the sum of the tensors of elastic deformation as well as of the plastic deformation [7]

$$\varepsilon_{ij}=\varepsilon^{e}_{ij}+\varepsilon^{p}_{ij}. \tag{1}$$

The tensor of elastic deformation can be evaluated through Hook's law (written using Einsten's convention)

$$\varepsilon_{ij}=\frac{1+\nu}{E}\sigma_{ij}-\frac{\nu}{E}\sigma_{ij}\delta_{ij}, \tag{2}$$

where : σ_{ii} represents the stress tensor ; δ_{ij} is the spherical tensor ; E and ν are the Young's modulus and Poisson's coefficient respectively. Differentiating (1) the differential strains are obtained

$$de_{ij}=de^{e}_{ij}+de^{p}_{ij}, \tag{3}$$

where de^{e}_{ij} and de^{p}_{ij} are the differential elastic and differential plastic strains respectively. It had to be outlined that this process of differentiation is a consistent operation due to the fact that the strain tensors are symmetrical

gradients of the displacements vectors which under the fundamental hypothesis of the theory of elasticity and plasticity should have continuous variations. To be able to calculate the plastic deformations the differentials from (3) have to be evaluated.

The differential of the elastic strain tensor is obtained direct from (2)

$$d\varepsilon_{ij}^{e} = \frac{1+\nu}{E} d\sigma_{ij} - \frac{\nu}{E} d(\sigma_{ii})\delta_{ij} . \tag{4}$$

The differential of plastic strain tensor can be written in the following from [2]

$$d\varepsilon_{ij}^{p} = \frac{3}{2} \frac{d\bar{e}_p}{\bar{\sigma}_e} S_{ij}, \tag{5}$$

where $d\bar{e}_p$ is the differential of the intensity of plastic strain tensor ; $\bar{\sigma}_e$ is the intensity of the stress tensor ; S_{ij} is deviatoric stress tensor.

The Ramberg-Osgood's equation

$$\bar{e} = \frac{\bar{\sigma}_e}{E} + \left(\frac{\bar{\sigma}_e}{B}\right)^N \tag{6}$$

is used to establish the link between the stress tensor and the intensity of the strain tensor. In (6) $\bar{e}$ is the intensity of the strain tensor, B is a material constant, N — a function of strain hardening. It can be seen that $\bar{\sigma}_e/E$ represents the elastic component and $(\bar{\sigma}_e/B)^N$ represents the plastic component

$$\bar{e}_p = \left(\frac{\bar{\sigma}_e}{B}\right)^N . \tag{7}$$

Differentiating (7)

$$d\bar{e}_p = \frac{N\bar{\sigma}_e^{N-1} d\bar{\sigma}_e B^N - \bar{\sigma}_e^N N B^{N-1} dB}{B^{2N}} . \tag{8}$$

Since B is a material constant, $dB=0$, so that

$$d\bar{e}_p = \frac{d\bar{\sigma}_e N\bar{\sigma}_e^{N-1}}{B^N} , \quad \text{or} \quad d\bar{e}_p = \frac{N\bar{\sigma}_e^{N-1}}{B^N} d\bar{\sigma}_e ,$$

$$\frac{d\bar{\sigma}_e}{d\bar{e}_p} = \frac{B^N}{N(\bar{\sigma}_e)^{N-1}} . \tag{9}$$

The slope of the plastic portion of Ramberg-Osgood's curve is

$$H' = \frac{d\bar{\sigma}_e}{d\bar{e}_p} = \frac{B^N}{N\bar{\sigma}_e^{N-1}} , \tag{10}$$

so

$$d\bar{e}_p = \frac{d\bar{\sigma}_e}{H'} = \frac{N(\bar{\sigma}_e)^{N-1}}{B^N} d\bar{\sigma}_e . \tag{11}$$

Replacing (11), (5) and (4) in Eq. (3) the following equation is obtained

$$d\varepsilon_{ij}=\frac{1+\nu}{E}d\sigma_{ij}-\frac{\nu}{E}\delta_{ij}d(\sigma_{ii})+\frac{3}{2}\frac{S_{ij}}{\bar{\sigma}_e H'}d\bar{\sigma}_e. \tag{12}$$

The last equation establishes a link between the components of the stress tensor and the components of the total strain tensor. In this form the equation is very difficult to handle, but some observation will be made to permit a more suitable form.

i) The Eq. (12) is valid in any reference connected with the considered point of the material.

ii) Both parts of Eq. (12) get their principal directions simultaneously so that the Eq. (12) can be written in the reference formed with principal directions.

In this system

$$\sigma_{ij}=\begin{cases}0 & \text{for } i\neq j,\\ \sigma_i & \text{for } i=j;\end{cases}\qquad \varepsilon_{ij}=\begin{cases}0 & \text{for } i\neq j,\\ \varepsilon_i & \text{for } i=j;\end{cases}$$

$$S_{ij}=\begin{cases}0 & \text{for } i\neq j,\\ \sigma_i=\frac{1}{3}\sigma_{kk} & \text{for } i=j.\end{cases}$$

Multiplying by $2\bar{\sigma}_e$ the last fraction of the right part of Eq. (12) one obtains

$$d\varepsilon_{ij}=\frac{1+\nu}{E}d\sigma_{ij}=\frac{\nu}{E}\delta_{ij}d(\sigma_{kk})+\frac{3}{4}\frac{S_{ij}}{\bar{\sigma}_e^2 H'}d(\bar{\tau}_e^2). \tag{13}$$

Putting

$$\begin{aligned}A_1&=2\sigma_1-\sigma_2-\sigma_3,\\ A_2&=2\sigma_2-\sigma_3-\sigma_1,\\ A_3&=2\sigma_3-\sigma_1-\sigma_2,\end{aligned} \tag{14}$$

the Eq. (13) becomes

$$d\varepsilon_i=\frac{1+\nu}{E}d\sigma_i-\frac{\nu}{E}d(\sigma_{kk})+\frac{A_1}{4\bar{\sigma}_e^2 H'}\left[\sum\frac{\partial(\bar{\sigma}_e^2)}{\partial\sigma_i}d\sigma_i\right]. \tag{15}$$

If in Eq. (14) $\bar{\sigma}_e$ is considered given by von Mises plasticity criterion one obtains

$$\bar{\sigma}_e^2=\frac{3}{2}S_{ij}S_{ij}=\frac{3}{2}\sum(\sigma_i-\tfrac{1}{3}(\sum\sigma_i))^2. \tag{16}$$

Performing the partial differentiations

$$\frac{\partial(\bar{\sigma}_e^2)}{\partial\sigma_i}=A_i,\qquad i=1,2,3, \tag{17}$$

one obtains

$$d\varepsilon_i=\frac{1+\nu}{E}d\sigma_i-\frac{\nu}{E}\sum_j d\sigma_j+\frac{A_i}{4\bar{\sigma}_e^2 H'}\sum_j A_j d\sigma_j. \tag{18}$$

It can be noted that the Eq. (17) can be written also in matrix form

$$\begin{bmatrix} d\varepsilon_1 \\ d\varepsilon_2 \\ d\varepsilon_3 \end{bmatrix} = [A_{ij}] \cdot \begin{bmatrix} d\sigma_1 \\ d\sigma_2 \\ d\sigma_3 \end{bmatrix}, \tag{19}$$

where

$$[A_{ij}] = \left[\frac{1}{E}\delta_{ij}\right] + \left[\frac{\nu}{E}(\delta_{ij}-1)\right] + \left[\frac{A_i A_j}{4\bar{\sigma}_e^2 H'}\right]. \tag{20}$$

3. Simplifying Hypothesis and Numerical Solution. For loads that exceed the elastic limit only by a relatively small factor the differences between elastic and elasto-plastic contact in the plastic range are manifested through relatively small variations in the shape and in the area of the pressure ellipse and consequently strains must be approximately equal for both types of loading. It should be noted that the equations of equilibrium and those of compatibility are not always fully satisfied. The numerical solution used to solve the expressions just developed is known as the compatibility technique, which satisfies displacement restrictions in entire the solid body. This method suggests that the force should be applied in small increments till it reaches the required value.

As each load is applied, differential stress and stratus are related through the coefficients in the A_{ij} matrix. The A_{ij} matrix can be determined from the previous load increment. Stresses and strains, after each load increment are computed by summing all previous stress and strain differentials. An explanation of the compatibility technique is shown in Fig. 1, where results of a uniaxial tensile test are recorded. If material was loaded up to point A, the following load increment, brings about a total strain ε_t which is assumed to be equal to the elastic strain calculated using Hooke's law (point B on the dotted line).

Using Eq. (19) by inversing A_{ij} matrix the variation of the stress tensor $d\sigma_{ij}$ is obtained. This variation added to the stress tensor gives the real stress tensor corresponding to the point C. Using the stress tensor σ_r the elastic strain ε^e is computed that is then substrating from the total strain ε_t in order to obtain the incremental plastic strain $d\varepsilon^p$. These incremental plastic strains are summed till the required load is achieved. In this way the plastic strain at a certain depth and for a particular load was obtained.

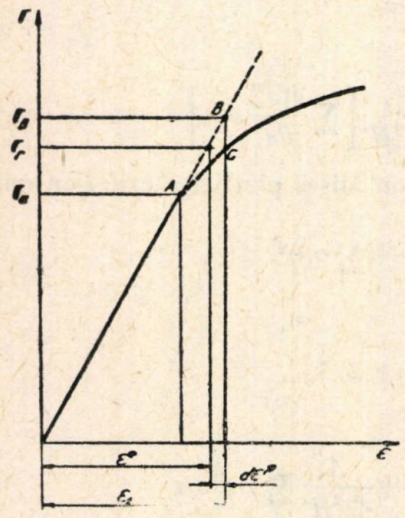

Fig. 1

The whole process is repeated for every depth and a numerical dependence of plastic deformation with depth is obtained.

In order to obtain the total plastic deformation (permanent deformation)

the total plastic strain in the Z coordinate direction must be evaluated. This implies the integration of plastic strains in the Z direction

$$W_Z = \int_0^{Z_p} \varepsilon_{ZZ}^p dZ. \tag{21}$$

The limit Z_p in the integral (21) represents the depth at which the strain ε_{ZZ}^p becomes zero.

4. Results of Numerical Solution. A FORTRAN IV programme for the CORAL 4011 computer has been elaborated. The flow chart of the programme is given in Fig. 2.

The numerical method was applied for the simpler case of line contact, Fig. 3. The dependence of plastic deformation with depth is presented in Fig. 4 for four different loads.

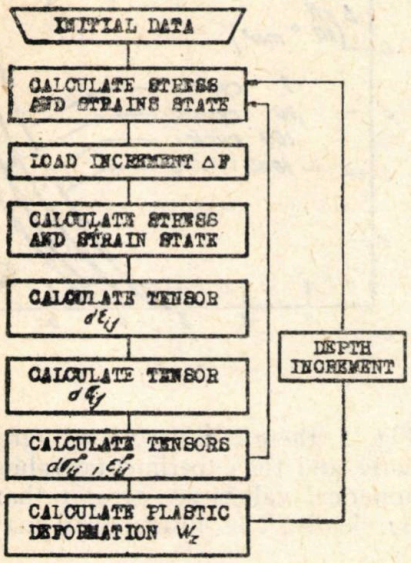

Fig. 2

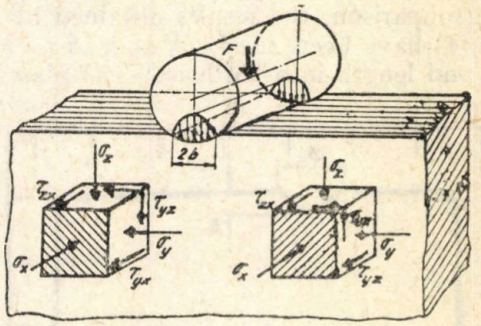

Fig. 3

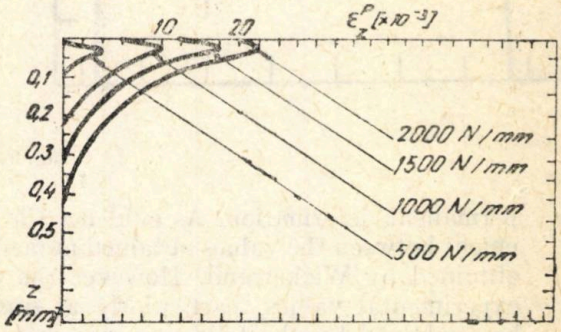

Fig. 4

The results of the numerical integration along the Z coordinate of the curves from Fig. 4 represents the permanent deformation and is presented in Fig. 5.

5. Comparision with Experimental Results. Plastic deformations measurements have been carried out in point contact.

The inner rings of the NU 206 cylindrical roller bearing and toroidal discs have been used as test specimens, Fig. 6. The profile of plastic deforma-

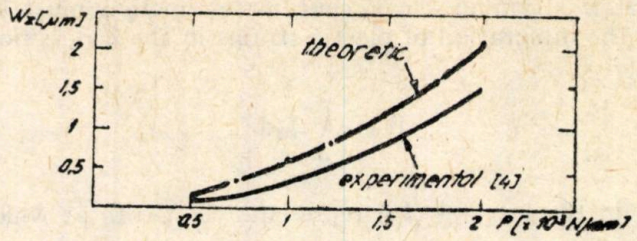

Fig. 5

tions has been obtained using the Taylor-Hobson apparatus (Fig. 6 *a*). The results of the measurements are plotted in Fig. 6 *b* as against maximum Hertz stress σ_0. It can be noted that the curves have the same shape with that obtained by numerical solution. In order to achieve a quantitative comparison, the results obtained by N. Wickstrand in line contact [4] have been used. Wickstrand loaded rollers of various diameters and length into hardened steel plates and measured the resulting depth of

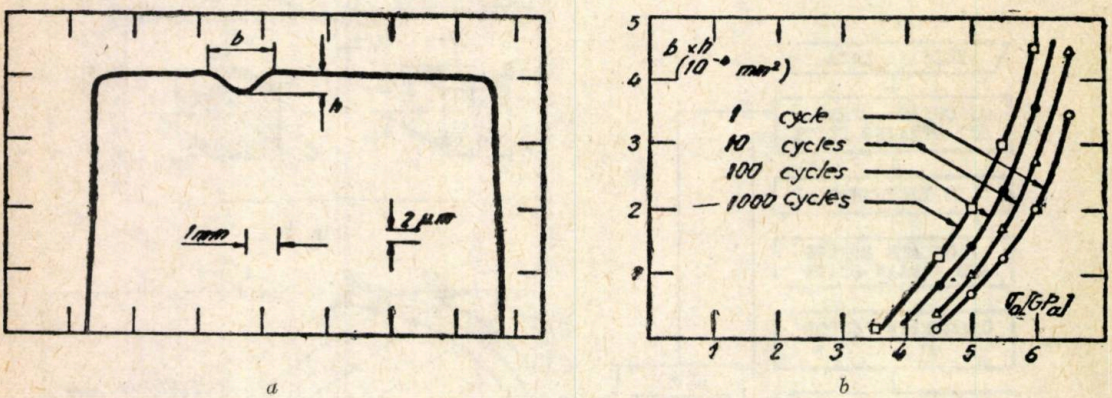

a *b*

Fig. 6

permanent deformation. As evidenced in Fig. 5, there is a very good agreement between the values obtained numerically and the experimental values obtained by Wickstrand. However the numerical values are greater than experimental values, particularly at greater loads. This discrepancy may be explained by the following statements :

i) the compatibility technique used in the computation does not strictly respect the equations of equilibrium and those of compatibility ;

ii) the load increment used had a finite value (50 N) and was not able to predict strains, with a sufficient accuracy at high values of stress.

6. Conclusions. 1. The incremental theory of plasticity incorporating both the Mises-Hencky yield criterion and the Ramberg-Osgood strain hardening equation, has been used to predict the load-depth of permanent deformation relationship in the case of line contact (contact of a roller and a halfspace).

2. Experimental investigations carried out to relate the depth of plastic deformation to various loading levels have conducted to an exponential dependence.

3. There is a very close agreement between displacements obtained from the compatibility technique and the experimental measurements presented in the literature.

Received November 25, 1985

Polytechnic Institute, Jassy,
Department of Machine Design

REFERENCES

1. Creţu S. Sp., Ph. D. Thesis, Jassy Politechnic Institute, 1978.
2. Palazatto A. N., Morris N. F., *An Elastic-plastic Plane Stress Solution Using the Incremental Theory*. Int. J. of Mech. Sci., **13**, 97 (1971).
3. Hartnett M. J., Palazatto A. N., *Permanent Deformation of Bearing Raceway Surfaces*. ASLE Trans., **19**, *2*, 115–124 (1976).
4. Wickstrand N. M., *Depth of Permanent Indentation in Flat Plates Due to Loaded Cylindrical Rollers*. Trans. of ASME, J. of Lub. Engng., series **F**, *163* (1970).
5. Williams F. J., Schwartz A., *An Investigation of Permanent Deformation (Brinelling) of Ball and Roller Specimens*. Trans. of ASME, J. of. Lub. Technol., **91**,*2*, 618–630 (1968).
6. Hoeprich M. R., Zantopulos H., *Line Contact Deformation; a Cylinder between Two Plates*. Trans. of ASME, J. of Lub. Technol., **103**, *1*, 21–25 (1981).
7. Olszak W. ş.a. *Teoria plasticităţii*. Ed. tehn., Buc., 1970.
8. Орлов А. В., Пинегин С. В., *Остаточные напряжения деформации при контактом нагружении*, Машиностоение, М., 1971.

ANALIZA NUMERICĂ A DEFORMAŢIEI PLASTICE LA CONTACTUL LINIAR ELASTO-PLASTIC

(Rezumat)

Este tratat analitic procesul de deformare plastică la contactul hertzian liniar. Studiul se bazează pe ecuaţiile Prandtl-Reuss din teoria curgerii plastice şi pe criteriul de plasticitate al lui von Mises. Legătura între tensiuni şi deformaţii se realizează prin utilizarea curbei Ramberg-Osgood.

Rezolvarea este realizată numeric folosind tehnica compatibilităţii. Rezultatele obţinute teoretic sînt comparate cu măsurători experimentale atît ale autorilor cît şi din literatură, constatîndu-se o strînsă corelare.

BULETINUL INSTITUTULUI POLITEHNIC DIN IAȘI
Tomul XXXI (XXXV), Fasc. 1—4, 1985
Secția IV
CONSTRUCȚII DE MAȘINI

D.C. 621—185

ANALYTICAL METHOD FOR THE DETERMINATION OF RADIUS OF CURVATURE IN THE CASE OF PLANE CAMS

BY

CEZAR DUCA and ADRIAN POPOVICI

0. Introduction. The radius of curvature is a very important parameter for the optimal design of cam mechanisms. The minimum value of the radius of curvature has implications in the problem of avoiding the undercutting phenomenon and is directly connected to the performance of cam-follower system.

The paper offers the cams designers an analytical method of the radius of curvature determination. This method is simple and convenient if compared to other methods [2], [3]. It can be used to elaborate an optimization algorithm [1] or to make an ordinary design.

1. The Kinematic Equations of the Higher-pair Joint. Fig. 1 represents a higher-pair joint formed by the moving links *1* and *2*. Active curves T_1 and T_2, contacting in P, are attached to links *1* and *2*, respectively.

The velocity equations are

$$\bar{v}_P=\bar{v}_{P_1}+v_{PP_1}, \tag{1}$$

$$\bar{v}_P=v_{P_2}+\bar{v}_{PP_2}, \tag{2}$$

where : $\bar{v}_P$—velocity of the contact point P with respect to the fixed system; $\bar{v}_{P_1}$—velocity of the point P_1 on body *1*, which coincides, at instant, with P; $\bar{v}_{PP_1}$—relative velocity of point P with respect to the moving system *1*. The trajectory of this motion is T_1, therefore $\bar{v}_{PP_1} \| tt$; $\bar{v}_{P_2}$—velocity of the point P_2 on body *2*, which coincides, at instant, with P ; v_{PP_2} — relative velocity of point P with respect to the moving system *2*. The trajectory of this motion is T_2, therefore $\bar{v}_{PP_2} \| tt$.

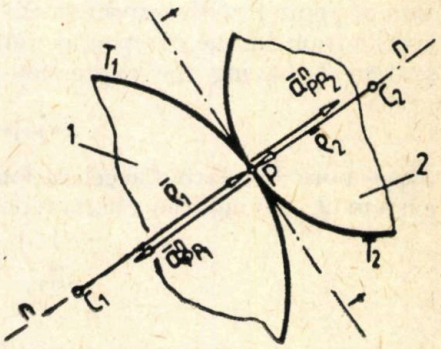

Fig. 1

The acceleration equations are

$$\bar{a}_P=\bar{a}_{P_1}+\bar{a}^c_{PP_1}+\bar{a}^n_{PP_1}+\bar{a}^t_{PP_1}, \tag{3}$$

$$\bar{a}_P=\bar{a}_{P_2}+\bar{a}^c_{PP_2}+\bar{a}^n_{PP_2}+\bar{a}^t_{PP_2}, \tag{4}$$

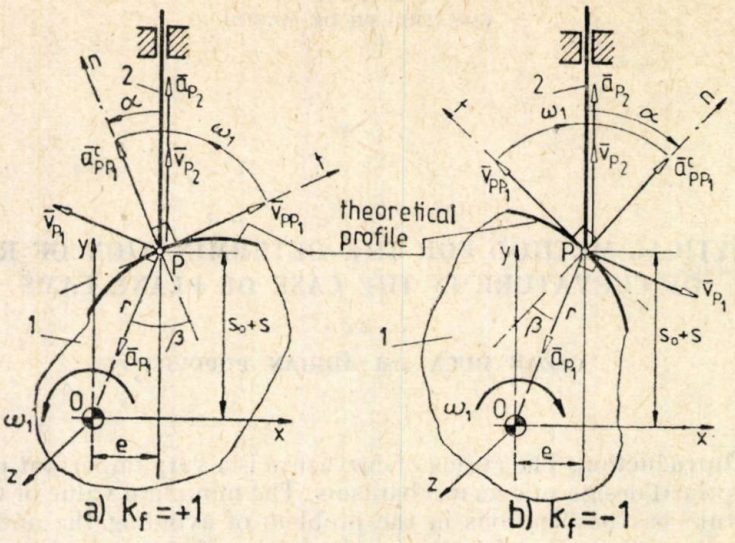

Fig. 2 — Disc cam with translating roller-ended follower.

in which : $\bar{a}_P$—acceleration of the point P with respect to the fixed system ; a_{P_1}— acceleration of the point P_1 on body *1*, which coincides, at instant, with P ; $\bar{a}^c_{PP_1}$ — Coriolis acceleration in the compound motion of point P by means of the moving system *1*, having the expression

$$\bar{a}^c_{PP_1} = 2\bar{\omega}_1 \times v_{PP_1} ;$$

$\bar{a}^n_{PP_1}$—normal relative acceleration of point P with respect to the moving system *1*, having the characteristics

$$\bar{a}^n_{PP_1} = -\frac{v^2_{PP_1}}{\rho_1} ; \quad \| nn ;$$

ρ_1— radius of curvature of curve T_1 in P ; $\bar{a}^t_{PP_1}$— tangential relative acceleration of point P with respect to the moving system *1* ; $\bar{a}^t_{PP_1} \| tt$; $\bar{a}^c_{PP_2}$— Coriolis acceleration in the compound motion of point P by means of the moving system *2*, having the expression

$$\bar{a}^c_{PP_2} = 2\bar{\omega}_2 \times \bar{v}_{PP_2} ;$$

$\bar{a}^n_{PP_2}$— normal relative acceleration of point P with respect to the moving system *2*, having the characteristics

$$\bar{a}^n_{PP_2} = -\frac{v^2_{PP_2}}{\rho_2} \quad \| nn ;$$

ρ_2—radius of curvature of curve T_2 in P; $a^t_{PP_2}$— tangential relative acceleration of point P with respect to the moving system *2* ; $\bar{a}^t_{PP_2} \| tt$.

2. The Radius of Curvature of the Cam Profile. If we consider link *1* as a cam and link *2* as its follower, the radius of curvature of the cam profile in the contacting point P has the expression $\rho_1 = -v^2_{PP_1}/a^n_{PP_1}$, or

$$\rho_1 = -\frac{(v_{PP_1}/\omega_1)^2}{a^n_{PP_1}/\omega_1^2}. \tag{5}$$

The sign — intervenes in the formula (5) because the vectors $\bar{\rho}_1$ and $\bar{a}^n_{PP_1}$ have opposite senses (Fig. 1), and the scalars ρ_1 and $a^n_{PP_1}$ have opposite signs.

The magnitude v_{PP_1}/ω_1, which intervenes in (5), can be determinated by equating the expressions (1) and (2), projecting the obtained equation on the common tangent in P and dividing by ω_1 :

$$\frac{v_{PP_1}}{\omega_1} = \frac{(v_{P_2})_t}{\omega_1} + \frac{v_{PP_2}}{\omega_1} - \frac{(v_{P_1})_t}{\omega_1}. \tag{6}$$

Similary we determine $a^n_{PP_1}/\omega_1^2$, by equating expressions (3) and (4), projecting the obtained equation on the common normal in P and dividing by ω_1^2 :

$$\frac{a^n_{PP_1}}{\omega_1^2} = \frac{(a_{P_2})_n}{\omega_1^2} + \frac{a^c_{PP_2}}{\omega_1^2} + \frac{a^n_{PP_2}}{\omega_1^2} - \frac{(a_{P_1})_n}{\omega_1^2} - \frac{a^c_{PP_1}}{\omega_1^2}. \tag{7}$$

The common normal in P has conventionally the sense of crossing the cam profile from its inside to the outside. The sense of the common tangent is obtained by turning 90° the normal in the opposite sense with respect to the cam angular velocity (Figs. 2...5). Thus, when ρ_1 results positive, the profile is convex, and when it results negative, is concave.

Starting from the indicated definitions of the terms which apear in (6) and (7), we infered their calculating expressions. These are given in Table 1 for the principal types of planar cam mechanisms. The notations are the following : φ—cam angle rotation, measured from the beginning of the phase ; k_f—phase coefficient.

In the case of the translating follower mechanisms, the value of k_f is : $k_f = +1$ if $v/\omega > 0$ and $k_f = -1$ if $v/\omega < 0$, where v is follower velocity and ω—cam angular velocity. The signs of the parameters v and ω results from comparing the senses of vectors $\bar{v}$ and $\bar{\omega}$ with the axes Oy and Oz of the right-handed coordinate system. This system has the origin in the cam rotation center, the axis Ox is perpendicular to the follower and is orientated towards it, the axis Oy is paralel to the follower and the axis Oz completes the right-handed system (Fig. 2).

In the case of the oscillating follower mechanisms k_f has the values: $k_f = +1$ if the cam and the follower rotate in the same sense and $k_f = -1$ if the cam and the follower rotate in opposite senses. Further one, s—space (displacement of follower) (the functions $s(\varphi)$, $\frac{ds}{d\varphi}(\varphi)$ and $\frac{d^2s}{d\varphi^2}(\varphi)$ characterize the motion law of the translating follower) ; ψ—follower angle

Table 1

	Disc cam with translating roller-ended follower (Fig. 2)	Disc cam with translating flat-faced follower (Fig. 3)	Disc cam with oscillating roller-ended follower (Fig. 4)	Disc cam with oscillating flat-faced follower (Fig. 5)
$\frac{(v_{P_2})_t}{\omega_1}$	$k_f \frac{ds}{d\varphi} \sin\alpha$	0	$-k_f \frac{d\psi}{d\varphi} l \sin\alpha$	0
$\frac{v_{PP_2}}{\omega_1}$	0	$\frac{d^2s}{d\varphi^2}$	0	$\frac{d\frac{d^2\psi}{d\varphi^2}\cos(\psi_0+\psi) - k_f d \frac{d\psi}{d\varphi}\left(1-k_f\frac{d\psi}{d\varphi}\right)\sin(\psi_0+\psi)}{\left(1-k_f\frac{d\psi}{d\varphi}\right)^2}$
$\frac{(v_{P_1})_t}{\omega_1}$	$-r\cos\beta$	$-(s_0+s)$	$-r\cos\beta$	$-d\sin(\psi_0+\psi)$
$\frac{(a_{P_2})_n}{\omega_1^2}$	$\frac{d^2s}{d\varphi^2}\cos\alpha$	$\frac{d^2s}{d\varphi^2}$	$-\left(\frac{d\psi}{d\varphi}\right)^2 l\sin\alpha + \frac{d^2\psi}{d\varphi^2} l\cos\alpha$	$\frac{d^2\psi}{d\varphi^2}\frac{d\cos(\psi_0+\psi)}{1-k_f\frac{d\psi}{d\varphi}}$
$\frac{a^c_{PP_2}}{\omega_1^2}$	0	0	0	$2k_f\frac{d\psi}{d\varphi}\left(\frac{v_{PP_2}}{\omega_1}\right)$
$\frac{a^n_{PP_2}}{\omega_1^2}$	0	0	0	0
$\frac{(a_{P_1})_n}{\omega_1^2}$	$-r\cos\beta$	$-(s_0+s)$	$-r\cos\beta$	$-d\sin(\psi_0+\psi)$
$\frac{a^c_{PP_1}}{\omega_1^2}$	$2\frac{v_{PP_1}}{\omega_1}$	$-2\left(\frac{d^2s}{d\varphi^2}+s_0+s\right)$	$2\frac{v_{PP_1}}{\omega_1}$	$2\frac{v_{PP_1}}{\omega_1}$

rotation (the functions $\psi(\varphi)$, $\frac{d\psi}{d\varphi}(\varphi)$ and $\frac{d^2\psi}{d\varphi^2}(\varphi)$ characterize the motion law of the oscillating follower ; e — offset distance (Fig. 2) ; s_0 — distance between cam rotation center and origin of the space, measured parallel to the follower ; l—lenght of oscillating follower arm ; d—distances between the centers of rotation of cam and follower ; ψ_0—angle between the line of centers and the origin of angle ψ ; r—radius of contacting point (Table 2); α—pressure angle (Table 2) ; β—angle between the normal to the profile in the contacting point and radius of this point (Table 2).

Table 2

	Disc cam with translating roller-ended follower	Disc cam with oscillating roller-ended follower
r	$\sqrt{e^2+(s_0+s)^2}$	$\sqrt{l^2+d^2-2ld\cos(\psi_0+\psi)}$
α	$\operatorname{arctg}\dfrac{k_f\dfrac{ds}{d\varphi}-e}{s_0+s}$	$\operatorname{arctg}\left\{-\dfrac{k_f\dfrac{d\psi}{d\varphi}-(l-d\cos(\psi_0+\psi))}{d\sin(\psi_0+\psi)}\right\}$
β	$\left\lvert\operatorname{arctg}\dfrac{e}{s_0+s}+\alpha\right\rvert$	$\left\lvert\arcsin\left(\dfrac{d}{r}\sin(\psi_0+\psi)\right)+\alpha-\dfrac{\pi}{2}\right\rvert$

To understand the way in which we obtained the formulas written in Table 1, the velocities and the accelerations which intervene in (6) and (7) are representated in Figs. 2...5.

It is necessary to make an explanation in connection with the expressions of the parameter v_{PP_2}/ω_1 for the flat-faced follower mechanisms. We obtained the expressions by differentiating the distance TP for the translating follower (Fig. 3) and the distance O_2P for the oscillating follower (Fig. 5) with respect to φ. This distance are

$$TP=\frac{ds}{d\varphi}, \qquad O_2P=\frac{d\cos(\psi_0+\psi)}{1-k_f\dfrac{d\psi}{d\varphi}}.$$

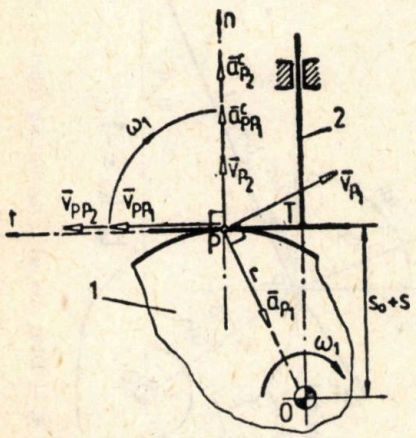

Fig. 3. — Disc cam with translating flat-faced follower.

It will be observed that the already known formula

$$\rho=s_0+s+\frac{d^2s}{d\varphi^2}$$

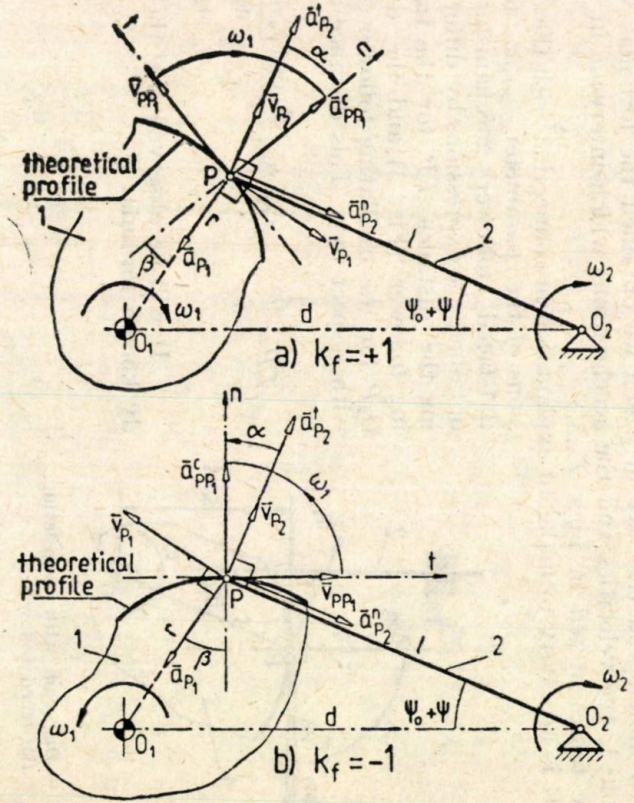

Fig. 4. — Disc cam with oscillating roller-ended follower.

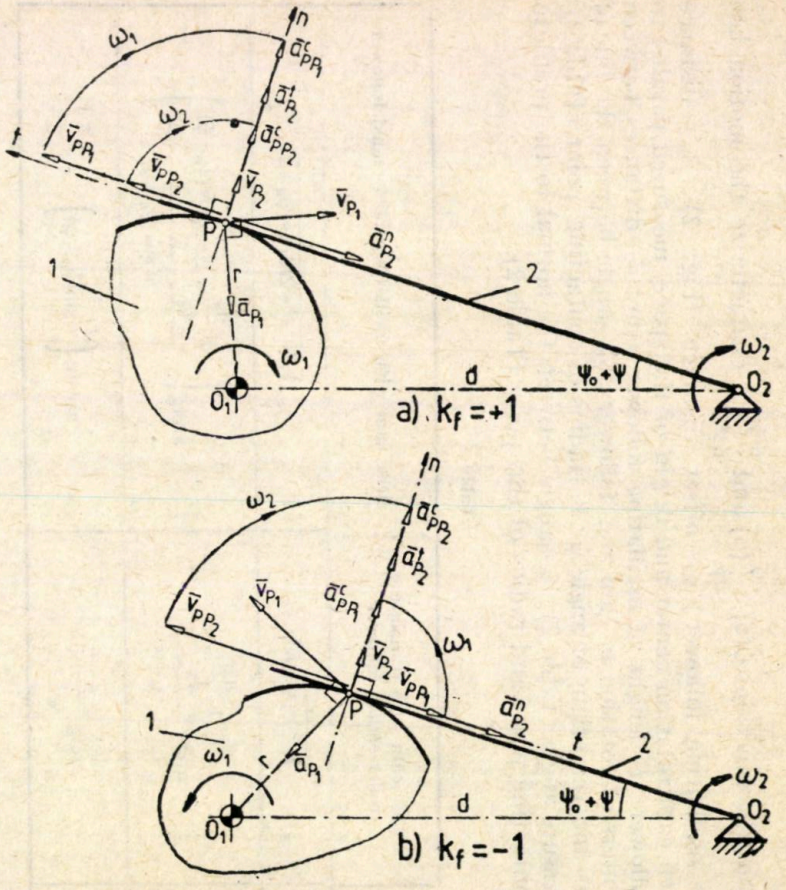

Fig. 5. — Disc cam with oscillating flat-faced follower.

for the disc cam with translating flat-faced follower, is to be found here, too.

3. Conclusion. 1. The above method permits to determine the profile radius of curvature, depending on the following elements :

a) The position of the cam expresed by angle φ.

b) The basic geometric parameters of the mechanism (e, s_0, l, d, ψ_0).

c) The phase coefficient k_f.

d) The motion law expressed by functions $s(\varphi)$, $\frac{ds}{d\varphi}(\varphi)$, $\frac{d^2s}{d\varphi^2}(\varphi)$ or $\psi(\varphi)$, $\frac{d\psi}{d\varphi}(\varphi)$, $\frac{d^2\psi}{d\varphi^2}(\varphi)$.

The enumerated elements are, usually, known by the designer who is not obliged to calculate the supplementary expressions as other methods [2], [3] require.

2. The method, also, reflects the connection between the radius of curvature and the other functional and constructive parameters of the mechanism. This fact suggests the possibilities of their correlation to find an optimal solution.

Received March 14, 1985

Polytechnic Institute, Jassy,
Department of Mechanisms and
Machine Design

REFERENCES

1. Duca C., *Problema optimizării parametrilor geometrici de bază ai mecanismelor cu came.* Simpozionul, „Mecanisme și Transmisii Mecanice", Inst. polit. Timișoara, Vol. I, pp. 145—153, 1980.
2. Chakraborty J., Dhande S. G., *Kinematics and Geometry of Planar and Spatial Cam Mechanisms.* Wiley, Eastern Ldt., New Delhi/Bangalore, 1977.
3. Юдин В. А., Петрокас Л. В., *Теория механизмов и машин.* Изд. „Вышая школа", М., 1977
4. Maros D., *Mecanisme.* Vol. I, Inst. polit. Cluj-Napoca, 1980.

METODĂ ANALITICĂ PENTRU DETERMINAREA RAZEI DE CURBURĂ A PROFILULUI ÎN CAZUL CAMELOR PLANE

(Rezumat)

Metoda expusă în lucrare se bazează pe relația binecunoscută dintre viteza unui punct accelerația normală și raza de curbură a traiectoriei. Această relație se aplică pentru mișcarea punctului de contact, în raport cu planul camei, avînd ca traiectorie profilul. Se ajunge la relația de calcul a razei de curbură pentru următoarele mecanisme : cu tachet de translație și rolă, cu tachet oscilant și rolă, cu tachet de translație și talpă plană și cu tachet oscilant și talpă plană. În formulele obținute figurează numai parametri funcționali și constructivi care, în mod obișnuit, sînt cunoscuți de către proiectant, care nu este astfel obligat să efectueze calcule suplimentare.

Metoda poate fi utilizată atît pentru verificarea razei de curbură în legătură cu subtăierea, interferența sau portanța cuplei superioare, cît și în procesul de elaborare a unui algoritm de optimizare a construcției mecanismelor cu came.

BULETINUL INSTITUTULUI POLITEHNIC DIN IAȘI
Tomul XXXI (XXXV), Fasc. 1—4, 1985
Secția IV
CONSTRUCȚII DE MAȘINI

D.C. 531.787

CRITERIA OF BOURDON TUBE SELECTION FOR THE INDUSTRIAL MANOMETERS

BY

V. MERTICARU and DĂNUȚ RECEANU

Notations

f_{max} — maximum sag to corresponding of the maximum pressure, mm
Δf — deviation of the sag comparatively with theoretic value, mm
Δx — total error of mechanical amplifier, mm
Δx_t — theoretic error of the mechanical amplifier, mm
Δx_C — constructive error, mm
Δx_H — error of the elastic behaviour, mm
Δx_a — tolerable error of the manometer, mm
x_c — displacement of the joint C, mm (Fig. 3)
γ — precision class of the manometer, %
λ — density of the dislocations, mm^{-2}
p_{max} — maximum pressure of the manometers, bar
E^*, R^*, L^* and φ^* — optimized dimensions of the mechanical amplifier
Δx_A, Δy_A, Δx_C and Δy_C — dimensional deviations of the joints A respectively C (Fig. 3)

1. Consideration with Regard to the Precision of the Manometers. Experimental Techniques. Bourdon tube is an elastic element. Then, it presents hysteresis and non-linearity.

The characteristic of the relative errors are presented in the Fig. 1. The Fig. 2 shows the experimental equipment.

The error is

$$\Delta x_H = \frac{\Delta f}{f_{max}} 100. \tag{1}$$

The errors of the elastic behaviour have great values. For the future, these errors must be considered.

For the field $0 - p_{max}$, the total error of the entire mechanical amplifier is

$$\Delta x = \Delta x_C + \Delta x_t + \Delta x_H \cdot \tag{2}$$

The tolerable error is

$$\Delta x_H = \Delta x_a - \Delta x_t - \Delta x_a, \tag{3}$$

where

$$\Delta x_a = \frac{\gamma f_{max}}{100}. \tag{4}$$

The displacement of the joint C is

$$x_C = x_C(\varphi, R, L, E).$$

The error of joint C results by differentiating the equations of the vectorial contour, **R**, **L**, $\mathbf{x}_{c_0}$ and **E** (Fig. 5).

Therefore

$$\Delta x_C = \frac{\cos(\varphi-\psi)}{\cos\psi} R + \frac{1}{\cos\psi}\Delta L - \Delta E \operatorname{tg}\psi. \tag{5}$$

The dimensions R and L are adjustable

$$\Delta x_C = -\Delta E \operatorname{tg}\psi, \tag{6}$$

where

$$E = (x_A - x_C)\sin(-\pi+\gamma+\varphi^*) + (y_C - y_A)\cos(-\pi+\gamma+\varphi^*) \tag{7}$$

and

$$\psi_{max} = \text{arc sin}\,\frac{E^* + \Delta E - R^*\sin\varphi^*}{L^*}. \tag{8}$$

ΔE has maximum and positive value when

$$\Delta x_A > 0, \quad \Delta y_A > 0, \quad \Delta x_C < 0 \quad \text{and} \quad \Delta y_C > 0. \tag{9}$$

The Fig. 4 shows the optimum programming of the dimensions E, R, L and φ. Simultaneously, this programme calculates Δx_H.

For the manometers with $p_{max} = 10$ bar, $\varnothing$ 60 Fig. 6 shows : *a*) the theoretic error ; *b*) the constructive error ; *c*) the tolerable error of the elastic behaviour.

The internal structure of the Bourdon tube influences the resistance, the internal friction and the attack by chemical action.

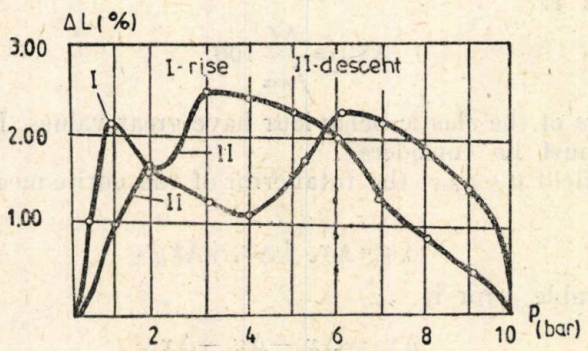

Fig. 1

The metallic surface of the Bourdon tube, which contains internal tensions, is attacked by mercurous azotate and appears a selective corro-

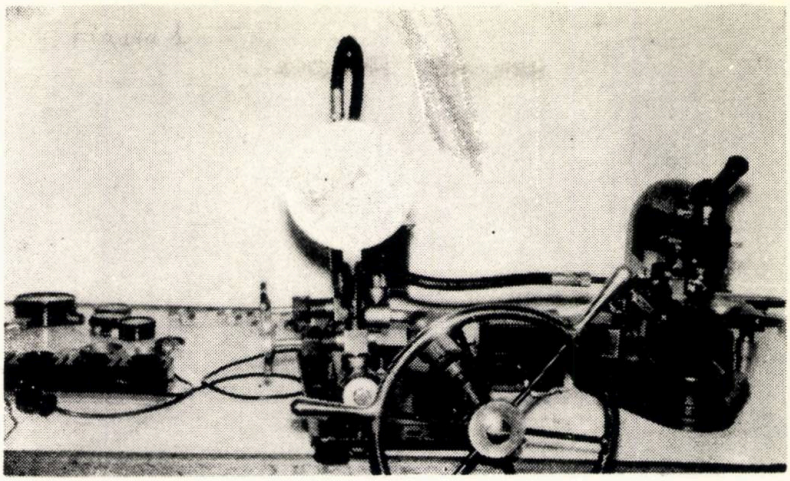

Fig. 2

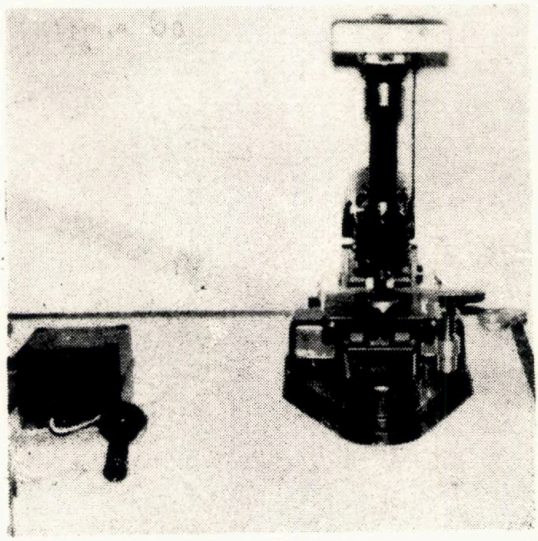

a

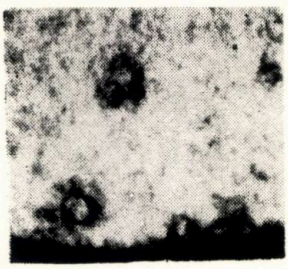

b

Fig. 3

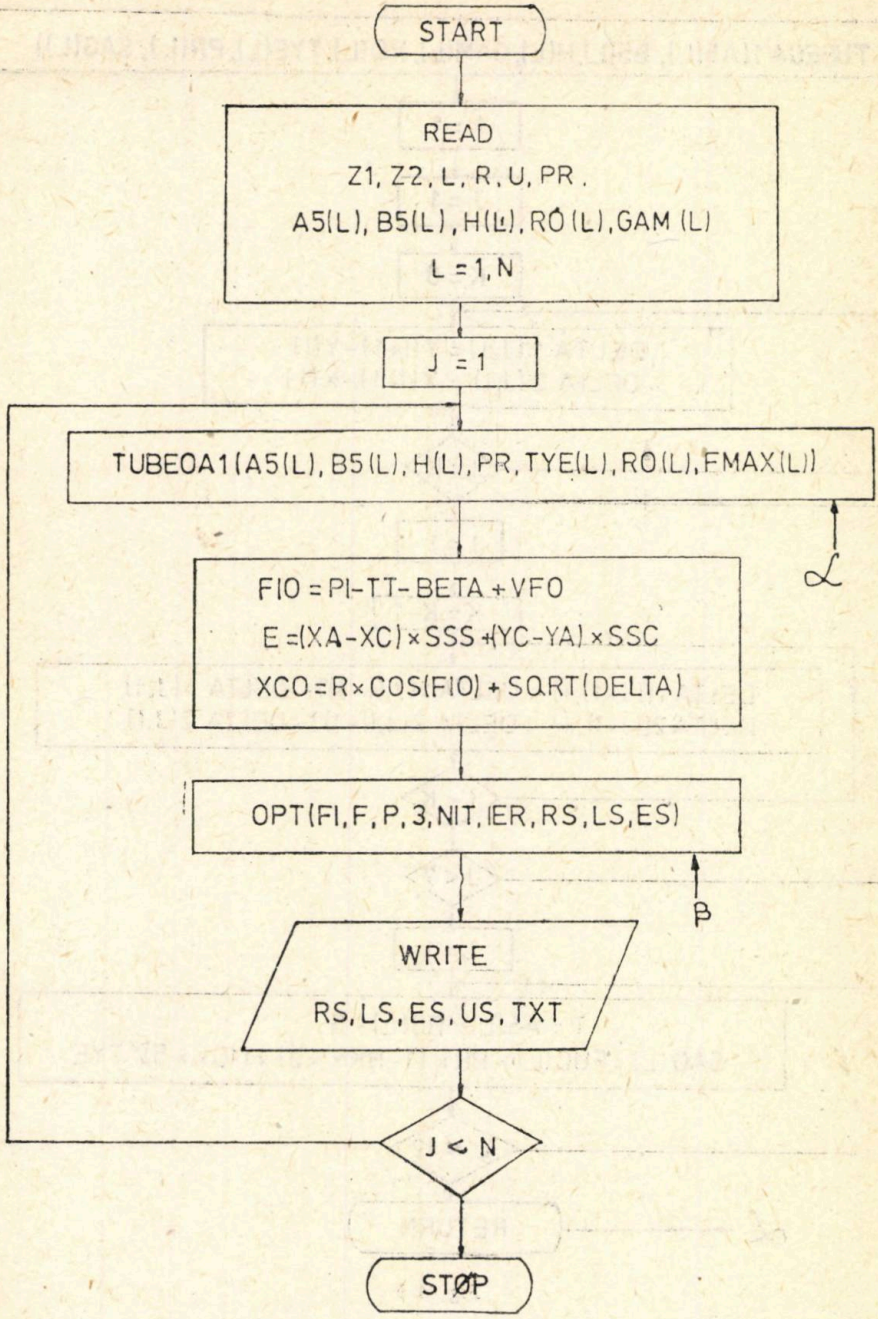
START
READ
Z1, Z2, L, R, U, PR,
A5(L), B5(L), H(L), RO(L), GAM(L)
L = 1, N
J = 1
TUBEOA1(A5(L), B5(L), H(L), PR, TYE(L), RO(L), FMAX(L))
L
FIO = PI-TT-BETA+VFO
E = (XA-XC) × SSS + (YC-YA) × SSC
XCO = R × COS(FIO) + SQRT(DELTA)
OPT(FI, F, P, 3, NIT, IER, RS, LS, ES)
B
WRITE
RS, LS, ES, US, TXT
J < N
STOP

Fig. 4 *a*

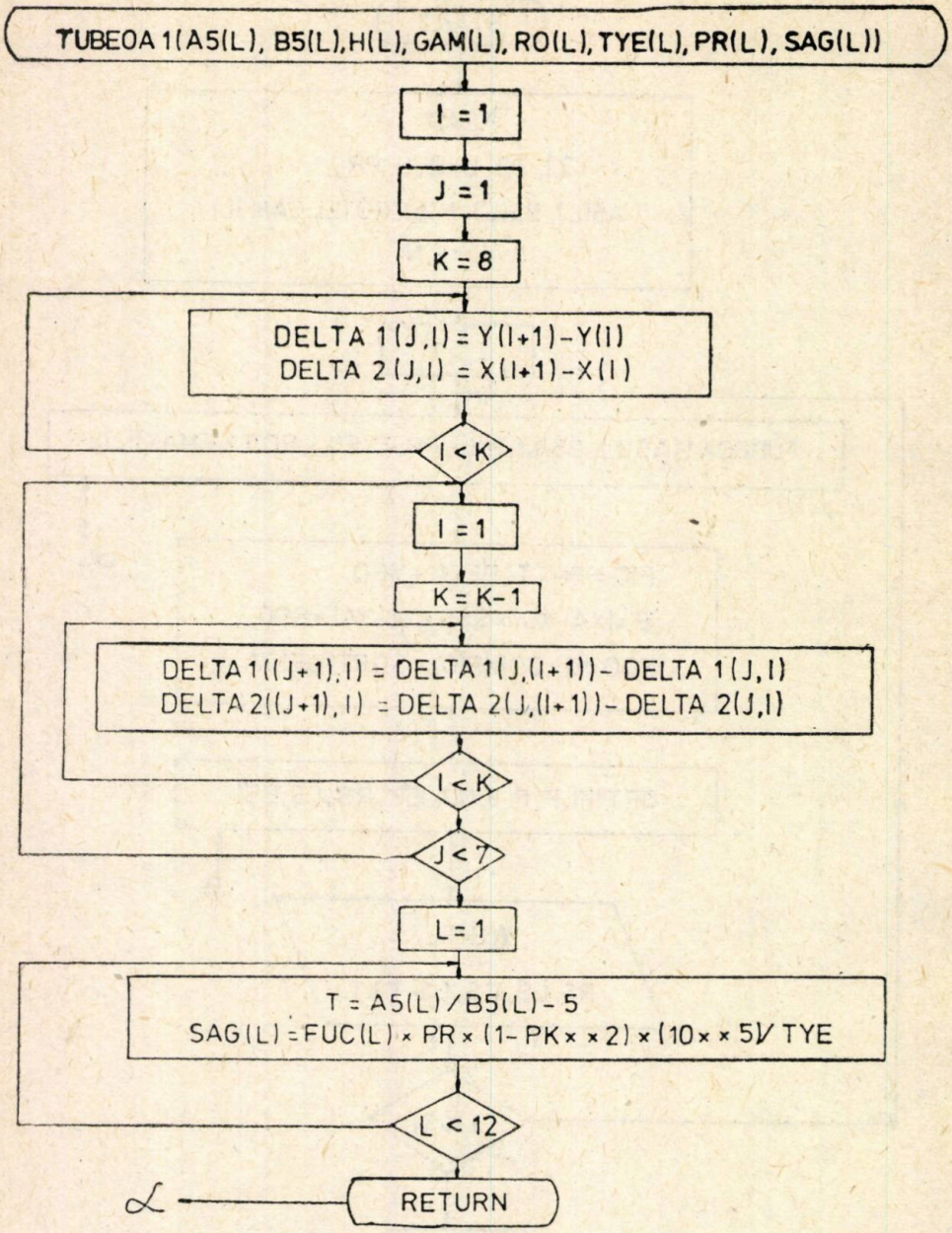
TUBEOA 1(A5(L), B5(L),H(L), GAM(L), RO(L), TYE(L), PR(L), SAG(L))
I = 1
J = 1
K = 8
DELTA 1(J,I) = Y(I+1)-Y(I)
DELTA 2(J,I) = X(I+1)-X(I)
I < K
I = 1
K = K-1
DELTA 1((J+1),I) = DELTA 1(J,(I+1))- DELTA 1(J,I)
DELTA 2((J+1),I) = DELTA 2(J,(I+1))- DELTA 2(J,I)
I < K
J < 7
L = 1
T = A5(L)/B5(L)-5
SAG(L) = FUC(L) × PR × (1-PK××2) × (10××5)/ TYE
L < 12
RETURN

Fig. 4 *b*

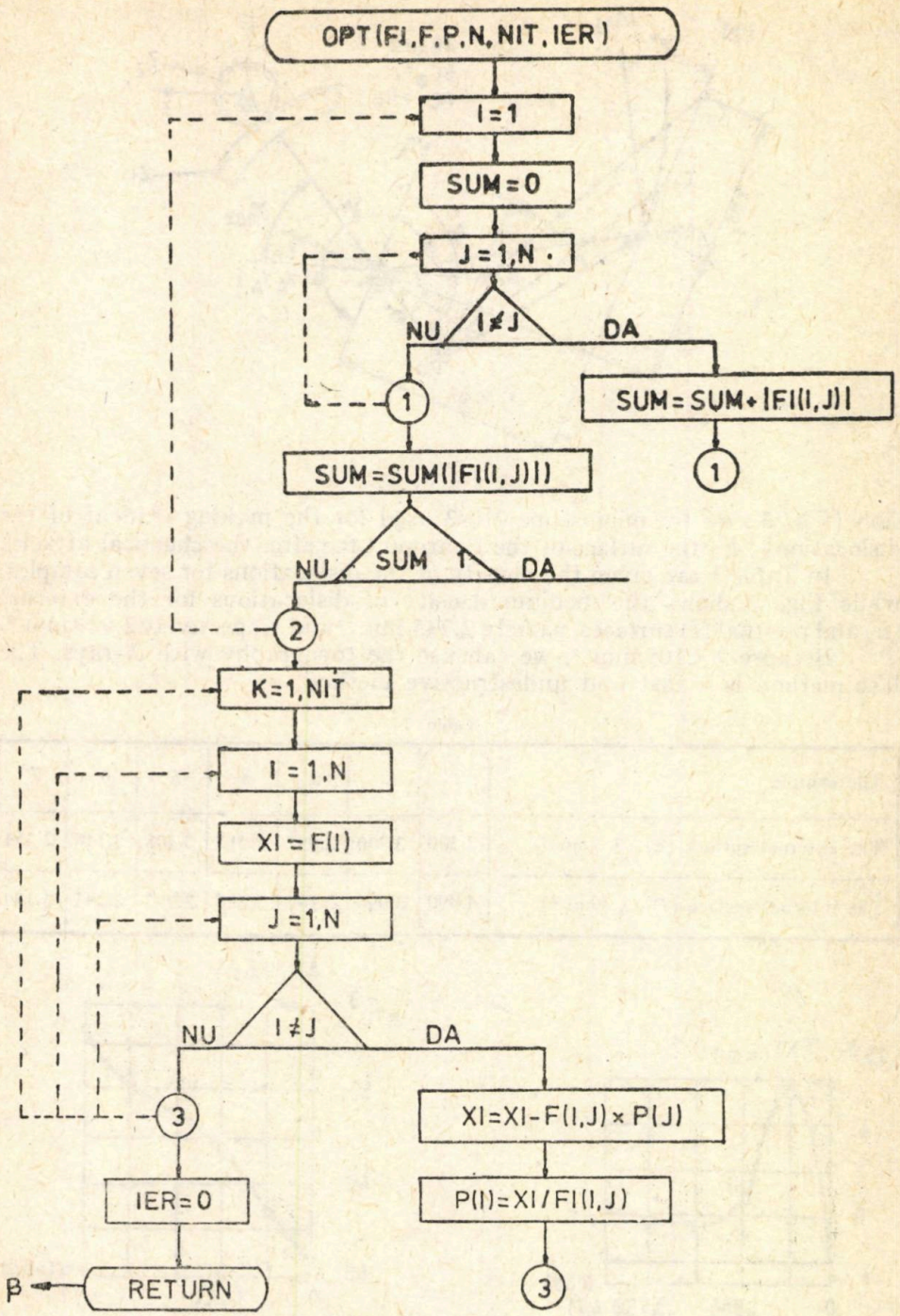
OPT(FI,F,P,N,NIT,IER)
I=1
SUM=0
J=1,N
NU
I≠J
DA
SUM=SUM+|FI(I,J)|
1
SUM=SUM(|FI(I,J)|)
NU
SUM
1
DA
2
K=1,NIT
I=1,N
XI=F(I)
J=1,N
NU
I≠J
DA
3
XI=XI-F(I,J)×P(J)
IER=0
P(I)=XI/FI(I,J)
β
RETURN
3

Fig. 4 *c*

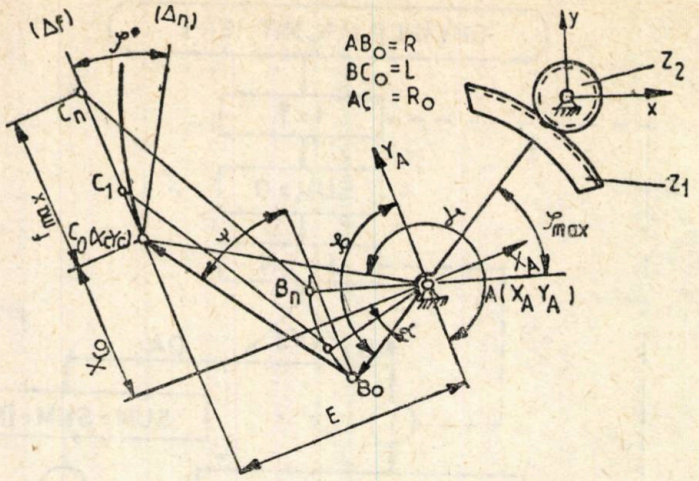

Fig. 5

sion (Fig. 3 : *a*—the microscope MC-2 used for the making evident of the dislocations ; *b*—the surface of the Bourdon tube after the chemical attack).

In Table 1 are given the density of the dislocations for seven samples, while Fig. 7 shows the medium density of dislocations for the external (E) and internal (I) surfaces, namely 2.745 mm^{-2} and respectively 2.929 mm^{-2}.

Because $\lambda < 10^4$ mm^{-2}, we can use the topography with X-rays. The last method is a fast and undestructive method.

Table 1

The sample	*1*	*2*	*3*	*4*	*5*	*6*	*7*
The external surface (E)—λ (mm^{-2})	2.300	3.700	2.097	2.513	3.108	3.146	2.354
The internal surface (I)—λ (mm^{-2})	4.400	3.090	2.407	2.226	2.993	2.241	3.139

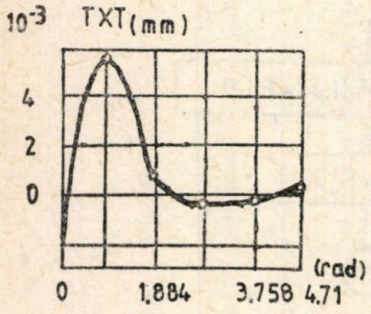

a

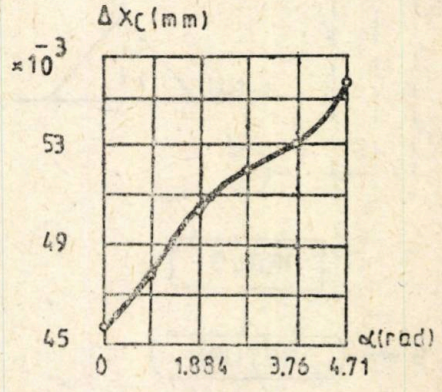

b

Fig. 6

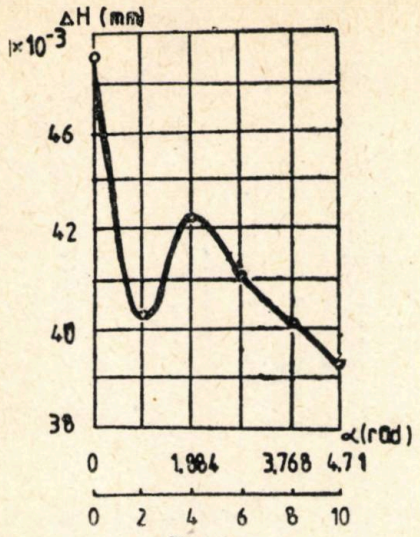

Fig. 6 *c*

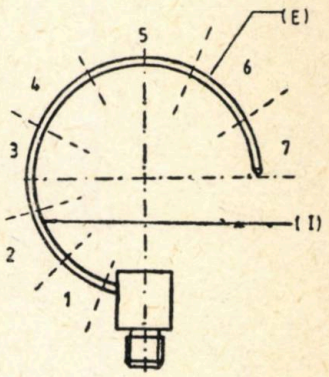

Fig. 7

3.1 **Conclusions.** 1. The calculation of the error Δx_H is a momentous action in the selection of the Bourdon tubes. This conditions the construction of the manometers in the prescribed precision class.

2. The methods of testing of the internal tensions are important in the optimizing of the tensional state from the crystal lattice. Thus, Bourdon tube shall have a good stability and a small hysteresis.

Received April 8, 1985

Polytechnic Institute, Jassy,
Department of Mechanisms and
Machine Design

REFERENCES

1. Bally D., Beneș L., Mihăilă R., *Difracția razelor X și a neutronilor*. Ed. tehn., Buc., 1972.
2. Dancea I., *Metode de optimizare*. Ed. „Dacia", 1976.
3. Merticaru V., Receanu D. și colab., *Elementul elastic și influența sa asupra funcționării manometrelor industriale*. Simpozionul „Fiabilitatea în construcția de mașini", Iași, 1983.
4. Mitnyan M. L., *Sensitivity of Compensating Tubular Spring Instruments*. Periodica Polytechnica, **6**, 3 (1962).
5. Popovici M. M., *Contribuții la perfecționarea mecanismelor din manometrele cu element elastic*. Teză de doctorat, București, 1981.
6. Receanu D. și colab., *Frecarea internă la elementele elastice din manometrele industriale*. Simpozionul „Tribotehnica", Iași, 1984.

CRITERII DE SELECȚIONARE A TUBURILOR MANOMETRICE DIN COMPONENȚA MANOMETRELOR INDUSTRIALE

(Rezumat)

Se prezintă un model de calcul și în același timp de selecționare a tuburilor manometrice din punct de vedere al comportării lor elastice. De asemenea sînt indicate metodele de măsurare a stabilității indicațiilor, stabilitate care depinde, în cea mai mare măsură, de tratamentul termic aplicat tuburilor manometrice după îndoire și lipire pe cep.

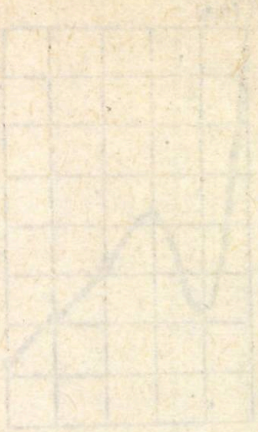

BULETINUL INSTITUTULUI POLITEHNIC DIN IAȘI
Tomul XXXI (XXXV), Fasc. 1—4, 1985
Secția IV
CONSTRUCȚII DE MAȘINI

D.C. 621.822.8

THE OPTIMUM DESIGN OF THE CONTACT GEOMETRY FOR CYLINDRICAL ROLLER BEARINGS

BY

SPIRIDON CREȚU and CEZAR RACOCEA

1. Introduction. The fatigue life of cylindrical roller bearing is heavily influenced by the crowning of the rollers [1]. Because the contact pressure distribution, as well as, the stress concentrations are nonlinearly dependent on the load level, the optimal crowning profile varies with the magnitude of the applied load.

Also, the global stiffness of the roller bearing is affected by the crowning profile. The design of cylindrical rolling elements in roller bearings is critical [2] ... [4].

When the crowned roller are studied the Hertz's solution is not longer accurate and does not give the possibility to study the critical zones at the end of the roller where important stress concentrations exist. G. Lundberg [6] solved the integral equation in the non-Hertzian case occurring in roller bearings under the assumptions that the contact pressure distribution will be constant along the roller and acting on a rectangular contact area and the stiffness will be that of a halfspace. The resulting profile is known today as Lundberg's crowned profile but it can not be competitive obtained even with modern technologies.

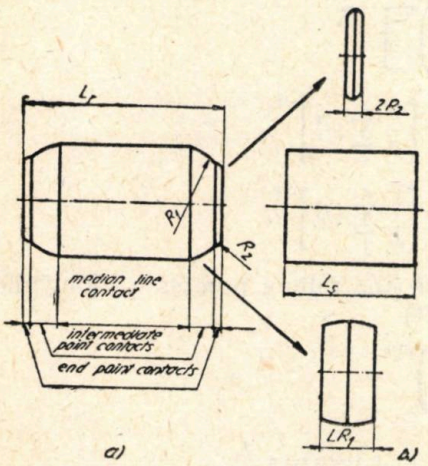

Fig. 1

An alternative solution for reducing of the stress concentrations at the end of the contact area can be the modification of the geometry of ideal line contact by introducing at the end of the roller of two zones with point contact. In the practical case of cylindrical roller bearings the proposed modification of the roller profile consists in the adjusting of the median cylinder with two zones with different radii of curvature (Fig.1).

2. The Sectionning Method. In order to study the elastic contact

between a crowned roller and a bearing ring with straight raceway, the modified line contact has been divided into a sum of three contacts, as is shown in Fig. 2*b*.

1. A median zone *I*, with line contact.

2. An intermediate zone *II* with point contact, having the value R_1 for the radius of curvature and being geometricaly adjusted with the adiacent zones.

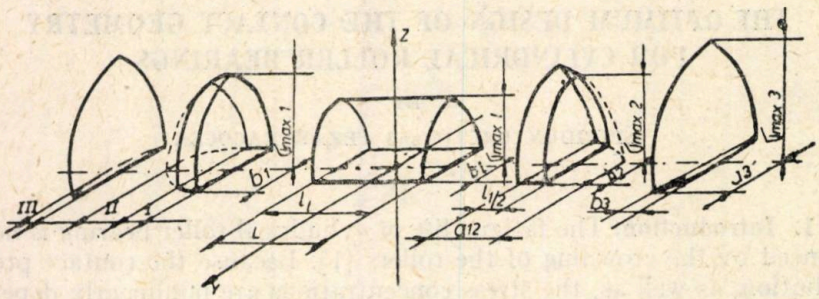

Fig. 2

3. An end zone *III* also with point contact, having the value R_2 for the radius of curvature.

Each of these zones have been considered as elementary rolling bearings, and dependence equations between loads and deformations have been determined by considering equilibrium equations, compatibility equations and Hooke's law. These dependence equations have been considered then in the general theory worked out by L u n d b e r g and P a l m g r e n [5] regarding the rolling contact fatigue. Finally the computing equations for the dynamic capacity of each of three situations have been obtained.

1. *For the zone I with line contact*

$$C_l = C_{l_\mu}\left[1+\left(\frac{C_{l_\mu}}{C_{l_\nu}}\right)^{9/2}\right]^{-2/9}, \tag{1}$$

$$C_{l_\mu} = ZQ_{l_\mu}\frac{J_r}{J_1}, \quad Q_{l_\mu} = \left[\frac{1}{Z}\sum_1^z Q_j^4\right]^{1/4}, \tag{2}$$

$$C_{l_\nu} = ZQ_{l_\nu}\frac{J_r}{J_2}, \quad Q_{l_\nu} = \left[\frac{1}{Z}\sum_1^z Q_j^4\right]^{1/4}. \tag{3}$$

2. *For the zone II with point contact* (the rolling process is along the minor axes of the corresponding contact)

$$C_p = C_{p_\mu}\left[1+\left(\frac{C_{p_\mu}}{C_{p_\nu}}\right)^{10/3}\right]^{-0.3}, \tag{4}$$

$$C_{p_\mu} = 10.8\left(\frac{2R_1}{D}\right)^{0.41}\frac{(1-\gamma)^{1.39}}{(1+\gamma)^{1/3}}\gamma^{0.3}Z^{2/3}D^{1.8}\frac{J_r}{J_1}, \tag{5}$$

(6) $$C_{p_\nu}=10.8\left(\frac{2R_1}{D}\right)^{0.41}\frac{(1+\gamma)^{1.39}}{(1-\gamma)^{1/3}}\gamma^{0.3}Z^{2/3}D^{1.8}\frac{J_r}{J_2}.$$

3. *For the zone III also with point contact* (the rolling process is along the major axes of the corresponding contact ellipse)

(7) $$C_p=C_{p_\mu}\left[1+\left(\frac{C_{p_\mu}}{C_{p_\nu}}\right)^{10/3}\right]^{-3/10},$$

(8) $$C_{p_\mu}=5.92256\left(\frac{2R_2}{D}\right)^{0.65}\frac{(1-\gamma)^{1.15}}{(1+\gamma)^{1/3}}\gamma^{0.3}D^{1.8}\frac{J_r}{J_1}Z^{2/3},$$

(9) $$C_{p_\nu}=5.92256\left(\frac{2R_2}{D}\right)^{0.65}\frac{(1+\gamma)^{1.15}}{(1-\gamma)^{1/3}}\gamma^{0.3}Z^{2/3}D^{1.8}\frac{J_r}{J_2}.$$

In the prior equations the μ index is reffering to the rotating ring (in the studied case, the inner ring) and the ν index to the stationary ring. The quantities J_r, J_1, J_2 and γ are defined by the following equations :

(10) $$J_r=\frac{1}{Q_{\max}}\frac{1}{Z}\sum_1^z Q_j\cos\varphi_j,$$

(11) $$J_1=\frac{1}{Q_{\max}}\left[\frac{1}{Z}\sum_1^z Q_j^3\right]^{1/3},$$

$$\gamma=\frac{D}{D_m}.$$

(12) $$J_2=\frac{1}{Q_{\max}}\left[\frac{1}{Z}\sum_1^z Q^{10/3}\right]^{0.3},$$

The equivalent basic dynamic capacity of the entire roller bearing is calculated by

(13) $$C=g_RC_1.$$

The coefficient g_R is given by

(14) $$g_R=F_R\left\{F_1^{W_l}+C_1^{W_l}\left[\left(\frac{F_{12}}{C_1}\right)^{W_p}-\left(\frac{F_2}{C_2}\right)^{W_p}+\left(\frac{F_3}{C_3}\right)^{W_p}\right]\right\}^{-\frac{1}{W_R}},$$

where : F_R is the total load which acts upon roller bearing ; F_{12} is the load which could be taken by intermediate zones in the case that a complete ellipse is formed (Fig. 2) ; F_2 is the force taken by the zones that are removed from the intermediate zones (Fig. 2) ; F_3 is the load taken by the end zones of the roller.

It is obvious that the zone *III* from the end of each roller comes in contact with the raceway and participates in overtaking process of the load only after the deformation δ is greater than a critical value δ_{cr}. The critical value is determined by pure geometrical considerations. The values of the exponents W_l, W_p, W_r have been established following T. Harris [3], [4]

$$W_l=\frac{9}{2},\qquad W_p=\frac{10}{3},\qquad W_R=\frac{9}{2}.$$

3. Some Considerations Regarding the Classic Design Process. When a bearing has to be designed the designer establishes some parameters with straight influence on basic dynamic capacity which are called basic parameters. The other parameters which does not influence directly the value of basic dynamic capacity are called auxiliary parameters. The basic parameters would be considered optimum when they will determine the maximum value for the basic dynamic capacity. In classical design methods, the basic parameters are appreciated by some empirical formulae, which were verified only for few dimensions. The basic parameters are not precise determined, the designer has to choose a value from a certain domain. In order to determine the correct values of the basic parameters an optimization process has been carried out considering the slicing method presented above.

4. Optimum Design Algorithm. A numerical algorithm has been worked out by which the optimum values of the following basic parameters are obtained :

i) the roller diameter, D_R ;
ii) the length of the zones I with straight generatrix, L_S ;
iii) the radius of curvature in the intermediate zone II, R_1 ;
iv) the radius of curvature in the end zones III, R_2.

The initial data of the algoritm are the main dimensions of the cylindrical roller bearing (the outer diameter D_E, the inner diameter d, the total length of roller L_t), the permissible stress, the minimum load F_{min} and the maximum load which can appear in the normal life of the bearing. It has to be pointed out that is wanted a specific optimum design, for a certain domain of the load level.

A FORTRAN IV programme for FELIX C-256 computer has been worked out, so that all the computation were automatically carried out.

The numerical computation has been carried out for the case of WJ 120 cylindrical roller bearing which has the following main dimensions : D_E=210 mm, d=120 mm, B=80 mm, L_T=48 mm. The basic dynamic capacity as is indicated in the bearing catalogues is C=500 kN. Using the algorithm just presented to obtain optimum values for basic parameters we get a greater value for the basic dynamic capacity, C_{opt}=620 kN. For the same condition of loading the roller bearing with optimum values for basic parameters will determine a 100% increase of the fatigue life in comparision with the clasic design.

5. Conclusion. An original method for optimum design of cylindrical roller bearing is presented. In this method the optimum values of the basic parameters of roller bearing are determined in order to minimize the stress concentration at the end of the contact ellipse. The maximum values for basic dynamic capacity are obtained.

Received December 16, 1985

Polytechnic Institute, Jassy,
Department of Machine Design

REFERENCES

1. Gafiţanu M., Năstase D., Creţu Sp., *Rulmenţi*. Ed. tehn., Buc., 1985.
2. Brandlein I., Wälzlagertechnik, *1*, 2—9 (1971).

3. Harris T. A., Trans. ASME, J. Lub. Tech., (*F*), 94, *2*, 181–187 (1972).
4. Harris T. A., ASLE Trans., **10**, *3*, 47–58 (1967).
5. Lundberg G., Palmgren A., Acta Polyt. 96, Mech. Engrs. Series, **2**, *4*, 1–32 (1952).
6. Lundberg G., Forschung auf dem Gebiete des Ingenieurwesens, **10**, *5*, 200–211 (1939).

PROIECTAREA OPTIMĂ A GEOMETRIEI DE CONTACT PENTRU RULMENŢII CU ROLE CILINDRICE

(Rezumat)

Se prezintă o metodă originală pentru proiectarea rulmenţilor radiali cu role cilindrice bazată pe ideea secţionării contactului liniar modificat.

Capacitatea dinamică de bază a rulmentului este calculată considerînd capacităţile dinamice de bază ale rulmenţilor intermediari derivaţi din secţionarea fiecărei role în trei zone. Pentru automatizarea calculelor este prezentat algoritmul unui program FORTRAN, care a fost aplicat pentru reproiectarea rulmentului WJ 120. Noua geometrie internă asigură creşterea capacităţii dinamice de bază de la 500 kN la 620kN, ceea ce conduce la o creştere cu 100 % a durabilităţii.

BULETINUL INSTITUTULUI POLITEHNIC DIN IAȘI
Tomul XXXI (XXXV), Fasc. 1—4, 1985
Secția IV
CONSTRUCȚII DE MAȘINI

D.C. 621.438

MATHEMATICAL MODEL FOR THE STARTING CONDITION OF THE GAS TURBO-ENGINES

BY

DAN URSESCU, VIRGIL GIURCĂ, I. RACOVIȚĂ and I. ȚÂRDEA

1. The starting condition determination, by calculation, is useful both to prototype and existing turbo-engines, which are going to drive another type of machine, to be started up by another kind of starting device or, even to use another type of fuel.

For such purposes, a mathematical model for the turbo-engine starting condition could be useful, delivering information as to :

i) the start-up period of time, up to the idling speed setting (of special importance for electric starting up devices) ;

ii) the firing speed values n_a and the idling speed values n_r ;

iii) the temperature condition before the turbine *starting up* ;

v) the fuel injection law in the firing chamber (or chambers) ;

vi) whether air exhausting through the antipumping valves is necessary during the starting up period, and which is the flow of air output ;

vii) whether the power of the starting device has been properly selected.

2. For a monoaxial turboengine, without recuperator (blast-heating apparatus) directly connected to the driven machine, a mathematical model, meeting the above-mentioned requirements, can be obtained from the following equation :

$$\Sigma P = I\omega \frac{d\omega}{d\tau}, \tag{1}$$

which represents the condition of power equilibrium for an accelerating turboengine. In (1) we have : I — the inertia moment of the rotor assembly, kg m² ; ω — the angular speed of the rotor assembly, rad s^{-1} ; ΣP — the required power for the rotor assembly acceleration, asummed to be constant, within the time element $d\tau$, W ; $d\tau$ — the time element required for the speed variation $d\omega$, s.

For the monoaxial turboengine, directly coupled with the driven machine, ΣP can be written as

$$\Sigma P = P_T + P_m - P_C - P_R, \tag{2}$$

where : P_P — the turbine output power at speed ω ; P_m — the output power of the starting engine at speed ω ; P_C — the power absorbed by the

compressor equiping the turboengine at speed ω ; P_R — the power absorbed by the driven machine at speed ω.

For computing reasons Eq. (1) can be written using finite differences

$$\Sigma P_m = I\omega_m \frac{\Delta\omega}{\Delta\tau}, \tag{3}$$

where : ΣP_m — the sum of the mean powers within the time element $\Delta\tau$; ω_m — the average angular speed within the time element $\Delta\tau$; I — the inertia moment of the rotor assembly.

The Eq. (3) can also be written as a function of the number of revolutions [r.p.m.].

If we put : n_j — the speed at the end of the time element $\Delta\tau_j$, r.p.m. ; n_{j-1} — the speed at the beginning of the time element $\Delta\tau_j$, r.p.m, then

$$\omega_m = \pi(n_j + n_{j-1})\frac{1}{60},$$

$$\Delta\omega = \pi(n_j - n_{j-1})\frac{1}{30}$$

and Eq. (3) becomes

$$\Delta\tau_j = 5\,478 \cdot 10^{-6} I \frac{n_j^2 - n_{j-1}^2}{\Sigma P_m}, \tag{4}$$

where ΣP_m is given in kW.

In Eq. 4,

$$\Sigma P_m = P_{Tm} + P_{mm} - P_{Cm} - P_{Rm},$$

P_{Tm}, P_{mm}, P_{Cm}, P_{Rm} are respectively, the turbine average output power, the starting device average output power, the average power absorbed by the turboengine compressor, and the average power absorbed by the driven machine, within the time element $\Delta\tau_j$.

These powers can be calculated using the following equations :

$$\begin{aligned} P_{Tm} &= 0.5(P_{T_j} + P_{T_{j-1}}), \\ P_{mm} &= 0.5(P_{m_j} + P_{m_{j-1}}), \\ P_{Cm} &= 0.5(P_{C_j} + P_{C_{j-1}}), \\ P_{Rm} &= 0.5(P_{R_j} + P_{T_{j-1}}), \end{aligned} \tag{5}$$

where P_{T_j}, $P_{T_{j-1}}$, P_{m_j}, $P_{m_{j-1}}$, P_{C_j}, $P_{C_{j-1}}$, P_{R_j}, $P_{R_{j-1}}$ represent, respectively, the turbine and the starting device output powers, the power absorbed by the compressor and the power absorbed by the driven machine at the speed n_j, respectively n_{j-1}.

The Eq. (4) can determine the dynamics of the turboengine starting operation as a function of τ, namely

$$n_j = \Phi(\tau) = \Phi(\Sigma\Delta\tau_j), \tag{6}$$

if the powers P_T, P_m, P_C, P_R can be calculated as a function of speed.

For the powers P_m and P_R, the question is relatively simple, because the designers provide for all kinds of starting devices and mostly for the driven machine, speed characteristics which can be written as

$$\begin{aligned} P_{mj} &= A_0 + A_1 n_j + A_2 n_j^2 + \ldots + A_i n_j^i + \ldots , \\ P_{Rj} &= B_0 + B_1 n_j + B_2 n_j^2 + \ldots + B_i n_j^i + \ldots . \end{aligned} \tag{7}$$

In case the driven machine is a compressor, the problem is more difficult, because frequently the designer does not provide experimental data at low speeds such as the starting speeds.

In this case, aproximative equations can be used

$$P_{Rj} = P_{R0} \left(\frac{n_j}{n_0} \right)^{\varkappa} , \tag{7'}$$

where P_{R0} is a known power at a speed n_0 as close to the speed n_j as possible.

For $\varkappa$, the literature recomands values between $\varkappa = 3$ and $\varkappa = 3.5$.

The determination of the speed characteristics $P_{Tj} = f_1(n_j)$ and $P_{Cj} = f_2(n_j)$ is also difficult, because the turbine output power depends on the air parameters at the compressor outlet and on the gas temperature at its inlet ; this temperature can be controlled by means of the burnt fuel quantity in the firing chamber.

Due to the above-mentioned relationships, the turbine power depends on the following parameters :

$$G_a,\ p_c,\ T_C,\ T_T,\ k,\ c_p,\ R,\ n_j ,$$

that is, on the flow in the compressor, the pressure at the compressor outlet, the temperature at the compressor outlet, the temperature at the turbine inlet, the physical characteristics of the gas expanding in the turbine (k, c_p, R) and of course on n_j.

3. The values G_a, p_C, T_C can be most accurately obtained by means of a computing program, subsequently referred to as CØMP.

This program is relatively easy to elaborate for centrifugal compressors, and far more difficult for axial compressors even if the precise dimensions and the profiles aero-dinamic characteristics are available.

If no such program is available the following aproximative relations can be used, in good concordance with the practical results [1] ... [3] :

$$\begin{aligned} & p_{Cj} = p_A \varepsilon_j , \\ & \varepsilon_j = 1 + (\varepsilon_0 - 1) \left(\frac{n_j}{n_0} \right)^{2.5} , \\ & T_{Cj} = T_A \left[1 + \frac{\varepsilon_j^{0.29} - 1}{\eta_C} \right] , \\ & G_{aj} = G_{a0} \left(\frac{n_j}{n_0} \right)^{\varkappa_1} \qquad \varkappa_1 = 1 \ldots 1.25 , \\ & P_{Cj} = P_{C0} \left(\frac{n_j}{n_0} \right)^{\varkappa} \qquad \varkappa = 3 \ldots 3.25 , \end{aligned} \tag{8}$$

where ε_0, G_{a0} and p_{C0} represent the compression ratio, the flow in the compressor and the power at a known rate and at a speed as close as possible to the speed n_j.

The temperature and the pressure at the turbine inlet, as well as the physical constants of the working agent, also require a computing program for the process of combustion.

At the Polytechnic Institute of Jassy such a program was developped with variable specific heat capacities ; it will be subsequently referred to as CØMB. This program provides the values of p_T, K, c_p, R and of the air excess α.

The gas temperature at the turbine inlet should be related to the speed and should not exceed the turbine maximum allowable value. The most convenient is a lineary variation law, depending on the speed, written as

$$T_{Tj}=T_{Tm}-m(n_j-n_a), \tag{9}$$

where T_{Tj} and T_{Tm} are, respectively, the temperature at speed n_j and the temperature at the maximum allowable speed on starting ; n_j and n_a represent the current speed and the firing speed, and m is a factor which must be selected depending on the starting period of time and on the value of the idling speed.

The working parameters of the turbine can also be determined by means of a program, whose complexity depends on the required accuracy and on the operating time.

At the Polytechnic Institute of Jassy such a program has been developped, using as initial data p_T, T_T, c_p, k, R, n_j and providing $P_{Tj}=f_1(n_j)$ and G_{Tj} — that is the flow on the turbine at speed n_g [4]. This program will be subsequently referred to as TURBØ 15.

If G_{Cj}, G_{Tj} and α are known, we can obtain the fuel flow at speed n_j and consequently, the fuel delivery law in the firing chambers, as well at the air quantity to be exhausted by the anti-pumping valves, from the equations

$$G_{Cbj}=\frac{G_{Tj}}{1+\alpha L_0}, \tag{10}$$

$$\Delta G=G_{Cj}-\frac{G_{Tj}}{1+\frac{1}{\alpha}L_0}, \tag{11}$$

where L_0 is the theoretically quantity of air required for the burning of 1 kg fuel.

4. The program CØMP, or the relation (8), together with the programs CØMB and TURBØ15, and the relations (9) and (10) permit the developping of an algoritm for the determination of $n_j=\Phi(\tau)=\Phi(\Sigma\Delta\tau_j)$ representing the starting operation dynamics with this end in view. The starting process should be divided into 3 stages that is :

1. *The cold acceleration of the engine, by means of the starting device,* up to the firing speed n_a. The condition characteristic of the end of this stage is

$$P_{mj}+P_{Tj}=P_{Cj}+P_{Rj}+\Delta P, \tag{12}$$

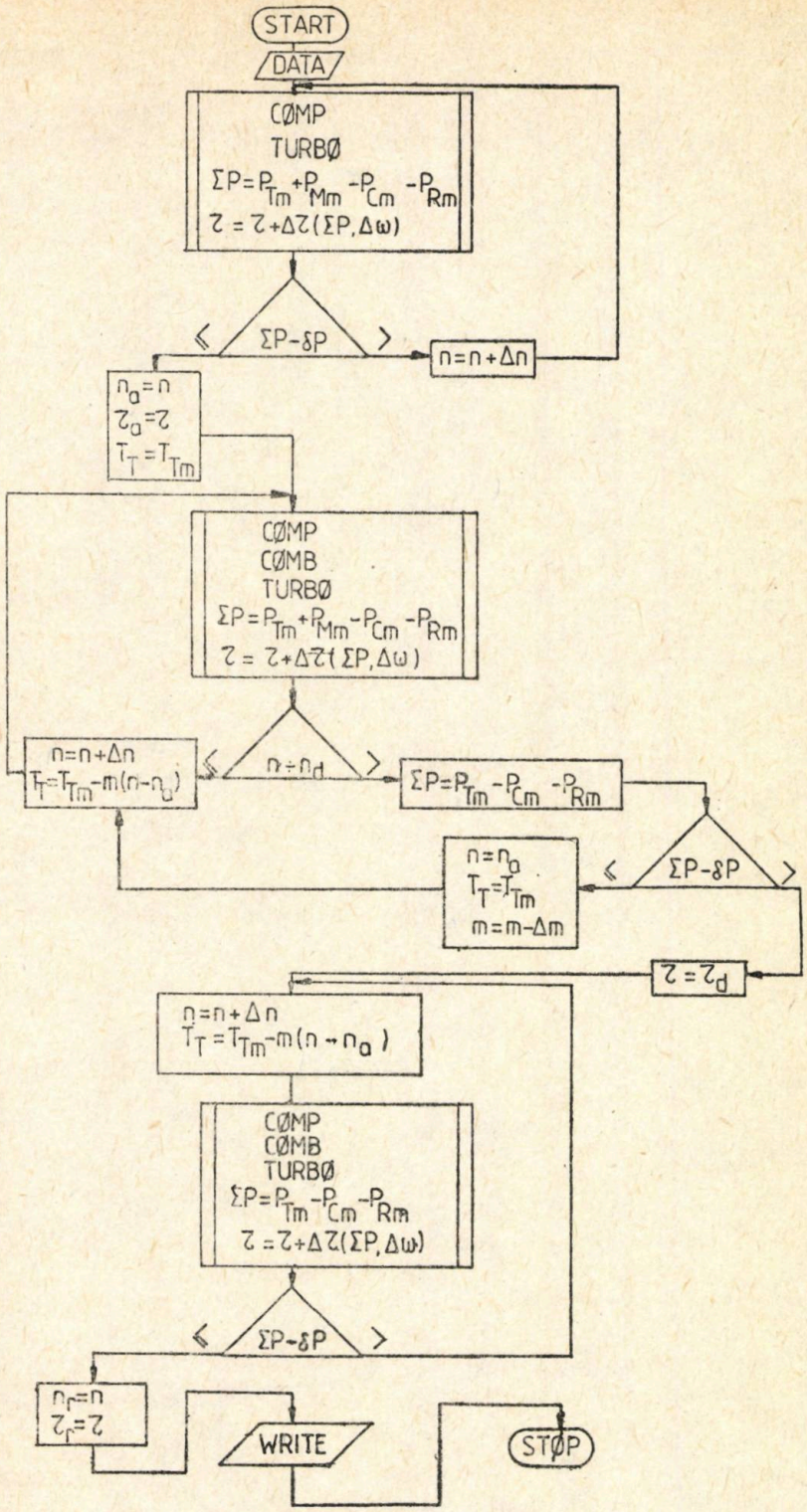
START
DATA
CØMP
TURBØ
ΣP=P_Tm+P_Mm-P_Cm-P_Rm
Z=Z+ΔZ(ΣP,Δω)
ΣP-δP
n=n+Δn
n_a=n
Z_a=Z
T_T=T_Tm
CØMP
CØMB
TURBØ
ΣP=P_Tm+P_Mm-P_Cm-P_Rm
Z=Z+ΔZ(ΣP,Δω)
n=n+Δn
T_T=T_Tm-m(n-n_a)
n÷n_d
ΣP=P_Tm-P_Cm-P_Rm
n=n_a
T_T=T_Tm
m=m-Δm
ΣP-δP
Z=Z_d
n=n+Δn
T_T=T_Tm-m(n-n_a)
CØMP
CØMB
TURBØ
ΣP=P_Tm-P_Cm-P_Rm
Z=Z+ΔZ(ΣP,Δω)
ΣP-δP
n_r=n
Z_r=Z
WRITE
STØP

Fig. 1

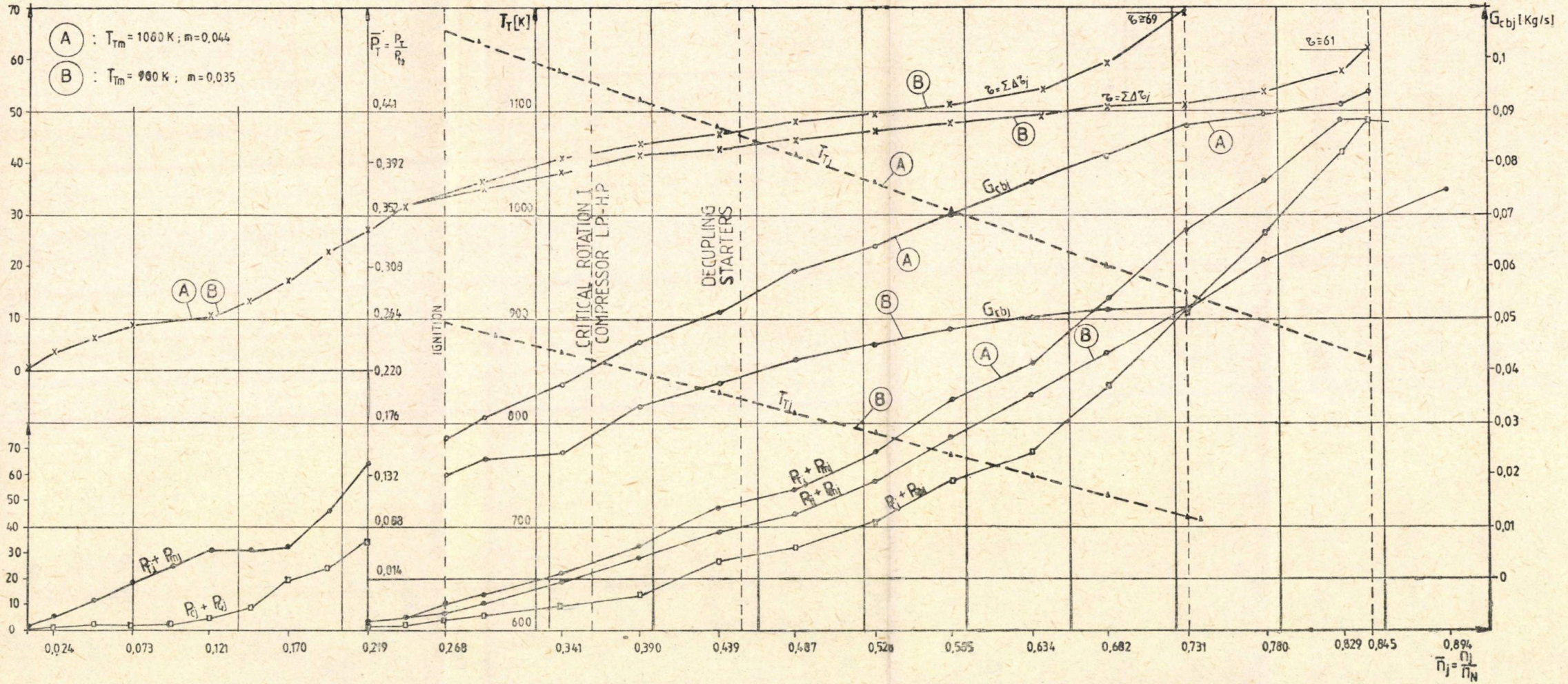
A : T_{Tm} = 1080 K ; m = 0,044
B : T_{Tm} = 980 K ; m = 0,035
$\overline{P}_T = \frac{P_T}{P_{T2}}$
T_T[K]
G_{cbj} [Kg/s]
$\overline{n}_j = \frac{n_j}{n_N}$
IGNITION
CRITICAL ROTATION I COMPRESSOR L.P.-H.P
DECUPLING STARTERS
$\tau_c = \Sigma \Delta \tau_{cj}$
$\tau_c \cong 69$
$\tau_c \cong 61$
T_{Tj}
G_{cbj}
$P_{Tj} + P_{mj}$
$P_{cj} + P_{cj}$

Fig. 2

where ΔP is a reserve source of power, necessary for maintaining a continuous acceleration of the engine.

All this time for the program TURBØ15 we must impos the following conditions :

2. *The heat acceleration of the engine, by means of the turbine and the starting device.* The condition characteristic of the end of this stage is

$$n_j = n_{md}, \tag{13}$$

where n_{md} is the starting device maximum working speed.

From now on, the condition of power equilibrium becomes

$$P_{Tm} - P_{Cm} - P_{Rm} = 5.478 \cdot 10^{-6} I \frac{n_j^2 - n_{j-1}^2}{\Delta\tau_j}. \tag{14}$$

3. *The acceleration of the engine only by means of the turbine,* stage which ends at the idling speed

$$n_j = n_r, \tag{15}$$

for which the following condition is obtained :

$$P_{Tj} - P_{Cj} - P_{Rj} = \Delta P, \tag{16}$$

where the difference ΔP can be no matter how small, because it is necessary only to permit the computer operation.

In the respective algoritm, the programs CØMP, CØMB and TURBØ enter as subroutines.

The precision of the procedure is greater especially as it operates with values $\Delta\tau_j$, and differences $n_j - n_{j-1}$, smaller. This implies a calculation for several working points.

In this case, the reducing of the operations time for the subroutines belonging to the algorithm get a special importance.

Mention must be made of the fact that subroutines CØMB and TURBØ 15 require respectively less than 1 second and 3 minutes for a working point.

Fig. 1 shows the computing algorithm for determining the function $n_j = \Phi(\tau)$ and Fig. 2 represents the dynamics of the starting point for a group consisting of an aircraft turbo prop engine used on land, for driving a pit gas compressor, determined by the above mentioned algorithm. The values represented in the diagram have the same significance as in the text.

The calculations have been made for 2 variation laws of T_{Tj}.

Notation

p_A, T_A — ambient pressure and temperature
c_{pA}, k_a — specific heat capacity at constant pressure and the air adiabatic exponent
c_p, k, R — specific heat capacity, adiabatic exponent and the status constant of gas in the turbine
α — air excess in the firing chamber
ν_c — pressure loss ratio in the firing chamber
g_c, g_h — hydrogen and carbon content of fuel
n_j — speed during τ_j, r.p.m.
n_a — firing speed, r.p.m.
n_{md} — maximum speed of the starting device, r.p.m.
n_r — idling speed, r.p.m.

Received May 10, 1985

Polytechnic Institute, Jassy,
Department of Thermotechnics and Thermic Engines

REFERENCES

1. Kulaghin I I., *Teoria motoarelor cu reacţie cu turbine cu gaz* (trad. din l. rusă). Ed. tehn., Buc., 1954.
2. Стечкин Б. С., Казанджан П. К., Алексеев Л. П., Городов А. Н., Нечаев Ю. Н., Федоров Р. М., *Теория реактивных двигателеи.* Оборонгиз, 1956
3. Гительман А. Й., *Динамика и управление судовых газотурбиных установок.* Цзд. „Судостроение", Ленинград, 1974.

MODEL MATEMATIC PENTRU REGIMURILE DE START ALE TURBOMOTOARELOR CU GAZE

(Rezumat)

Se prezintă un model matematic pentru calculul regimurilor de pornire a turbomotoarelor cu gaze monoax. Algoritmul permite determinarea timpului de pornire, stabilirea turaţiei şi parametrilor la regimul de ralanti şi legea de injecţie a combustibilului în perioada de pornire, aşa fel încît temperaturile la intrarea în turbină să se încadreze în limitele admise.

BULETINUL INSTITUTULUI POLITEHNIC DIN IAŞI
Tomul XXXI (XXXV), Fasc. 1—4, 1985
Secţia IV
CONSTRUCŢII DE MAŞINI

D.C. 621.643 ; 66.045

OPTIMAL GEOMETRY OF FINNED HEAT PIPES TO ACHIEVE A MAXIMUM HEAT FLOW PER UNIT WEIGHT

BY

BOGDAN HORBANIUC and EMIL LUCA

1. Introduction. The paper presents a method of geometrical optimization of heat pipes with circular fins of constant cross section for obtaining a maximum heat flow per unit weight. The principle of this method may be used in the optimization of heat pipes of other fin types. First the evaporator and the condenser are subject to separate optimization, leading to optimal values of fin height, thickness and pitch for each, then they are „linked together" and an optimal ratio of their lengths is obtained. In this paper we used the results of heat flow/weight optimization of a finnless heat pipe [1] in the selection of the ratio of evaporator to condenser lengths.

2. Conditions for the Optimization of Q/m.

i) Tube and fins are made of the same material.

ii) The heat transfer is steady.

iii) Heat losses are negligible. The heat flow to the evaporator is equal to that from the condenser.

iv) The temperature drop across the pipe wall is negligible

$$t_{w,i} \simeq t_{w,0} = t_w.$$

v) The saturation temperature t_S, does not vary within the vapour space from evaporator to condenser.

vi) Optimization refers to the ratio of the heat transfer rate to the sum m of the evaporator and condenser masses. The mass of the adiabatic zone is not of significance for this optimization.

vii) Only the parameters with superscript — have to be choosen before optimization :

$$\bar{\lambda},\ \bar{d}_0,\ \bar{r},\ \bar{h}_{i,e(c)}\ (\bar{d}_0, \bar{r}),$$

$$\bar{h}_{0,e(c)} = \bar{h}_{0,e(c)}(\bar{d}_0,\ \bar{e}_{e(c)},\ p,\ R).$$

The outside heat transfer coefficients are given functions of d_0, e, p, R only. As L_e, L_c vary, $h_{i,e}$, $h_{i,c}$, $h_{0,e}$, $h_{0,c}$ remain constant.

3. Shape of the Function Q/m **Convenient for Optimization.** The equations of heat transfer at evaporator and condenser are

$$(1) \qquad Q = h_{i,e} A_{i,e} \theta_{w,e} = h_{0,e} (A_{w,e} + \eta_e A_{f,e}) (\theta_1 - \theta_{w,e}),$$

$$Q=h_{i,c}\,A_{i,c}\,(\theta_2-\theta_{w,c})=h_{0,c}\,(A_{w,c}+\eta_c A_{f,c})\,\theta_{w,c}. \tag{2}$$

Let us define the mass per unit inner surface area as

$$k_{im}=\frac{m_i}{A_i}=0.5\,\rho\,\frac{V_i}{A_i}. \tag{3}$$

We have considered one half of the evaporator tube wall volume corresponding to the inner surface, the other to the outer bare tube heat exchange surface.

The mass per unit outer reduced surface area is

$$k_{0m}=\frac{m_0}{A_w+\eta_i A_f}=\frac{\rho(0.5\,V_i+V_f)}{A_w+\eta_i A_f}. \tag{4}$$

With the notations

$$a_e=\frac{h_{i,e}}{k_{im,e}},\quad b_e=\frac{h_{0,e}}{k_{0m,e}},\quad c_e=\frac{a_e}{b_e}\in(0,\,+\infty),\quad x_e=\frac{\theta_{w,e}}{\theta_1}\in(0,\,1)$$

one obtains from the Eqs. (1), (3) and (4)

$$\frac{m_e}{Q}=\frac{m_{i,e}}{Q}+\frac{m_{0,e}}{Q}=\frac{k_{im,e}A_{i,e}}{Q}+\frac{k_{0m,e}(A_{w,e}+\eta_e A_{f,e})}{Q}=$$

$$=\frac{k_{im,e}}{h_{i,e}\theta_{w,e}}+\frac{k_{0m,e}}{h_{0,e}(\theta_1-\theta_{w,e})}=\frac{1}{a_e\theta_1 x_e}+\frac{1}{b_e\theta_1(1-x_e)}, \tag{5}$$

$$\frac{Q}{m_e}=a_e\theta_1 f_e(x_e,\,c_e), \tag{6}$$

where $f_e=[x_e^{-1}+c_e/(1-x_e)]^{-1}$.

The same procedure leads to the following results for the condenser :

$$\frac{m_c}{Q}=\frac{m_{i,c}}{Q}+\frac{m_{0,c}}{Q}=\frac{k_{im,c}}{h_{i,c}(\theta_2-\theta_{w,c})}+\frac{k_{0m,c}}{h_{0,c}\,\theta_{w,c}}=\frac{1}{a_c\theta_2(1-x_c)}+\frac{1}{b_c\theta_2 x_c}, \tag{7}$$

where $a_c=\dfrac{h_{i,c}}{k_{im,c}}$, $b_c=\dfrac{h_{0,c}}{k_{0m,c}}$, $x_c=\dfrac{\theta_{w,c}}{\theta_2}\in(0,\,1)$;

$$\frac{Q}{m_c}=a_c\theta_2 f_c(x_c,\,c_c), \tag{8}$$

where

$$c_c=\frac{a_c}{b_c}\in(0,\,+\infty)\qquad\text{and}\qquad f_c=\left[\frac{1}{1-x_c}+\frac{c_c}{x_c}\right]^{-1}.$$

4. The Expressions of c and x for Circular Fins of Constant Cross Section.

$$k_{im,e}=\frac{m_{i,e}}{A_{i,e}}=0.5\,\rho\pi\,\frac{d_0^2-d_i^2}{4}\,\frac{L_e}{\pi d_i L_e}=0.125\,\rho d_0\left(r-\frac{1}{r}\right), \tag{9}$$

$$k_{0m,e}=\frac{m_{0,e}}{A_{w,e}+\eta_e A_{f,e}}=\frac{\rho[0.125\,\pi L_e(d_0^2-d_i^2)+N_e e_e\,\pi(d_{i,e}^2-d_0^2)/4]}{\pi d_0(L_e-N_e e_e)+2\eta_e N_e\pi(d_{i,e}^2-d_0^2)/4}=$$

$$=\frac{0.5\,\rho\,d_0[0.5(1-r^{-2})+p_e e_e(R_e^2-1)]}{2(1-p_e e_e)+p_e\eta_e d_0(R_e^2-1)}, \tag{10}$$

$$(11)\qquad c_e=\frac{a_e}{b_e}=\frac{h_{i,e}k_{om,e}}{h_{0,e}k_{im,e}}=4\frac{h_{i,e}}{h_{0,e}}\;\frac{r}{r^2-1}\;\frac{0.5(1-r^{-2})+e_e p_e(R_e^2-1)}{2(1-e_e p_e)+\eta_e p_e d_0(R_2^e-1)}.$$

The expression of x_e results from Eq. (1) as follows :

$$(1')\qquad h_{i,e}A_{i,e}\theta_1 x_e=h_{0,e}\,(A_{w,e}+\eta_e A_{f,e})\;\theta_1(1-x_e),$$

$$(12)\qquad \frac{1-x_e}{x_e}=\frac{h_{i,e}A_{i,e}}{h_{0,e}(A_{w,e}+\eta_e A_{f,e})},$$

$$(12')\qquad \frac{1}{x_e}=1+\frac{h_{i,e}}{h_{0,e}}\;\frac{\pi d_i L_e}{\pi d_0(L_e-N_e e_e)+2\eta_e N_e\pi(d_{i,e}^2-d_0^2)/4},$$

$$(13)\qquad x_e=\left\{1+\frac{1}{r}\,\frac{h_{i,e}}{h_{0,e}}\;\frac{1}{1-e_e p_e+0.5\eta_e p_e d_0(R_e^2-1)}\right\}^{-1}.$$

Proceeding in the same way one obtains for the condenser

$$(14)\qquad k_{im,c}=k_{im,c}=0.125\;\pi d_0\left(r-\frac{1}{r}\right),$$

$$(15)\qquad k_{0m,c}=\frac{0.5\pi d_0[0.5\,(1-r^{-2})+p_c e_c(R_c^2-1)]}{2(1-p_c e_c)+p_c\eta_c d_0(R_c^2-1)},$$

$$(16)\qquad c_c=4\,\frac{h_{i,c}}{h_{0,c}}\;\frac{r}{r^2-1}\;\frac{0.5(1-r^{-2})+e_c p_c\,(R_c^2-1)}{2(1-e_c p_c)+\eta_c p_c d_0(R_c^2-1)},$$

the expression of x_c being derived from Eqs. (2) as x_e resulted from (1)

$$(17)\qquad x_c=\left\{1+r\,\frac{h_{0,c}}{h_{i,c}}\,[1-e_c p_c+0.5\eta_c p_c d_0(R_c^2-1)]\right\}^{-1}.$$

5. Optimization of Q/m_e and Q/m_c (First Step of Optimization). The first step in our procedure consists in maximizing separately the functions $f(x, c)$ for the evaporator and condenser.

The fin efficiency η_i for circular fins of constant cross section is given by

$$(18)\qquad \eta_i=\frac{\tanh MH}{MH},$$

where $M=(2h_0/e\lambda)^{0.5}$ and $H=0.5\,d_0(R-1)\,\{1+0.35\,[\ln(R)]\}$.

To be able to compute x and c (from the Eqs. (11), (13), (16), (17)) and f thereafter, taking into account the relation (18) for the fin efficiency, one must only know λ, e, h_0, h_i, r, p, R, d_0. It is important to notice that parameters as θ_1, θ_2, L_e, L_c (through which Q can be finally modified) do not change optimization results for f_e, f_c.

Before optimization let us fix the following superscripted elements

$$\bar{\lambda},\ \bar{d}_0,\ \bar{r},\ \bar{h}_i\,(\bar{d}_0, \bar{r}),\qquad \bar{h}_0(\bar{d}_0, e, p, R).$$

The outside heat transfer coefficients must not necessarily be given as constants (as it has been done in the application) but as known functions of only

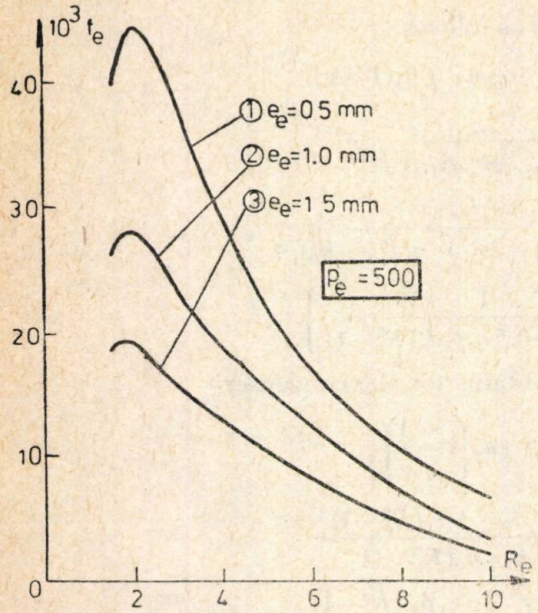

Fig. 1

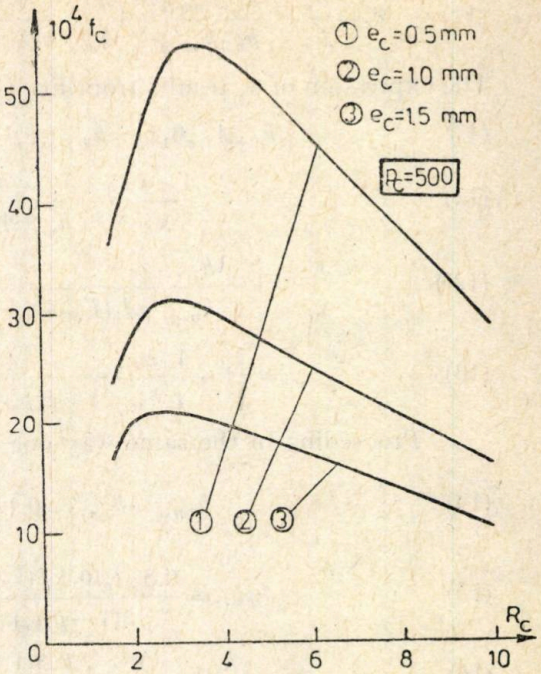

Fig. 2

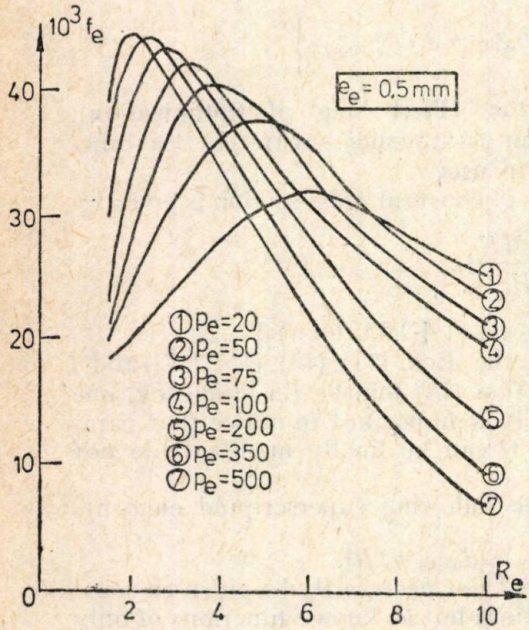

Fig. 3

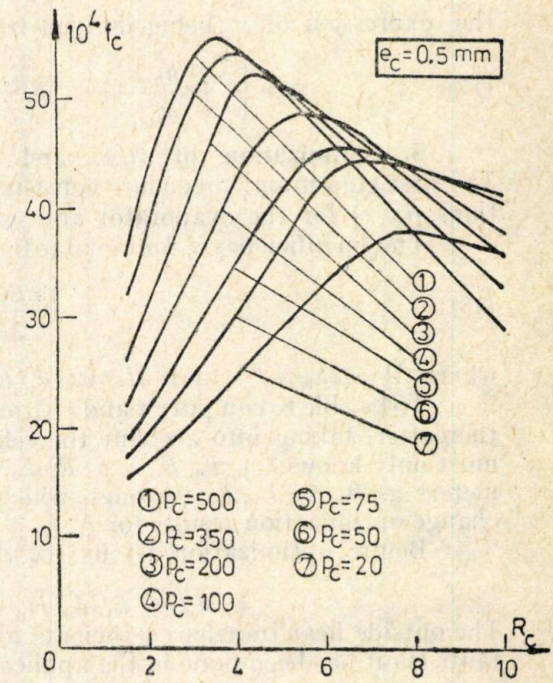

Fig. 4

d_0, e, p, R (see the application from [2]). With the restrictions above, x and c remain functions of three variables, e, p and R.

The easiest way to find $f_{\max}(x(e, R)\ ;\ c(e, R))$ for a fixed value of p is to give values to e and R and to trace the graphs $f(R,\ e$—parameter, $p=$ =const.), as it was done in the application (see Figs. 1,2 for $p = 500$ fins/m).

The results of optimization according to [3] are also shown in Figs. 1 and 2 ; it is obvious, however, they do not match in our case.One selects the best situated curves $f(R,\ e)$ from the graphs traced for different p-values (i.e., as we established, those for which $e=e_{\text{opt}}=0.5$ mm in the application). These curves are plotted together in Fig. 3 (for the evaporator) and 4 (for the condenser), where p is the parameter. At p=const., f always admits a maximum with respect to R.

The best situated point of maximum (with respect to p) gives the solution of the first optimization step.

6. Optimization of Q/m (Second Step of Optimization). Let us consider now the evaporator and condenser (optimized separately in the first step) linked together,

$$\frac{m}{Q}=\frac{m_e}{Q}+\frac{m_c}{Q}=\frac{1}{a_e\theta_1 f_{e,\max}}+\frac{1}{a_c\theta_2 f_{c,\max}}, \tag{19}$$

(see Eq. (6) and (8)) ;

$$a_e=\frac{h_{i,e}}{k_{im,e}}=\frac{8\bar{h}_{i,e}\bar{r}}{\rho\bar{d}_0(\bar{r}^2-1)}=\text{const.}, \tag{20}$$

$$a_c=\frac{h_{i,c}}{k_{im,c}}=\frac{8\bar{h}_{i,c}\bar{r}}{\rho\bar{d}_0(\bar{r}^2-1)}=\text{const.} \tag{21}$$

From the Eqs. (19) we notice that as a_e, a_c, $f_{e,\max}$, $f_{c,\max}$ are constants, m/Q can be optimized with respect to θ_1 and θ_2, these parameters being linked by the condition

$$\theta_1+\theta_2=\theta. \tag{22}$$

From (19) we infer that

$$\frac{Q}{m}=\frac{a_c f_{c,\max}\theta}{a_c f_{c,\max}(x_{HP}a_e f_{e,\max})^{-1}+(1-x_{HT})^{-1}}=\frac{a_c f_{c,\max}\theta}{c_{HP}/x_{HP}+(1-x_{HP})^{-1}}, \tag{23}$$

where

$$x_{HP}=\theta_1/\theta\in(0,\ 1),$$

$$c_{HP}=a_c f_{c,\max}/a_e f_{e,\max}=(\bar{h}_{i,c}/\bar{h}_{i,e})\ (f_{c,\max}/f_{e,\max})=\text{const.}\in(0,\ +\infty).$$

As a_c, $f_{c,\max}$, c_{HP} are constants, Q/m is a function of a single variable, i.e. x_{HP}. The mathematical study of this function shows that Q/m always admits a maximum for a value of x_{HP} from the interval (0, 1). Thus

$$x_{HP,\text{opt}}=\frac{c_{HP}^{0.5}}{1+c_{HP}^{0.5}}\in(0,\ 1). \tag{24}$$

Selecting from (1) and (2) the convenient equations we may write

$$h_{i,e}\pi d_i L_e x_e\theta_1=h_{i,c}\pi d_i L_c\theta_2(1-x_c), \tag{25}$$

$$h_{i,e} L_e x_e x_{HP} \theta = h_{i,c} L_c (1 - x_c)(1 - x_{HP})\,\theta, \tag{26}$$

$$\frac{L_e}{L_c} = \frac{h_{i,c}}{h_{i,e}} \frac{1 - x_c}{x_e} \left(\frac{1}{x_{HP}} - 1 \right). \tag{27}$$

As $x_c = x_{c,\mathrm{opt}}$ (known from the first optimization step), $x_e = x_{e,\mathrm{opt}}$ (known from the first step), $h_{i,c} = \bar{h}_{i,c}$, $h_{i,e} = \bar{h}_{i,e}$ (known) the condition (24) will be observed only if

$$\frac{L_e}{L_c} = \left(\frac{L_e}{L_c} \right)_{\mathrm{opt}} = \frac{\bar{h}_{i,c}}{\bar{h}_{i,e}} \frac{1 - x_{c,\mathrm{opt}}}{x_{e,\mathrm{opt}}} \frac{1}{c_{HP}^{0.5}} = \frac{1 - x_{e,\mathrm{opt}}}{x_{e,\mathrm{opt}}} \left(\frac{f_{e,\max}}{f_{c,\max}} \right)^{0.5} \left(\frac{h_{i,c}}{h_{i,e}} \right)^{0.5}. \tag{28}$$

The second step in the optimization allows us to find an optimal value of the ratio of evaporator to condenser lengths.

The value of Q still remains variable through the variation of L_e and L_c keeping their ratio optimal (Eq. (28)).

7. Application. For example, assume

$\bar{\lambda} = 372\ \mathrm{W\,m^{-1}K^{-1}}$
$e_e = e_c = 0.5\ /1.0\ /\ 1.5\ \mathrm{mm}$
$\bar{d}_0 = 13\ \mathrm{mm}$
$\bar{r} = 1.3$
$R \in [1.2,\ 15]$

$\bar{h}_{i,e}(\bar{d}_0, \bar{r}) = \mathrm{const.} = 2\,000\ \mathrm{W\,m^{-2}\,K^{-1}}$
$\bar{h}_{i,c}(\bar{d}_0, \bar{r}) = \mathrm{const.} = 7\,500\ \mathrm{W\,m^{-2}\,K^{-1}}$
$\bar{h}_{0,e}(\bar{d}_0, e_e, p, R) = \mathrm{const.} = 50\ \mathrm{W\,m^{-2}\,K^{-1}}$
$\bar{h}_{0,c}(\bar{d}_0, e_e, p, R) = \mathrm{const.} = 15\ \mathrm{W\,m^{-2}K^{-1}}$
$p \in [20,\ 500]$ fins/m

Calculating x_e from Eq. (13), c_e from Eq. (11), x_c from Eq. (17) and c_c from Eq. (16) (where the fin efficiency η results from Eq. (18)) for different values of R and e (within the ranges mentioned above) and for p = const., one obtains the curves $f(R, e)$. For $p = 500$ fins/m, such curves are plotted in Fig. 1 (for the evaporator) and Fig. 2 (for the condenser). From all the graphs ($p = 20,\ 50,\ 75,\ 100,\ 200,\ 350,\ 500$ fins/m) we established that $e_{\mathrm{opt}} = 0.5$ mm, as this e-value leads to the highest values of f_e, f_c.

We retained only the curves for which $e = e_{\mathrm{opt}}$ and plotted them in Figs. 3 and 4.

For $f_{e,\max}$ and $f_{c,\max}$ one may select the following optimal values:

$e_{e,\mathrm{opt}} = 0.5$ mm
$R_{e,\mathrm{opt}} = 2.4$
$p_{e,\mathrm{opt}} = 350$ fins/m
$x_{e,\mathrm{opt}} = 0.27012$
$f_{e,\max} = 004425$

$e_{c,\mathrm{opt}} = 0.5$ mm
$R_{c,\mathrm{opt}} = 3.5$
$p_{c,\mathrm{opt}} = 500$ fins/m
$x_{c,\mathrm{opt}} = 0.914$
$f_{c,\max} = 0.005462$

Although $f_{e,\max(R)}$ ($p_e = 500$ fins/m), $f_{e,\max(R)}$ ($p_e = 350$ fins/m), the difference is quite small (Fig. 3) so as to justifiy the selection of $p_{e,\mathrm{opt}} = 350$ fins/m.

The optimal value of the ratio of evaporator to condeser lengths results from Eq. (28)

$$\left(\frac{L_e}{L_c} \right)_{\mathrm{opt}} = 1.76.$$

The optimal value of the dimensionless saturation temperature is given by Eq. (24)

$$x_{HP,\mathrm{opt}} = 0.4044.$$

The fin heights for evaporator and condenser are given by $R_{e,\mathrm{opt}}$ and $R_{c,\mathrm{opt}}$, the two fin densities are $p_{e,\mathrm{opt}}$ and $p_{c,\mathrm{opt}}$; $e_{e,\mathrm{opt}}$ and $e_{c,\mathrm{opt}}$ are the optimal fin thicknesses.

The ratio of evaporator length to condenser length must be 1.76 so as to reach the maximum of Q/m. The heat pipe heat transfer rate may be finally equalized to an imposed value $\bar{Q}$ by choosing L_e to observe the relation

$$L_e = \frac{\bar{r}\bar{Q}}{\pi \bar{h}_{i,e} \bar{d}_0 x_{e,\mathrm{opt}} x_{HP,\mathrm{opt}} \bar{\theta}} = 0.1457 \frac{\bar{Q}}{\bar{\theta}}; \tag{29}$$

$\bar{\theta}$ must now be given.

8. Conclusions. 1. For heat pipes with circular fins of constant cross section, if $\bar{\lambda}, \bar{d}_0, \bar{r}, \bar{h}_{i,e(c)}, \bar{h}_{0,e}(\bar{d}_0, e_e, p, R), \bar{h}_{0,c}(\bar{d}_0, e_c, p, R)$ are given it is possible to find the optimal fin heights, thicknesses and pitches for evaporator and condenser, and an optimal ratio of evaporator to condenser lengths so as Q/m to be maximum. The heat pipe heat transfer rate Q does not affect results.

2. The optimization method may also be used for other fin types.

3. From the application we noticed that the thinner and more numerous the fins are, the better it is from the point of view of this optimization.

Notation

a — ratio of inside heat transfer coefficient to mass per unit inner surface area (W kg^{-1}K^{-1})
A — area of heat exchange surface (m^2)
b — ratio of fin side heat transfer coefficient to mass per unit outer reduced surface area (W kg^{-1}K^{-1})
$c_{e(c)}$ — dimensionless criterion given by the ratio a/b
c_{HP} — dimensionless criterion for heat pipe
d — diameter (m)
e — fin thickness (m)
f — dimensionless function of x and c
h — heat transfer coefficient (W m^{-2}K^{-1})
H — equivalent fin height in the calculation of the fin efficiency (m)
k_m — mass per unit surface area (kg m^{-2})
L — length (m)
m — mass (total mass if no subscript) (kg)
M — criterion in the calculation of the fin efficiency (m^{-1})
N — number of fins
p — fin pitch (fins/m)
Q — heat pipe heat transfer rate (W)
r — ratio of tube outside to inside diameters
R — ratio of the diameter at fin tops to their bottom diameter
t — temperature (K)
t_1 — average hot fluid temperature (K)
t_2 — average cold fluid temperature (K)
V — volume (m^3)
x — dimensionless ratio of temperature differences

$x_e = \theta_{w,e}/\theta_1$, $x_c = \theta_{w,c}/\theta_2$, $x_{HP} = \theta_1/\theta$

ρ — density of the material of tube and fins (kg m^{-3})
λ — thermal conductivity of the fin material (W m^{-1}K^{-1})
η — fin efficiency (dimensionless)
$\theta = t_1 - t_2$ (K)
$\theta_1 = t_1 - t_S$ (K)
$\theta_2 = t_S - t_2$ (K)
$\theta_{w,e} = t_{w,e} - t_S$ (K)
$\theta_{w,c} = t_{w,c} - t_2$ (K)

Subscripts

c — condenser
e — evaporator
f — fin
i — inside
m — mass
o — outside
S — saturation
t — at fin top
w — wall
HP — heat pipe
max — maximum
opt — optimal

Superscript

— for elements to be known before optimization

Received November 25, 1985

Polytechnic Institute, Jassy,
Laboratory for Thermotechnics
and
Department of Physics

REFERENCES

1. Peretz R., *Relation Between Evaporator and Condenser Lengths of a Finless Heat Pipe to Achieve a Maximum Heat Flow per Unit Weight*. Int. J. Heat and Fluid Flow, **3**, 3, 147–148 (Sept. 1982).
2. Peretz R., Horbaniuc B., *Optimal Heat Pipe Heat Exchanger Design*. J. Heat Recovery Systems, *4*, 9–24 (1984).
3. Brown A., *Optimum Dimensions of Uniform Annular Fins*. Int. J. Heat and Mass Transfer, Vol. **8**, Pergamon Press, 1965, pp. 655–662.

OPTIMIZAREA GEOMETRICĂ A TUBURILOR TERMICE CU ARIPIOARE ÎN SCOPUL OBȚINERII UNUI FLUX TERMIC MAXIM PE UNITATEA DE GREUTATE

(Rezumat)

Se prezintă o metodă de optimizare geometrică a tuburilor termice cu aripioare circulare de grosime constantă, în scopul obținerii unui flux termic maxim pe unitatea de greutate. Principiul metodei constă în optimizarea separată a vaporizatorului și condensatorului tubului termic, rezultînd pentru aceste două zone valori optime ale înălțimii și grosimii aripioarei, precum și ale pasului de aripioare. În final rezultă și valoarea optimă a raportului dintre lungimea vaporizatorului și cea a condensatorului.

La sfîrșitul lucrării este dat un exemplu numeric de optimizare a unui tub termic gravitațional.

BULETINUL INSTITUTULUI POLITEHNIC DIN IAŞI
Tomul XXXI (XXXV), Fasc. 1—4, 1985
Secţia IV
CONSTRUCŢII DE MAŞINI

D.K. 621.743

UNTERSUCHUNHGEN ZUR REDUZIERUNG DER MASSE VON KUNSTHARZBINDERN IN DEN KALTSELBSTERSTARRENDEN FORMMISCHUNGEN

VON

C. CIOCHINĂ, EMIL ANDREI, AURELIAN SIMIONESCU, OVIDIU CALANCIA, RADU DĂNILĂ, LEONACHE DRĂGOI und FLORIN ANDREI

1. Allgemeines. In den letzten zwanzig Jahren hat in der Gußteilherstellung die Anwendung von unterschiedlichen Kunstharzen, auf deren Basis viele Varianten von Formherstellungsverfahren entwickelt wurden, an Umfang zugenommen [1]. Eines dieser Verfahren ist die Herstellung von Gießformen aus kaltselbsterstarrenden Formmischungen.

Zum Gießen von dickwandigen und mittelkomplizierten Gußeisenteilen in der Gießerei des Schwermaschinenbau-Kombinates (C.U.G.) aus Jassy wurden Formen aus kaltselbsterstarrenden Mischungen, die aus Sand, Kunstharz und Katalysator bestehen, hergestellt.

Der Sand ist vom Typ Aghireș-Cornești mit folgenden Eigenschaften: aussehen der Kornoberfläche, scharfe Kanten und rauhige Oberfläche; auswaschbare Anteile, 0,2%; mittlere Körnung (M 50), 0,18%; Gleichmäßigkeitsgrad (GU), 65% ; Siliziumdioxyd (SiO_2), 98,5% ; Eisenoxyd (Fe_2O_3), 0,4% ; Kalziumoxyd und Magnesiumoxyd (CaO und MgO), 0,5% ; Alkalioxyde (Na_2O und K_2O), 0,6%; Schwefel in Form von Sulfiden, — ; Grundanteil, 77,3% auf Sieben von 0,4 bis 0,2.

Als Bindemittel wurden zwei Sorten von Kunstharzen, die vom Chemischen Kombinat „Victoria" aus Făgăraș geliefert wurden, verwendet : a) Phenolformaldehydkunstharz zum Kerngießen, STAS 11492-80 ; b) Kalterstarrendes Furanharz für die Gießerei Typ FR-1, STAS 11294/1-79.

Die technischen Güteanforderungen dieser Kunstharze sind in der Tabelle 1 zusammengestellt.

Zur Erstarrung beider Harze wird als Katalysator Benzolschwefelsäure Typ SBA-21, STAS 11294/2-79, dessen technische Güteanforderungen in der Tabelle 2 zusammengestellt sind, verwendet.

Nachdem die Kalterstarrungsreaktion stattgefunden hat, werden die Gießformen mit värmebeständiger, in organischen Lösungsmitteln gelöster Farbe Typ VET2-s angestrichen, welche im allgemeinen beim Gießen großer, hochkomplizierter Werkstücke aus Grauguß mit Wanddicken von 80 bis 120 mm angewendet wird.

In der Werkspraxis beim C.U.G. Jassy wird in den kalterstarrenden, oben aufgeführten Formmischungen ein recht hoher Anteil von Kunst-

Tabelle 1

Technische Güteanforderungen der Kunstharze

Charackteristiken	Anforderungen an	
	Bindemittel a)	Bindemittel b)
Aggregatzustand	homogene zähe Flüssigkeit	zähe Flüssigkeit
Farbe	gelb-braun	rötlich braun
Spezifische Masse bei 20°C, g/cm³	1,205±0,020	1,185±0,025
Viskosität bei 20°C, mPas (CP) max.	650	28±6
Freies Phenol, % (max.)	14	—
Harz, %	—	—
Freies Formaldehyd, % (max.)	0,8	1,7
pH	7,2 ... 7,8	6,5 ... 7,5
Stickstoff, % (max.)	—	5
Biegefestigkeit, N/mm² (min.)		
nach 30 min	0,8	—
nach 5 h	3,0	—
nach 20 h	3,0	—

Tabelle 2

Technische Güteanforderungen an den Katalysator Typ SBA-21

Charakteristiken	Anforderungen
Zustand	opaleszente Flüssigkeit
Farbe	schwarz
Spezifische Masse, g/cm³	1,265±0,015
Säuregehalt (H_2SO_4), %	20 ... 22

harz (4 bis 5%) und von Katalysator (>1%) verwendet, um dadurch hohe physikalisch-mechanische Eigenschaften (hohe mechanische Festigkeiten der Mischungen, hohe Durchlässigkeit u.a.) in der am kürzesten erwünschten Zeit des Kalterstarrungsreaktionsablaufes zu erzielen.

2. **Versuche.** Da die Fachliteratur keine Informationen bezüglich des Zusammenhanges zwischen den mechanischen Festigkeiten der Formen und der Kerne, der Menge des Kunstharzes und des Katalysators und der Ablaufszeit der Kalterstarrungsreaktion enthält, versucht die vorliegende Arbeit diesen Zusammenhang für die beiden Sorten der rumänischen Bindemittel, die in C.U.G.—Jassy realisierten Fommischungen angewendet wurden, festzustellen.

Zu diesen Zweck wurden Untersuchungen mit Probestücken unter Versuch- und Standardbedigungen im Labor der Graugußgießerei des C.U.G.—Jassy durchgeführt ([2], S. 2—8).

Die untersuchten Prüfstücke wurden aus Formischungen nach folgender Mischungsformel hergestellt:

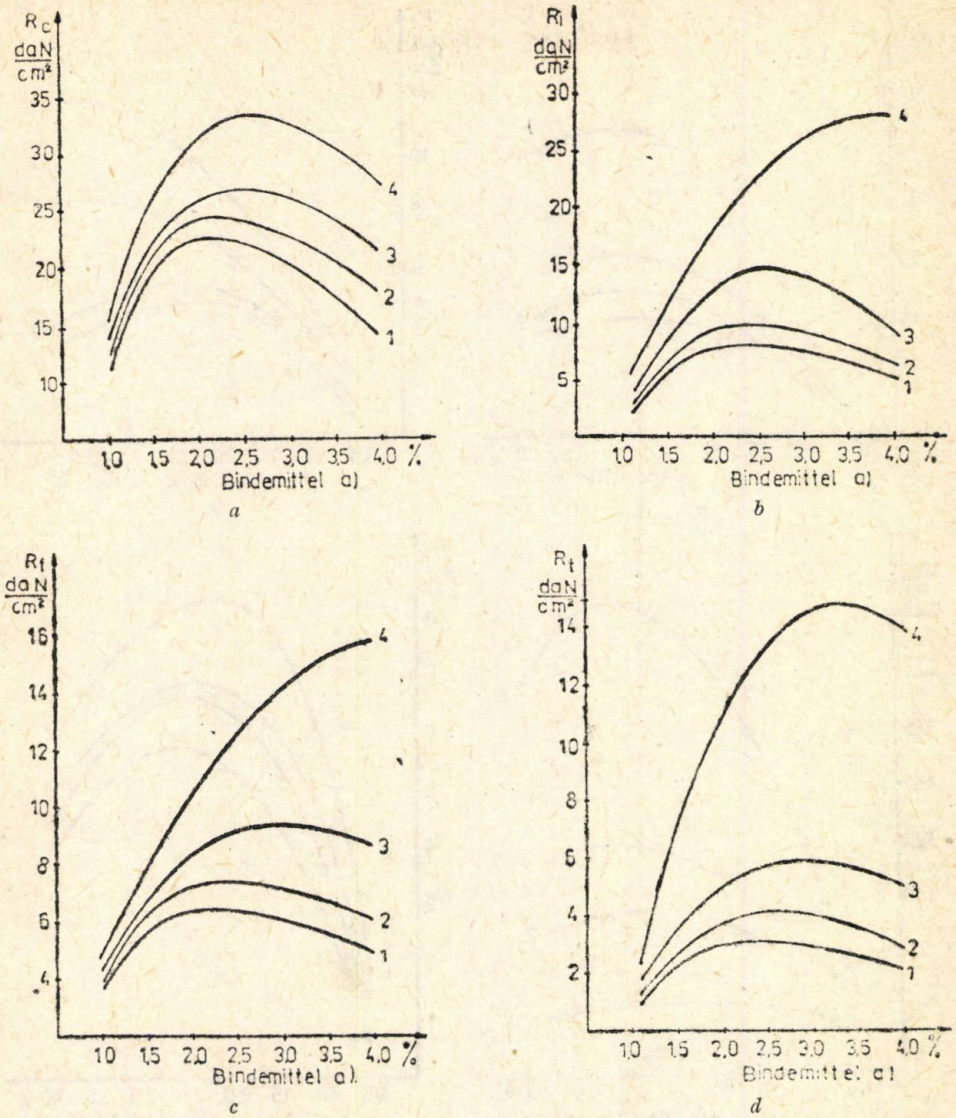

Abb. 1 — Die Abhängigkeit der mechanischen Festigkeiten der kalterstarrenden Formmischungen, bei denen das Bindemittel a) verwendet wurde, von der Kunstharzmenge und von der Erstarrungsdauer : *a* — Erstarrte Probestücke nach 1 Stunde ; *b* — Erstarrte Probestücke nach 2 Stunden ; *c* — Erstarrte Probestücke nach 4 Stunden ; *d* — Erstarrte Probestücke nach 24 Studen .

a) Katalysator 1% ;
b) Kunstharz 0,5% , 1% , 1,5% , 2% , 2,5% , 3% , 3,5% , 4% ;
c) Neusand.

Für die Versuche wurde ein Georg-Fischer-Versuchskasten verwendet, wobei die Prüflinge nach 1, 2, 4 bzw. 24 Stunden nach Beginn der Kalt-

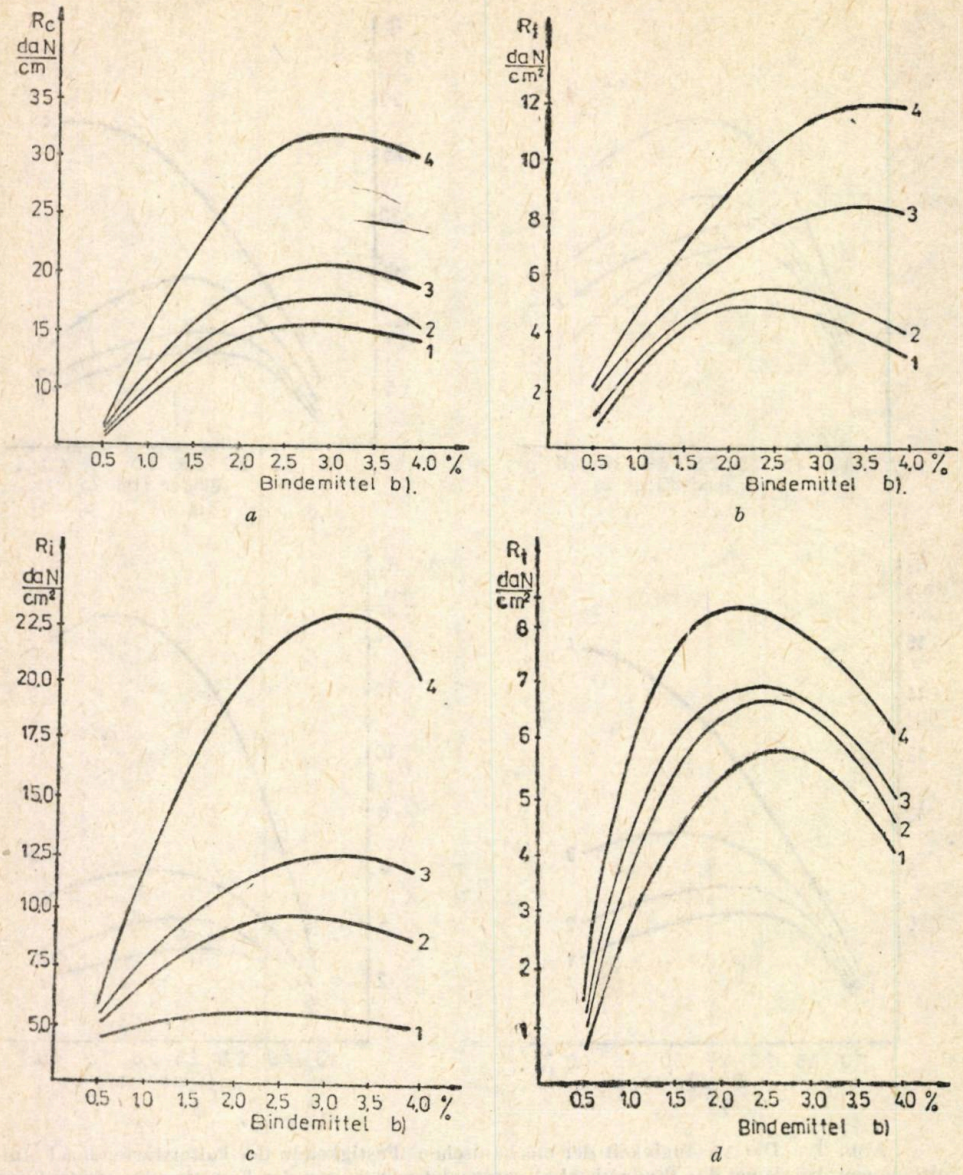

Abb. 2 — Die Abhängigkeit der mechanischen Festigkeiten der kalterstarrenden Formmischungen, bei denen das Bindemittel b) verwendet wurde, von der Kunstharzmenge und von der Erstarrungsdauer : *a* — Erstarrte Probestücke nach 1 Stunde ; *b* — Erstarrte Probestücke nach 2 Studnen ; *c* — Erstarrte Probestücke nach 4 Stunden ; *d* — Erstarrte Probestücke nach 24 Stunden.

erstarrungsreaktion untersucht wurden. Die bei den Probestücken erhaltenen Festigkeiten der kalterstarrenden Formmischungen (Druckfestigkeit R_c, Biegefestigkeit R_i, Zugfestigkeit R_t und Scherfestigkeit R_f) sind in den Abbn. 1 und 2 graphisch dargestellt.

3. **Auswertung der Versuchsergebnisse.** Die Analyse der durch die Kurven dargestellten Versuchsergebnisse zeigt, daß fast alle untersuchten mechanischen Festigkeiten für etwa 2,5% Kunstharz erhöhte Werte aufweisen.

Die Werte der mechanischen Festigkeiten der mit kalterstarrenden Formmischungen, die 2,5% Kunstharz beinhalten, hergestellten Formen erhauben die Einhaltung der physikalisch-mechanischen Eigenschaften der Formen und der Kerne bei ihrer Manipulation und bei den notwendigen Montageoperationen, sowie auch während der Dauer des Gießens des flüssigen Graugußes zur Erzeugung von mittelkomplizierten und dickwandigen Teilen.

Die im Labor festgestellte Durchlässigkeit ist sehr gut. Sie ist größer als 250 Durchlässigkeitseinheiten bei den Bindemitteln a) und b) für alle analysierten Mischungsformeln.

Deshalb zieht man die Schlußfolgerung, daß folgende optimale Mischungsformeln empfehlenswert sind :

2,5% Bindemittel a), 1% Katalysator, 96,5% Neusand bzw.
2,5% Bindemittel b), 1% Katalysator, 96,5% Neusand.

Tabelle 3

Die mechanischen Festigkeiten für kalterstarrende Formmischungen, die 2,5% Bindemittel a) oder b), 1% SBA-21 und 96,5% Neusand enthalten

Erstarrungsdauer in Stunden	Mechanische Festigkeiten, daN/cm²							
	R_c		R_i		R_f		R_t	
	a)	b)	a)	b)	a)	b)	a)	b)
1	22,0	15,5	8,0	5,7	6,3	4,8	3,0	5,8
2	24,0	17,5	10,0	9,7	7,5	5,4	4,2	6,7
4	26,5	20,0	14,5	12,2	9,2	7,6	5,8	6,9
24	33,5	31,0	22,5	22,0	12,6	10,4	13,4	8,3

In Tabelle 3 werden die Werte der mechanischen Festigkeiten der kalterstarrenden Formmischungen, die für die beiden optimalen Mischungsformeln identisch sind, angegeben.

4. Schlußfolgerungen. 1. Die festgestellten optimalen Mischungsformeln wurden beim Gießen von Graugußteilen vom Typ „Steiger" in der Graugußgießerei vom C.U.G.– Jassy erprobt. Die vorgeschlagenen Mischungsformeln führten, im Vergleich zu den bis jetzt angewandten Mischungsformeln, zur Reduzierung der Bindemittelmenge von 1,5...2,5%.

Infolge dieser Reduzierung wurde auch bedeutend der Preis für eine Tonne kalterstarrende Formmischung gesenkt.

2. Die mechanischen Eigenschaften und die Struktur der in mit kalterstarrenden Formmischungen hergestellten Formen gegossenen Teile sind praktisch identisch mit denen der Teile, die in Formen gegossen wurden mit den ursprünglich angewandten Mischungsformeln ([2], S. 13—34).

3. Die neuen Mischungsformeln haben den Vorzug, daß sie ein leichteres Ausschlagen der gegossenen Teile und eine teilweise Wiederverwendung der in den Anlagen vom C.U.G.—Jassy angewandten Formmischungen gestatten.

Eingegangen am 12. Juni, 1985

Technische Hochschule, Jassy,
Lehrstuhl für Technologie

LITERATURVERZEICHNIS

1. Coşneanu C., Cohn E., Popescu B., Dumitrescu D., Pîrvu V., *Materiale auxiliare pentru turnători*. Ed. tehn., Buc., 1983.
2. Andrei E., Ciochină C., Simionescu A., Calancia O., Dănilă R., *Cercetări privind obţinerea amestecurilor de formare cu autoîntărire pentru piese din fontă şi oţel cu lianţi economici şi posibilităţi de regenerare. Faza experimentări industriale*. Contract de cercetare ştiinţifică între Inst. polit. Iaşi şi C. U. G. — Iaşi, 1984.
3. Buzilă S., *Proiectarea şi executarea formelor*. Ed. did. şi ped., Buc., 1976.

CERCETĂRI EXPERIMENTALE PRIVIND REDUCEREA CANTITĂŢILOR DE LIANŢI ORGANICI DIN COMPONENŢA AMESTECURILOR DE FORMARE AUTOÎNTĂRITOARE LA RECE

(Rezumat)

Se studiază variaţia valorilor rezistenţelor mecanice (la compresiune, forfecare, încovoiere şi tracţiune) a amestecurilor de formare autoîntăritoare la rece cu lianţi organici româneşti (răşini sintetice pe bază de fenolit sau urelit), în funcţie de timpul de autoîntărire şi de procentajul de răşină utilizată, în scopul stabilirii unor reţete optime.

BULETINUL INSTITUTULUI POLITEHNIC DIN IAȘI
Tomul XXXI (XXXV), Fasc. 1—4, 1985
Secția IV
CONSTRUCȚII DE MAȘINI

D.C. 621.785

THE DIMENSIONAL STABILIZATION OF PIECES DEFORMED UNDER THERMIC TREATMENT

BY

I. HOPULELE, CARMEN NEJNERU and M. ȘTEFAN

1. Introduction. After applying an improvement thermic treatment, in most cases, the rods and prismatic pieces result with no internal tensions, but with deformations which surpass the admitted limits. For fitting into the following correction dimensions the pieces deformed by thermic treatment are subjected to a correction process. The correction under a plastic-elastic deformation leads to the appearance of some high value strains, which are distributed again through discharge in the correction and exploitation process, distorting the piece.

By applying a technology of alternative correction with controlled parameters, one can obtain a minimal deformation, but at the same time, minimal internal tensions in the external strata, too.

The researches carried out aim at pointing out the phenomena which take place in the correction of prismatic pieces, after applying an improvement or normalization thermic treatment. A solution for the optimization of the correction technological parameters is also proposed.

2. Theoretical Aspects regarding the Correction of Prismatic Pieces Deformed by Thermic Treatment. The volume variation of pieces subjected to a thermic treatment are the fundamental causes of remanent deformation, especially of those pieces which during the heating and cooling process undergo phase transformation accompanied by the change of the specific volume.

In the pieces subjected to an improvement thermic treatment the internal tensions, which caused the deformation, disappear in the process of high return (recurrence), so that the pieces come out distorted, but with no important internal tensions.

For the correction of a prismatic piece of length l which possesses an initial deformation f_{p0} which surpasses the admitted limits, there can be applied a force concentrated in the middle of the piece, which should lead to an elastic deformation f_e and to a plastic deformation f_{p1} so that at the return the remanent rise of the arch of the deformation should fit into the admitted limits.

According to this one can consider that a force P_e, necesary to the maximal elastic deformation f_e, will exist, to which a bending moment M_e will correspond. Then, a total force P will be necessary for the plastic de-

formation, to which a bending moment M and a total rise $f_t = f_{p0} + f_e$ will correspond.

In Fig. 1 the scheme of the correction process by elastic-plastic deformation with concentrated force is presented, where A represents the deformation diagram and B means the internal tensions diagram: *1* — in the maximum moment zone; *2* — in the intermediate zone; *3* — in the elastic deformation zone; D is the plastic articulation.

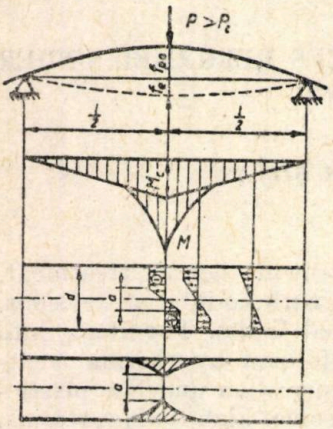

Fig. 1

In Fig. 1 one can see that in the zone of the maximum moment there will be a kernel of thickness a plastically undeformed which after removing the force P will stress the plastically deformed strata in the opposite direction.

The value of the height of the plastically undeformed kernel is calculated with the relation [1]

$$a = h\sqrt{3 - 2\frac{P_e}{P}}, \tag{1}$$

where h — thickness of the material (the prismatic bar).

The validity domain of this relation is

$$P_e \leqslant P \leqslant 1.5\, P_e.$$

For establishing a dependence between the elastic-plastic rise of the arch of the deformation and the deformation force, we use the relation [2]

$$\frac{f_t}{f} = 5\left(\frac{P_e}{P}\right)^2 - \sqrt{\frac{P_e}{P}}\left(3\frac{P_e}{P} + 1\right)\sqrt{3\frac{P_e}{P} - 2}\,. \tag{2}$$

The validity domain of the relation is

$$f_{p0} \leqslant 1.2\, f_e\,.$$

In order to determine the internal tension it is supposed that the elastic kernel partially discharges the plastically deformed strata after removing the deformation force. The value of the tension in the external strata will depend on the bending moment created by the elastic kernel [3]

$$\sigma_{rem} = \frac{\sigma_c}{2}\left(1 - \frac{a^2}{h^2}\right). \tag{3}$$

3. **Theoretical Contributions regarding the Correction with Dimensional Stabilization of Pieces Deformed under Thermic Treatment.** For removing the internal tensions after the straightening of the pieces, a solicitation in the opposite direction to the straightening one is applied, under a tension which should produce an elastic-plastic deformation having the same thickness as the elastic kernel, a.

Due to the superposition of the remanent tensions on the stressing tensions, the opposite maximum elastic rise of the arch of the deformation f_{e1} will be much smaller

$$f_{e1}=f_e\left(1-\frac{\sigma_{rem}}{\sigma_c}\right). \tag{4}$$

The obtaining of the opposite plastic rise f_{p1} supposes the deformation in the opposite direction with a plastic rise which should ensure an elastic kernel having a thickness a which corresponds to

$$\frac{f_e+f_{p0}}{f_e}=\frac{f_{e1}+f_{p1}}{f_{e1}} \quad \Rightarrow \quad f_{p1}=\frac{f_{e1}f_{p0}}{f_e}. \tag{5}$$

The deformation in the opposite direction, with a total rise f_{t1} leads to the disappearing of the tensions in the external strata

$$f_{t1}=f_{e1}+f_{p1}. \tag{6}$$

4. Experimental Researches regarding the Correction with Dimensional Stabilization of Improved Steel Pieces, 41MoCr11. The experimental cheking of the correction technological parameters analitically established, requires the using of a laboratory equipment for the deformation of samples, presented in Fig. 2. It is made up by a hand-worked hydraulic pump equipped with a gauge *1*, a hydraulic cylinder *2* and a mechanical deformation device *3*.

For meassuring the deformation a comparator with a scale is used, *4*.

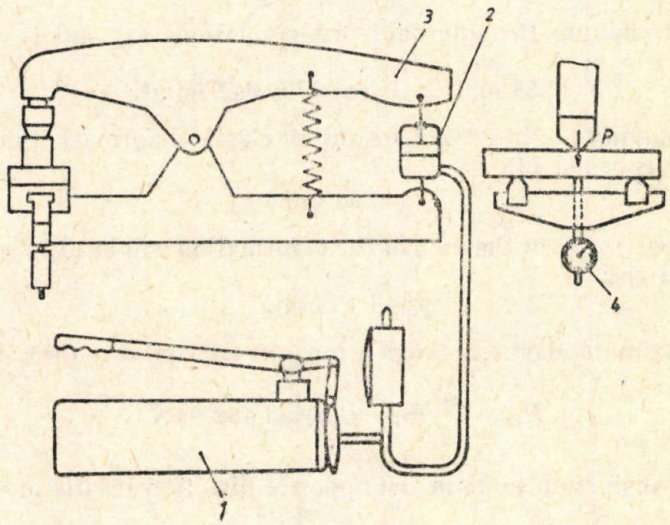

Fig. 2

The sample had a square section having a 20 mm side, the correction length being 20 mm, tempered in oil at 840°C temperature and brought back to a 500°C temperature for an hour.

After tempering and returning, the samples were selected two by two, having the same deformation. One of them was usually corrected by straightening and the other was subjected to a correction with dimensional stabilization.

For correcting the first group of pieces the samples having an initial deformation $f=1$ mm were selected having as a result the following parameters of the correction conditions :

$$f_e=\frac{l^2}{6hE}\sigma_c=1.24 \text{ mm}, \qquad P_c=\frac{2h^3}{3l}\sigma_c=2\,133 \text{ daN},$$

where f_e—the maximum elastic rise of the arch of the deformation ; l—the correction length = 200 mm ; h—the thickness of the sample = 20 mm ; E — the elasticity module = 21 500 daN/mm² ; σ_c—the flowing limit = =80 daN/mm² ; P_c—the force necessary for achieving the maximum elastic rise.

The total correction rise will be

$$f_t=f_{p0}+f_e=2.24 \text{ mm}.$$

The force necessary for the elastic-plastic deformation is determined using relation (2) and the result obtained is $P=3\,136$ daN.

As a consequence of the tests achieved, the following results were obtained : a total deformation $f_t=2.24$ mm under the elastic return 1.4 mm. Under the elastic deformation tests the 1.24 mm rise did not lead to plastic remanence.

These experiments lead to the conclusion that the elastic return is stopped.

For determining the internal tension relations (3) and (1) are used ; we get

$$a=4.88 \text{ mm}, \qquad \sigma_{rem}=37.6 \text{ daN/mm}^2.$$

For removing the internal tensions an elastic deformation in the opposite direction is asked (4)

$$f_{e1}=0.66 \text{ mm}.$$

The opposite rise of the arch of the deformation will be (5_2) $f_{p1}=0.53$ mm and the total rise

$$f_t=1.19 \text{ mm}.$$

The maximum elastic distortion force in the opposite direction will be

$$P_{c1}=\frac{2h^3}{3l}(\sigma_c-\sigma_{rem})=1\,130 \text{ daN}$$

and the total distortion force in the opposite direction results in

$$P_1=\frac{f_t}{f_e}P_{c1}=1\,662 \text{ daN}.$$

After the carried out tests of deformation in the opposite direction to the initial deformation in order to reduce the internal tension it is shown

that the piece plastically flowed under the smallest effort in the opposite direction, that is the elastic reserve for an effort $\sigma_c - \sigma_{rem}$ was not confirmed.

After the deformation with a total rise of 1.19 mm the elastic return was no longer 0.66 mm but only 0.38 mm which proves that the elastic return in the opposite direction is also prevented.

5. Conclusions. 1. The pieces deformed under thermic treatment simply corrected (straightened) do not fulfill the conditions for the subsequent processing (working) and exploiting because of the internal tensions introduced in the correction process.

2. The correction with dimensional stabilization is possible by applying of alternative deformation under controlled parameters.

3. The present theories regarding the elastic-plastic deformation of steel cannot be used in order to prescribe the optimum correction parameters.

4. Out of the experimental research carried out, there resulted that the internal tensions, after the simple correction, are very close to the flowing limit of the material because it is plastically deformed in the opposite direction under very small efforts.

5. For the optimization of the correction theory with dimensional stabilization the tackling of a theory regarding the elastic-plastic deformation of steel is necessary, theory which should be closer to the real correction conditions.

Received May 20, 1985

Polytechnic Institute, Jassy,
Laboratory of Thermal Treatments

REFERENCES

1. Buzdugan Gh., *Rezistența materialelor*. Ed. tehn., Buc., 1980.
2. Ponomariov S. D. și colab., *Calculul de rezistență în construcția de mașini* (trad. din l. rusă). Vol. II, Ed. tehn., Buc., 1963.
3. Posea N. și colab., *Mecanică aplicată pentru ingineri*. Ed. tehn., Buc., 1984.

STABILIZAREA DIMENSIONALĂ LA REDRESAREA PIESELOR DEFORMATE PRIN TRATAMENT TERMIC

(Rezumat)

Se prezintă contribuții teoretice și experimentale referitorare la problema redresării barelor deformate în urma tratamentului termic.

În prima parte sînt prezentate ipotezele de calcul și formula determinată pentru calcularea tensiunii remanente la o bară deformată plastic cu o anumită înălțime a arcului de deformare, cînd asupra ei acționează o forță concentrată P aplicată la mijloc. În partea a doua se propune o anumită strategie de dimensionare și justificarea acesteia din punct de vedere teoretic și practic, iar în ultima parte se prezintă rezultatele experimentale.

BULETINUL INSTITUTULUI POLITEHNIC DIN IAŞI
Tomul XXXI (XXXV), Fasc. 1—4, 1985
Secţia IV
CONSTRUCŢII DE MAŞINI

D. C. 621.9.01; 621.914

CONSIDÉRATIONS SUR LA CORRÉLATION ENTRE LA RUGOSITÉ DE SURFACE Ra ET LES PARAMÈTRES DE TRAVAIL AU FRAISAGE FRONTAL

PAR

DRAGOŞ PARASCHIV, OCTAVIAN PRUTEANU, V. BRAHA et GH. TEŞU

1. Considérations théoriques. L'usinage mécanique par fraisage constitue l'opération qui exige une forte proportion de main d'oeuvre et d'énergie entre les usinages que l'on applique aux surfaces planes. Le fraisage à outils munis de plaquettes de type Romascon s'est avéré une opération de haute productivité, la surface qui en résulte ayant une faible rugosité.

2. Matériaux employés. On a utilisé comme matériaux pour cette recherche trois sortes d'aciers alliés au Chr et Mo. Ces matériaux ont été traités thermiquement par recuit complet en vue de l'usinage mécanique.

3. Régimes de travail. On a utilisé pour le fraisage frontal deux modèles de fraises à affûtaje continu Romascon à 15 et 20 dents. Les régimes de travail assurés par une machine à fraiser verticale FV-32 représente la combinaison des paramètres présentés dans la fig. 1.

Les valeurs choisies correspondent à un large éventail de possibilités d'usinage pour les deux phases technologiques de dégrossissage et de finition.

4. Résultats expérimentaux. Pour réaliser la recherche, les éprouvettes usinées ont été soumises à des mesurages de la rugosité, tout en notant 11 valeurs pour chaque usinage. Ce nombre de mesurages, conformément au calcul statistique, correspond à un niveau de confiance $P=0{,}99$ à une précision égale à l'écart moyen carré standard empirique, s.

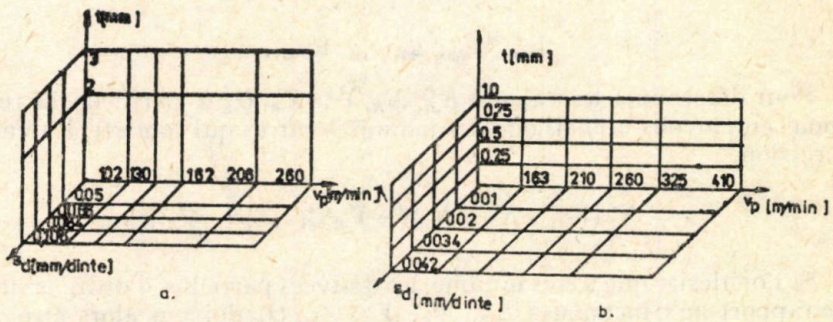

Fig. 1 — Régimes de coupe au fraisage : a — dégrossissage ; b — finition.

Dans le cas du fraisage, on considère que la rugosité Ra réelle des paramètres du régime de coupe à savoir : la vitesse de coupe v, l'avance par dent S_d, la profondeur de coupe t et le nombre des dents z, s'exprime par une relation telle que

$$\text{Ra} = K_R\, v^{X_R} S_d^{Y_R} t^{Z_R} z^{Q_R}. \tag{1}$$

Pour déterminer les valeurs des coefficients K_R et des exposants X_R, Y_R, Z_R, Q_R on part du tableau des données expérimentales

$$\begin{aligned} &(v_1,\ S_{d1},\ t_1,\ z_1,\ \text{Ra}_1),\\ &(v_2,\ S_{d2},\ t_2,\ z_2,\ \text{Ra}_2),\\ &\cdots\cdots\cdots\\ &(v_m,\ S_{dm},\ t_m,\ z_m,\ \text{Ra}_m), \end{aligned} \tag{2}$$

de sorte que la différence entre la valeur approximative Ra, déterminée par la relation (1), et la valeur Ra du tableau des données (2) soit minime.

Le logarithme de la relation (1) est donnée par

$$\log \text{Ra} = \log K_R + X_R \log v + Y_R \log S_d + Z_R \log t + Q_R \log Z\ ; \tag{3}$$

en posant

$$\begin{aligned} \log \text{Ra} &= \text{Ra}', & \log K_R &= K_R',\\ \log v &= v', & \log S_d &= S_d',\\ \log t &= t', & \log z &= z' \end{aligned}$$

on obtient la fonction linéaire

$$\text{Ra}' = K_R' + X_R v' + Y_R S_d' + Z_R t' + Q_R z'. \tag{4}$$

En logarithmant les valeurs du tableau (2) on obtient le tableau des données

$$\begin{aligned} &(v_1'\ S_{d1}',\ t_1',\ z_1',\ \text{Ra}_1'),\\ &(v_2',\ S_{d2}',\ t_2',\ z_2',\ \text{Ra}_2'),\\ &\cdots\cdots\cdots\\ &(v_m',\ S_{dm}',\ t_m',\ z_m',\ \text{Ra}_m'). \end{aligned} \tag{5}$$

Pour déterminer les valeurs K_R', X_R, Y_R, Z_R, Q_R à partir de la relation (3), nous employons la méthode des moindres carrés qui consiste à minimiser l'expression

$$s = \sum_{i=1}^{m} (\text{Ra}_i' - K_R' - X_R v_i' - Y_R S_{di}' - Z_R t_i' - Q_R z_i')^2. \tag{6}$$

Si l'on désire que s soit minime, les dérivées partielles d'ordre premier de s par rapport aux inconnues K_R', X_R, Y_R, Z_R, Q_R doivent alors être égaux à zéro et il en résulte un système de 5 équations linéaire à 5 inconnues :

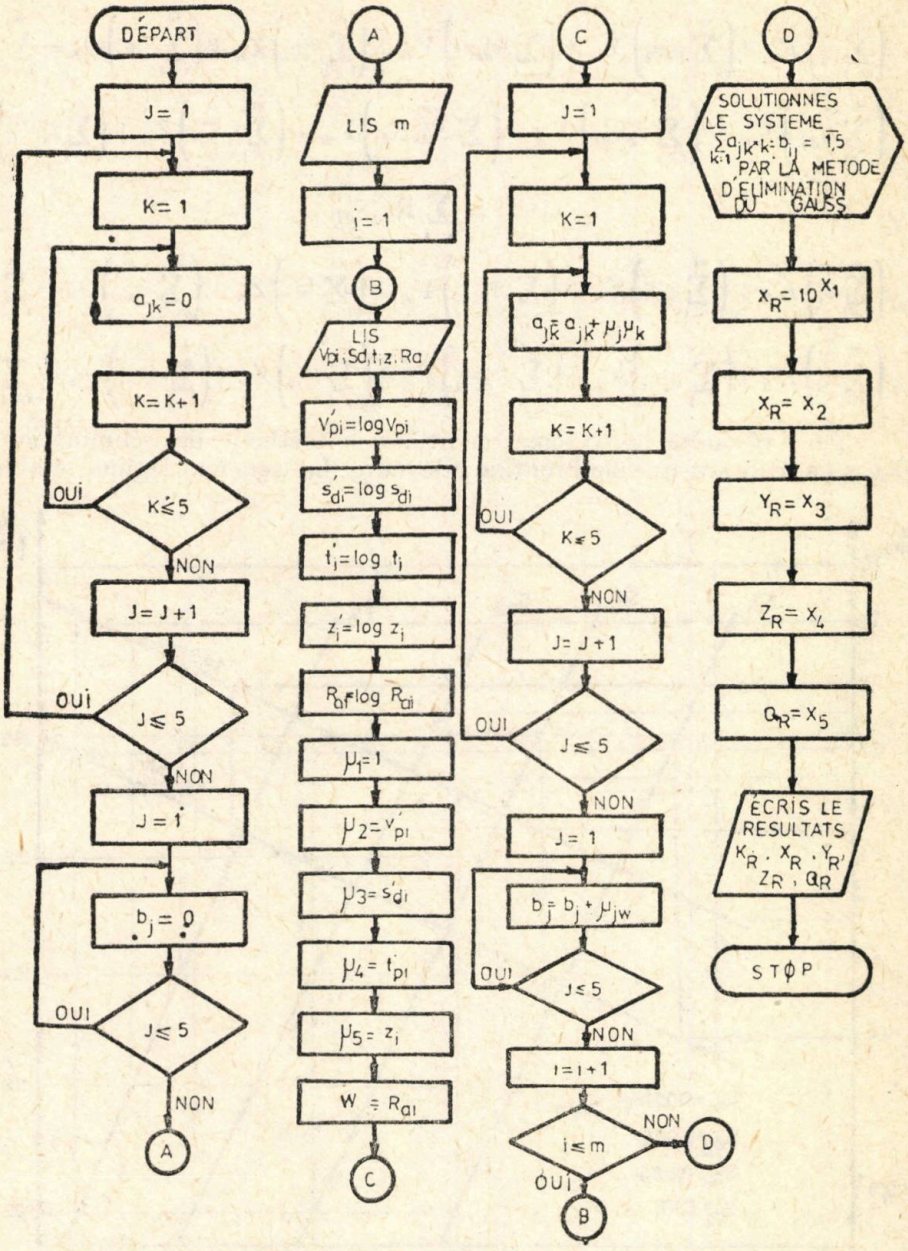

Fig. 2 — Schéma logique de calcul de la rugosité Ra en fonction des éléments du régime de coupe.

$$
\begin{aligned}
&mK'_R+\left(\sum_{i=1}^{m} v'_i\right)X_R+\left(\sum_{i=1}^{m} S'_{di}\right)Y_R+\left(\sum_{i=1}^{m} t'_i\right)Z_R+\left(\sum_{i=1}^{m} z'_i\right)Q_R=\sum_{i=1}^{m}\mathrm{Ra}'_i,\\
&\left(\sum_{i=1}^{m} v'_i\right)K'_R+\left(\sum_{i=1}^{m} v'_i v'_i\right)X_R+\left(\sum_{i=1}^{m} S'_{di}v'_i\right)Y_R+\left(\sum_{i=1}^{m} t'_i v'_i\right)Z_R+\left(\sum_{i=1}^{m} z'_i v'_i\right)Q_R=\sum_{i=1}^{m}\mathrm{Ra}_i v'_i,\\
&\left(\sum_{i=1}^{m} S'_{di}\right)K'_R+\left(\sum_{i=1}^{m} v'_i S'_{di}\right)X_R+\left(\sum S'_{di}S_{di}\right)Y_R+\left(\sum_{i=1}^{m} t'_i S'_{di}\right)Z_R+\left(\sum_{i=1}^{m} z'_i S'_{di}\right)Q_R=\\
&\qquad=\sum_{i=1}^{m}\mathrm{Ra}'_j S'_{dj},\\
&\left(\sum_{i=1}^{m} t'_i\right)K'_R+\left(\sum_{i=1}^{m} v'_i t'_i\right)X_R+\left(\sum_{i=1}^{m} S'_{di}t'_i\right)Y_R+\left(\sum_{i=1}^{m} t'_i t'_i\right)Z_R+\left(\sum_{i=1}^{m} z'_i t'_i\right)Q_R=\sum_{i=1}^{m}\mathrm{Ra}'_i t'_i,\\
&\left(\sum_{i=1}^{m} z'_i\right)K'_R+\left(\sum_{i=1}^{m} v'_i z'_i\right)X_R+\left(\sum_{i=1}^{m} S'_{di}z'_i\right)Y_R+\left(\sum_{i=1}^{m} t'_i z'_i\right)Z_R+\left(\sum_{i=1}^{m} z'_i z'_i\right)Q_R=\sum_{i=1}^{m}\mathrm{Ra}'_i z'_i.
\end{aligned}
\tag{7}
$$

Pour résoudre le système on utilise la méthode de l'élimination de Gauss en utilisant une soubroutine adéquate. Le schéma logique établi en

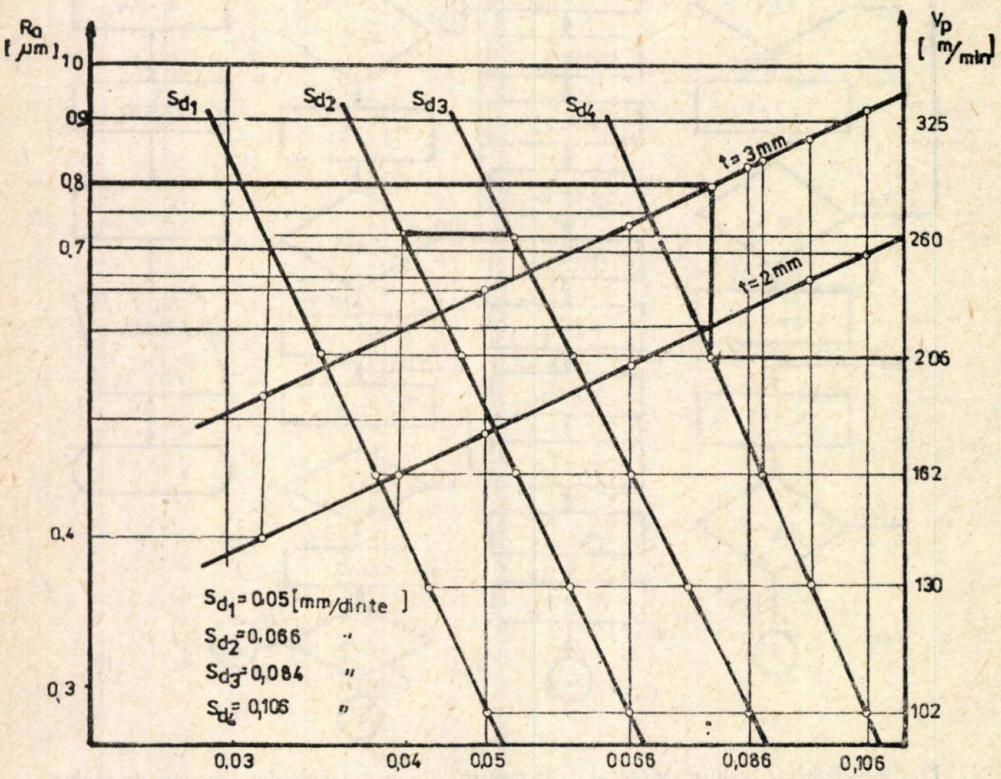

Fig. 3 — Nomogramme : variation de la rugosité Ra en fonction des éléments du régime de coupe au fraisage de dégrossissage.

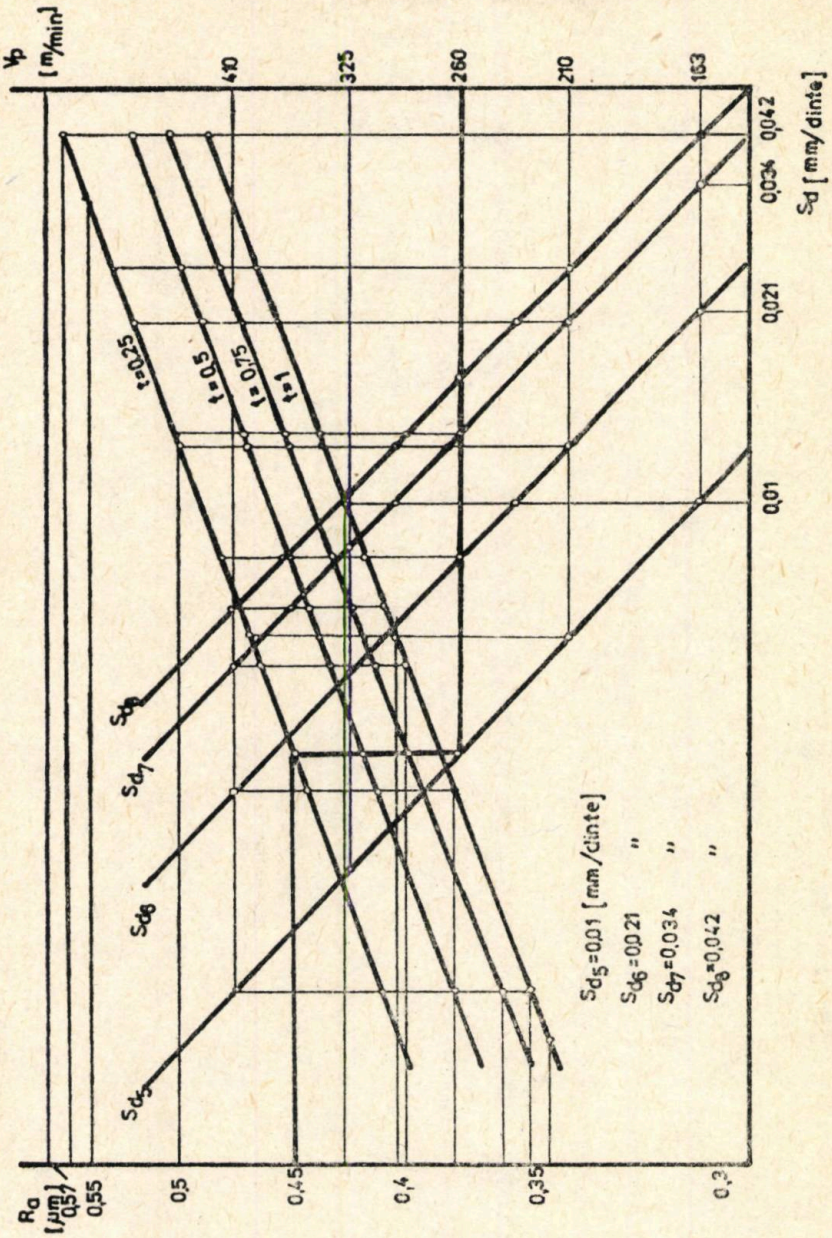

Fig. 4 — Nomogramme: variation de la rugosité Ra en function des éléments du régime de coupe au fraisage de finition.

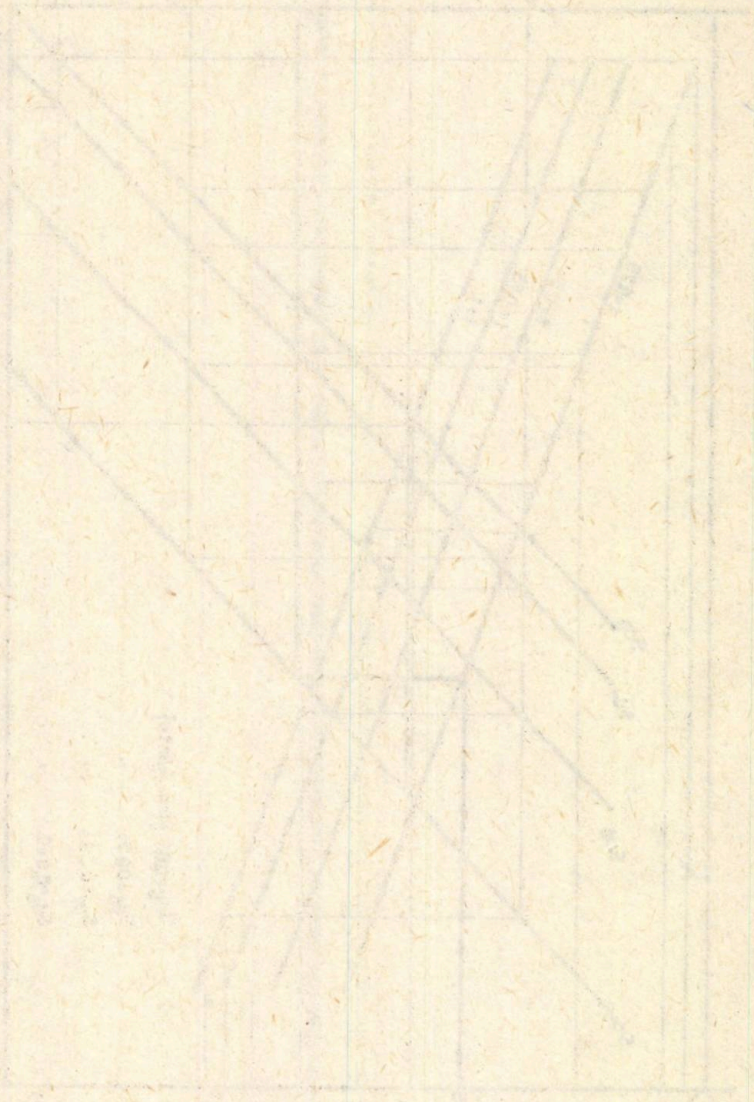

ce sens afin de déterminer le coefficient K_R et les exposants X_R, Y_R, Z_R, Q_R est donné dans la fig. 2, tandis que les valeurs obtenues sont données dans le Tableau 1.

Tableau 1

Coefficients et exposants	Fraisage de dégrossissage		Fraisage de finition		
	MoCN 15	RUL 2	MoCN 15	VMoCN 17	RUL 2
K_R	2,29	1,576	1,016	2,308	1,63
X_R	−0,192	−0,240	−0,117	−0,277	−0,254
Y_R	0,451	0,5	0,043	0,143	0,012
Z_R	0,164	1,172	0,048	0,022	−0,33
Q_R	0,288	0,153	−0,032	0,152	−0,015

L'emploi des coordonnées logarithmiques a permis d'établir les nomogrammes des figs. 3 et 4 d'où l'on détermine directement les éléments des régimes de coupe qui permettent d'obtenir une certaine rugosité.

5. Conclusions. Si l'on analyse le mode de variation de la rugosité de surface Ra, en fonction des paramètres des régimes de coupe et du nombre de dents de l'outil de coupe, on peut en tirer les conclusions suivantes.

1. La rugosité Ra a des valeurs comprises entre les limites 0,2...1,0 μm, ce qui permet de supprimer à l'opération de rectification de dégrossissage (rectification appliquée sur le matérial en état non recuit) le processus technologique de fabrication des pièces de ces matériaux.

2. L'usinage des matériaux étudiés avec des outils soigneusement affûtés et rodés permet d'obtenir sans exception une rugosité Ra au dessous de 0,8 μm.

3. On a obtenu de grandes valeurs de Ra au dégrossissage des matériaux avec des profondeurs et des avances importantes, à des petites vitesses de coupe.

4. On a obtenu au fraisage de finition de faibles valeurs de la rugosité Ra avec des profondeurs de 1 mm à des grandes vitesses de coupe.

5. La rugosité Ra est influencée par la qualité de l'affûtaje de l'outil, ayant de très grandes valeurs (2 à 3 fois plus grandes) dans le cas de l'outil récemment affûté par rapport à l'outil à l'état rodé. L'explication en est la rugosité des plaquettes tout spécialement du tranchant de passage et la non-uniformité de l'attaque frontal des dents fixés axialement et montés sur une surface conique.

Reçue le 18 Mars, 1985

Institut Polytechnique, Jassy,
Chaire de Technologie de la Construction des Machines

BIBLIOGRAPHIE

1. Belousov V., *Freze cu dinţi deşi şi superdeşi pentru prelucrarea rapidă a ghidajelor maşinilor-unelte.* Inst. polit. Iaşi, 1978.

2. Paraschiv Dr., *Contribuții la studiul influenței metodelor de prelucrare asupra proprietăților fizico-mecanice ale stratului superficial la unele materiale pentru scule și elemente de rulmenți*. Teză de doctorat, Inst. polit. Iași, 1981.
3. Pruteanu O. V., *Tehnologia construcției de mașini*. Ed. did. și ped., Buc., 1983.

CONSIDERAȚII PRIVIND CORELAȚIA DINTRE RUGOZITATEA DE SUPRAFAȚĂ Ra ȘI PARAMETRII DE LUCRU LA FREZAREA FRONTALĂ

(Rezumat)

Se prezintă rezultatele cercetărilor legate de modul de variație a rugozității de suprafață Ra în funcție de toți parametrii principali ai regimurilor de lucru. Se stabilește o relație empirică de legătură cu indicarea valorilor coeficienților și exponenților pentru fiecare tip de frezare în parte și pentru fiecare sortiment de material. În final se trasează o serie de nomograme care permit alegerea directă a regimurilor de lucru convenabile pentru obținerea unei anumite valori a rugozității de suprafață, Ra.

BULETINUL INSTITUTULUI POLITEHNIC DIN IAŞI
Tomul XXXI (XXXV), Fasc. 1—4, 1985
Secţia IV
CONSTRUCŢII DE MAŞINI

C.D. 621.914 ; 534.4

LES SOURCES DES VIBRATIONS DE TORSION DE LA MACHINE À FRAISER LES ENGRENAGES

PAR

STAN PANAIT, MIRCEA COZMÎNCĂ et I. ROMANESCU

1. Introduction. Dans le procesuss du travail avec la machine à fraiser les engrenages à fraise développante, l'apparition des oscillations torsionales à l'axe porte-pièce influence négativement la précision de la forme et les dimensions des paramètres géometriques de la roue-pièce.

La détermination de l'influence de ces facteurs (l'erreur constructive-fonctionelle des éléments cinématiques, les masses sans équilibrage, les forces de frottement variable etc) et des facteurs de l'extérieur de la chaîne cinématique (la variation du moment de fraisage, la surface obtenue comme un envelopement etc) nécessite un appareillage complexe, mais les essais expérimentaux avec une grande consommation des matériaux ne peuvent pas donner une information précise sur la source des vibrations de torsion [1], [3], [5].

Des études scientifiques sur ce domaine [1], [2], [4], il en résulte que pour évaluer l'amplitude et la fréquence des composantes de la vibration de torsion, surtout à l'axe porte-pièce de la machine à fraiser les engrenages à fraise développante, on utilise des méthodes analytiques et expérimentaux, mais les méthodes de détermination des ces grandeurs font appel aux mesures directes de l'amplitude et de la fréquence (oscilllogrammes, enregistrements magnétiques, visualité sur l'oscilloscope etc) et aux mesures indirectes comme celles obtenues au contrôle complexe de la roue-pièce.

Les recherches expérimentales [1], [3], [2], mettent en évidence comment l'amplitude de la vibration de torsion dépend des paramètres du régime de coupe et de la charge de la chaîne cinématique. À l'augmentation de la vitesse de coupe de 4...5 fois l'amplitude s'acroît avec 38...50% et à un régime de fonctionnement en charge l'amplitude augmente avec 20...180% par rapport au régime de fonctionement à vide (fig. 1).

Ainsi les fréquences des composantes harmoniques de la vibration de torsion doivent être parmi les fréquences relatives des élémentes de la chaîne cinématique (l'arbre vis sans fin, les roues dentées de l'engrenage diviseur, les engrenages coniques, l'arbre porte-outil etc), ainsi que du processus de coupe (l'entrée par la coupe des dents fraise-mère hélicoïdale).

Dans cet article, nous proposons une méthodologie à établir les grandeurs caractéristiques de la vibration de torsion produite par un des engre-

nages de la chaîne cinématique de roulage-division de la machine à fraiser les engrenages à fraise développante FD 250.

2. Détermination de la source de vibration de torsion. L'erreur cinématique d'un engrenage est l'effet des erreurs de construction et de montage de ses deux roues dentées qui deviennent actives en fonctionement.

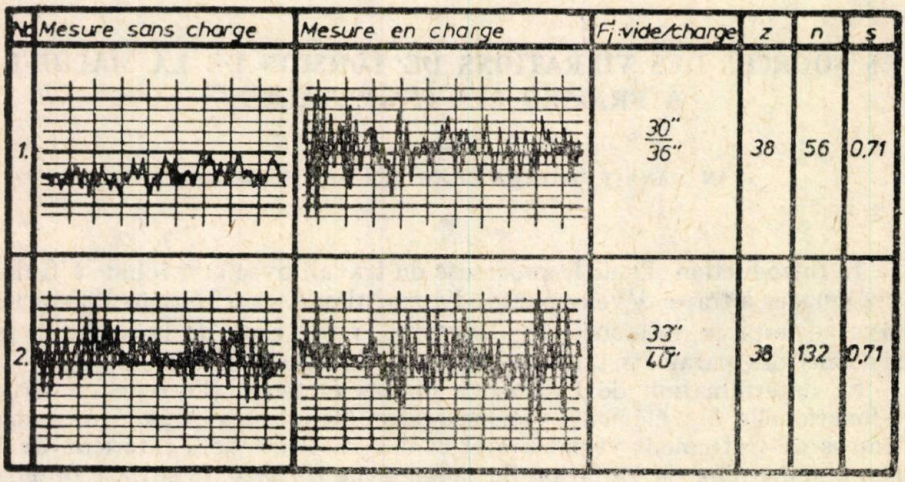

Fig. 1

Comme suite l'irrégularité de mouvement est composée par beaucoup de composantes harmoniques avec des différentes pulsations et amplitudes.

La variation du jeu circulaire entre les dents en contact représente un important facteur de l'apparition d'une vibration de torsion dans l'engrenage (son effet est de 2...4 fois plus grand que dans le cas de la déformation sous charge ou des erreurs au profil [1]). À cause de la variation du jeu entre les dents en engrenage, l'impulsion de la masse, qui actionne sur le dent de la roue dentée conduite, produira une accelération et une torsion de l'arbre conduit et conducteur.

À noter que l'engrenage se trouve dans la chaîne cinématique composée, le brin conducteur est freiné et le brin conduit est accéléré.

Aussi, dans la chaîne cinématique et les autres engrenages vont se produire des effets semblables, ainsi que la chaîne cinématique sera torsionée en différents points.

Pour établir la grandeur de l'amplitude et de la fréquence de la vibration de torsion, générée par la variation du jeu circulaire entre les dents en contact, il est nécessaire la détermination du moment d'une force, denommé en suite moment dynamique M_d, produit par l'effet des forces d'inertie de la chaîne cinématique.

Dans l'absence du jeu dans le système, sans considérer l'amortissement, l'arbre conduit $i+1$ se torsione avec l'angle φ determiné par

(1) $$\varphi = \frac{\omega_{i+1}}{\omega} \sin \omega t \qquad [\text{rad}],$$

où ω est la pulsation des vibrations de torsion du système équivalent (fig. 2) déterminée par

(2) $$\omega = \frac{2\pi}{\tau} \sqrt{\frac{k_{i+1}}{J_{i+1}}} \qquad [\text{s}^{-1}],$$

où τ est la période, k_{i+1} — la rigidité de l'arbre conduit (équivalent) et J_{i+1}—le moment d'inertie de la roue conduite $i+1$.

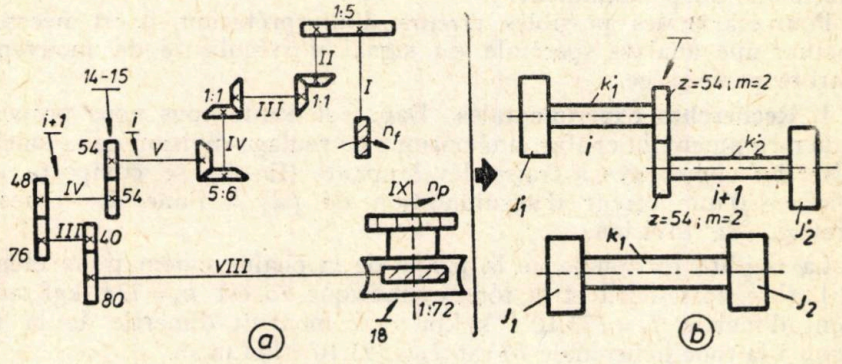

Fig. 2

Le moment qui exécute la torsion avec l'angle φ de l'arbre $i+1$ avec la rigidité k_{i+1} est

(3) $$M_d = k_{i+1}\varphi \qquad [\text{N.m}].$$

La roue conductrice donne à la roue conduite un mouvement proportionnel avec l'erreur cyclique f_{zkr} Si on considère cette erreur cyclique avec la répartition égale sur les deux roues dentées, alors le déplacement sera donné par la relation

(4) $$\varphi = \Delta = 2f_{zkr} \qquad [\text{rad}].$$

Après remplacement convenable on obtient

(5) $$M_d = \omega^2 J_{i+1} \Delta \qquad [\text{N.m}].$$

Pour la vitesse de variation du jeu circulaire $\dot{\Phi} = \omega\varphi$ [rad/s] la durée du déplacement sans charge du dent, au jeu entre les dents d'un engrennage φ_g, on peut écrire

(6) $$t = \frac{\varphi_g}{\dot{\Phi}}.$$

La fréquence de vibration de torsion pour le jeu entre dents φ_g est

(7) $$f = \frac{1}{2t + \tau} \qquad [\text{Hz}].$$

L'oscillation qui résulte est sinusoïdale. Après la première entrée forcée dans l'engrenage a lieu une diminution du moment et une décharge instantanée des arbres jusqu' au nouveau rattrapage du jeu, quand le même dent (ou le multiple) de la roue conductrice transmettra une nouvelle impulsion à la roue conduite. D'autre part entre les deux impulsions d'une valeur maxime, à l'arbre commandé apparaissent des autres vibrations, mais avec amplitude et fréquence différentes.

En réalité, dans la chaîne cinématique il y a des engrenage les sollicitations de torsion desquelles doivent être analysées simultanément, parce que chacun est lié élastiquement avec d'autres masses qui se déplacement indépendamment.

Pour écarter les possibles erreurs d'interprétation, il est nécessaire d'effectuer une analyse spectrale du signal d'irrégularité du mouvement du l'arbre porte-pièce.

3. **Recherches expérimentales**. Dans cet étude nous nous proposons d'étudier comment la chaîne cinématique de roulage division de la machine à fraiser les engrenages à fraise développante (fig. 2) se comporte dans la présence d'une erreur d'accumulation de pas à l'une des roues de l'engrenage de division.

La rigidité torsionale de la partie de la chaîne cinématique étendue entre l'arbre porte-outil et la roue cylindrique *15* est $k_1=723$ kgf/rad, le moment d'inertie $J_1=273.10^{-5}$ kgf.m s^2, le moment d'inertie de la roue *15* jusqu'à la roue hélicoïdale *18* est $J_2=593.10^{-5}$ kgf.m.s^2.

Si on considère un jeu normal entre les dents de l'engrenage *14* et *15* en négligeant l'amortissement, la pulsation du système équivalent est $\omega=\sqrt{k_1/J_1}=394{,}17$ s^{-1} et la période d'oscillation $\tau=0{,}0179$ s.

Pour trouver sans difficulté la fréquence de la vibration de torsion provenue de l'engrenage *14—15*, la roue *15* avec $z=54$ dents a été usinée par la machine à fraiser à fraise molette à tailler les engrenages et, sans être rectifiée, a été assemblée dans l'engrenage de division de la machine FD 250.

Pour cette roue dentée on a mesuré l'erreur cyclique f_{zkr} qui a été égale avec 430 μm (un angle de 0,007 rad). L'autre roue de l'engrenage a eu l'erreur cyclique $f_{zkr}=10$ μm (un angle de 0,00016 rad).

À supposer que les deux erreurs s'additionnent, il en résulte un angle de 0,00716 rad.

Au réglage cinématique correspondant à l'usinage d'une roue dentée avec $z=38$ dents on a choisi le nombre de tours à l'axe de l'outil $n_f=175$ rot/min. Dans cette situation les roues *14* et *15* ont le nombre de tours de 1 050 tr/min., mais la pulsation de l'erreur cumulée du pas est 3 fois la rotation de la roue.

Il resulté que la fréquence d'entrée dans l'engrenage de ces deux roues est $f_c=52{,}5$ Hz ($\omega_c=329{,}8$ s^{-1}).

L'amplitude du moment dynamique, à cause des defauts de l'engrenage *14—15*, calculée par la relation (5), est $M_{max}=4{,}43$ N.m et la deformation angulaire du système équivalent est $\varphi=M_{max}/k\approx 61.10^{-5}$ rad.

Le jeu mesuré (avec l'appareil) entre les flancs de l'engrenage *14* et *15* est égal à $J_{max}=0{,}2$ mm, ce qui corresponde à une course à vide de la

chaîne cinématique $\varphi = 32.10^{-4}$ rad. À une vitesse de variation du jeu $\dot{\Phi} =$ 0,2 rad/s, la course à vide a lieu dans une période $t = 0{,}016$ s.

La période des vibrations de torsion sera égale à $T = 2.0{,}016 + 0{,}0179 = 0{,}0499$ s et la fréquence $f \approx 20$ Hz.

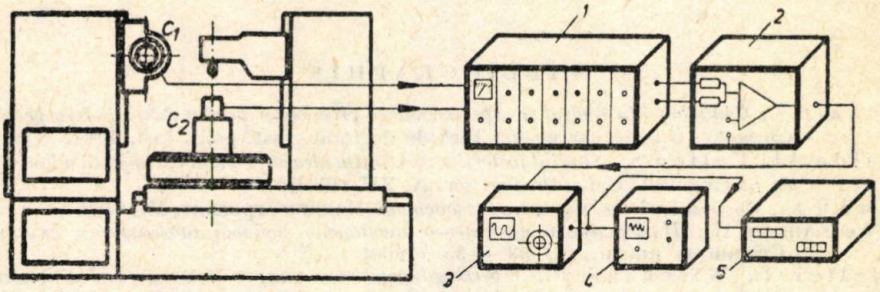

Fig. 3

Pour la détermination expérimentale des composantes de la vibration de torsion on a utilisé une installation de mesure avec un bloc-diagramme présenté dans la fig. 3. Les signaux électriques, transmis par les capteurs à masse inertiale C_1 et C_2, sont passés et traités dans un amplificateur tensométrique *1*, modèle N 2302.

À la suite, pour réaliser l'analyse en fréquence, à la sortie de cet amplificateur tensométrique on a connecté un analyseur de fréquence *3*, avec des possibilités d'hétérodyner le signal. Au moment où la fréquence d'hétérodine coïncide avec les fréquences du signal sur l'appareil indicateur ou sur le tube cathodique de l'oscilloscope *4* (EO102) aparaît un saut d'une certaine amplitude égale à la puissance par l'unité de largeur de la bande de fréquence (spectre de lignes). On lit la fréquence d'hétérodine sur un fréquencemètre compteur *5* (EO205) monté en parallèle avec l'oscilloscope *4*.

L'analyse du signal de l'irrégularité du mouvement de l'arbre porte-outil a mis en évidence une fréquence $f_m = 26{,}5$ Hz qui provient de l'engrenage diviseur.

Entre la fréquence calculée et celle mesurée on trouve une différence de 13%. La différence est due surtout à la grandeur du jeu réel entre les deux engrenages, tenant compte que la valeur $\varphi_g = 0{,}0032$ rad à été obtenue par la mesure sur l'appareil pour vérifier le jeu. De même, les moments d'inertie ont été calculés avec approximation.

4. Conclusions. 1. L'essai démontre que pour une modification périodique du jeu entre les dents des roues dentées qui doivent entrer en engrenage, a lieu l'apparition d'un moment dynamique qui produit une vibration torsionale qui influence les composantes du cycle de l'arbre porte-pièce ou porte-outil.

2. L'amplitude de cette vibration de torsion dépend de la grandeur du jeu et du rapport entre l'élément final et la roue d'où provient la vibration de torsion. Ainsi à l'arbre porte-outil l'amplitude de vibration sera environ 73'' et à l'arbre porte-pièce de 4''.

3. L'amplitude et la fréquence de la vibration de l'engrenage dépendent de l'érreur cyclique f_{zkr}, du moment d'inertie des élémentes de la chaîne cinématique et du jeu de l'engrenage.

Reçue le 4 Mars, 1985

Institut Polytechnique, Jassy,
Chaire de Machines-Outils

BIBLIOGRAPHIE

1. Panait S., *Contribuţii la studiul şi experimentarea procedeelor pentru determinarea preciziei cinematice a maşinilor unelte.* Teză de doctorat, Inst. polit. Iaşi, 1984.
2. Vaida Al., Velicu S., *Studiul factorilor care influenţează precizia cinematică a lanţurilor de filetare.* Bul. Univ. Braşov, ser. A, **XII** (1971).
3. Опиц Х., *Современая техника производства.* Машиностроение, М., 1975.
4. Степанек К., *Измерение и повышение точность зубообратывающих станков.* Станки и инстр., 2, 33 — 35 (1960).
5. Pfeifer T., Wiechenn R., *Übertragungsfehlermessung. Methodik und Einsatzmöglichkeiten bei kinematischen Untersuchungen an Werkzeugmaschinen.* Teil 2, *Kinematische Untersuchungen an mechanischen Übertragungssystemen.* Messwertanalyse, VDI-Z,. **122**, *3*, 81—86 (1980).

NATURA VIBRAŢIILOR TORSIONALE DIN MAŞINA DE FREZAT DANTURĂ

(Rezumat)

Pe baza unor studii teoretice şi experimentale, se determină una din cauzele apariţiei vibraţiilor torsionale în lanţul cinematic de rulare-divizare al maşinii de frezat dantura, model FD 250.

Cercetările evidenţiază că una din cauzele generatoare de vibraţii torsionale din maşina de frezat dantură o reprezintă variaţia jocului în angrenaj.

BULETINUL INSTITUTULUI POLITEHNIC DIN IAŞI
Tomul XXXI (XXXV), Fasc. 1—4, 1985
Secţia IV
CONSTRUCŢII DE MAŞINI

D.K. 621.941 ; 621.9.015

BEITRÄGE ZUM EINFLUSS DER ZENTRIFUGALKRAFT BEI UNWUCHT AUF DIE OBERFLÄCHENRAUHIGKEIT WÄHREND DES FEINDREHENS VON NICHTSTARREN WELLEN

VON

V. BRAHA, OCTAVIAN PRUTEANU, DRAGOŞ PARASCHIV, ROMEO CUDRIC und GAVRIL MUSCĂ

1. Vorwort. Infolge einer Reihe von Faktoren wie z.B. die Nichthomogenität des Materials, Ungenauigkeit beim Spannen des Werkstückes oder des Werkzeuges, die exzentrische Form des Werkstückes oder der Vorrichtungen, die das Werkstück in Rotationsbewegung setzen, Fehler beim Giessen, ungleichförmige Abnutzung des Schneidwerkzeuges usw., die in der laufenden Produktion praktisch nicht auszuschalten sind, fallen die Rotationsachse des Werkstückes oder des Werkzeuges und die des Gewichtsschwerpunktes nicht mehr zusammen.

Bei grossen Drehzahlen führt dieses Nichtzusammenfallen der beiden obengenannten Achsen, infolge der Zentrifugalkräfte bei Unwucht und der Trägheitsmomente, zum Auftreten von grossen Beanspruchungen an den Lagern. Durch die Einwirkung der Zentrifugalkräfte und der Trägheitsmomente infolge der statischen oder dynamischen Unwucht treten verschiedene Bearbeitungsfehler am Werkstück auf [1]...[3].

Bei unterschiedlichen Bearbeitungen, wie Aussendrehen, Innendrehen, Fräsen, Aussenschleifen, Innenschleifen und Bohren, werden die Werkstücke oder Werkzeuge infolge der unterschiedlichen Starrheit der Werkstücke und der Baugruppen der Werkzeugmaschinen und unter dem Einfluss der Schnittkräfte und der Zentrifugalkräfte in kreiselnde Bewegung gesetzt. Dadurch erfogt eine Abnahme der Bearbeitungsgenauigkeit und der Oberflächengüte des zu bearbeitenden Werkstückes [4],[5].

Zur Zeit wurde mit Erfolg im Falle des Aussenschleifens erreicht das Rotationssystem ins Gleichgewicht zu bringen.

Für die anderen Bearbeitungsfälle wurden Vorrichtungen zur Ausschaltung der Unwucht des Werkstückes entwickelt, auf die aber mit der Zeit verzichtet wurde, da diese Lösung zur Komplizierung der Werkzeugmaschinenkonstruktion oder zu nichterwarteten Ergebnissen führte [6].

Davon ausgehend, richteten sich die Untersuchungen in der letzten Zeit auf die Feststellung des Einflusses der Zentrifugalkräfte bei Unwucht auf die Oberflächenrauhigkeirt und auf die Formgenauigkeit der zu bearbeitenden Werkstücke. Dabei wird versucht, die Zusammenhänge zwischen ihnen und der Unwucht sowie auch der Einfluss der durch Unwucht aufgetretenen Abweichungen zu bestimmen [4]...[6].

2. **Arbeitsweise**. Dieser Beitrag befasst sich mit der Untersuchung des Einflusses der Zentrifugalkraft bei Unwucht auf die Oberflächenrauhigkeirt beim Feindrehen von nichtstarren Werkstücken.

Zur Bestimmung des Einflusses der Zentrifugalkraft bei Unwucht und also der Grösse der Unwucht des Halbzeuges wurde ein Dorn mit $L/D=12$ verwendet, auf den die für Untersuchungen verwendeten Prüflinge durch ein Spannbuchsensystem gespannt wurden.

Als Prüflinge wurden Ringe aus OLC 45, STAS 880-73, mit einer mittleren Härte von HB=197, die durch Glühbehandlung erreicht wurde, verwendet.

In dem vorgeschlagenen Modell kann die Zentrifugalkraft bei Unwucht bezüglich ihrer Grösse und Lage entlang der Drehachse des Werkstückes verändert werden. Ausserdem gestattet das Arbeitsmodell die Änderung der Lage der zu bearbeitenden Fläche entlang des Dornes (Abb.1)

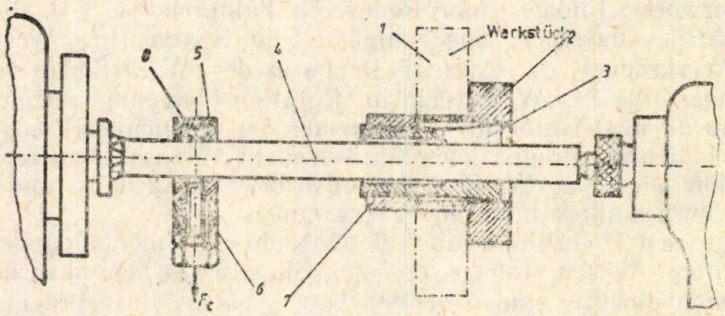

Abb. 1

Der Prüfling *1* wird auf den Dorn *4* mittels des Teiles *2* und der Spannbuchse *3* gespannt. Durch die Mutter *7* erfolgt das Spannen der Spannbuchse *3* auf den Dorn *4* sowie auch des Prüflings. Da sich die Spannbuchse *3* entlang des Dornes *4* bewegen kann, kann der Prüfling verschiedene Lagen in Bezug auf die Zentrifugalkraft bei Unwucht, erzeugt durch die auf dem Ring *5* angebrachten Gewichtet *6*, einnehmen.

Das angewendete Modell gestattet auch eine Änderung der Zentrifugalkraft bei Unwucht gegenüber der zu bearbeitenden Fläche durch die Lageänderung des Ringes *5*, der an verschiedenen Stellen auf dem Dorn mittels der Schraube *8* befestigt werden kann.

Die Versuche in der vorliegenden Arbeit wurden mit einem Drehmeissel mit mechanische festgeklemmten Wendeplatten aus der Gruppe P 20 durchgeführt, die folgende charakteristischen Werte aufweisen: $\varkappa=60°$, $\varkappa_1=30°$, $\alpha=4°$, $\gamma=6°$, $r=0{,}8$ mm. Um den Einfluss der Abnutzung auf die Oberflächenrauhigkeit auszuschalten, wurde in allen Untersuchungsfällen mit einer Spitze der Wendeplatte auf einer Länge von nur $l=10$ mm gedreht. Das dabei angewendete Arbeitsregime entspricht einem Feindrehen mit $t=1$ mm, $s=0{,}132$ mm/Umdrehung, wobei die Schnittgeschwindigkeit durch Benutzung von 5 verschiedenen Drehzahlen des Dreh-

zahlbereiches der Drehmaschine SNB 400 × 1 000 verändert wurde. Der Einfluss der Drehgeschwindigkeit auf die Oberflächenrauhigkeit wurde dadurch ausgeschaltet, dass nur höchstens 5 Läufe auf jedem Prüfling durchgeführt wurden. Entsprechend der 5 Drehzahlen wurden je 6 Unwuchtswerte bestimmt. Zum Vergleich für jede Gruppe von Untersuchungswerte wurde je ein Prüfling bei Unwucht gleich Null gedreht.

Für die Beurteilung der Rauhigkeit der bearbeiteten Oberfläche wurde der arithmetische Mittelwert der Rauhigkeit Ra ermittelt. Bei den Messungen wurde ein Profilschreiber-Profilmesser Typ AI, Modell 252, von der Firma Kalibri-UdSSR verwendet.

3. **Versuche.** Die Untersuchungen in dieser Arbeit wurden durchgeführt, um den Einfluss der Umwucht neben dem Spindelstock auf die Rauhigkeit der bearbeiteten Oberfläche für verschiedene Lagen auf dem Dorn zu studieren. Damit wurde der Zustand der durch den Mitnehmer erzeugten Unwucht modelliert.

Die notwendige Anzahl von Messungen für die Bestimmung des Rauhigkeitswertes bei einem vorgegebenen Vertrauenswert P kann mit Hilfe des folgenden Zusammenhanges berechnet werden [7]:

$$n \geqslant \left[\frac{t(P)}{\varepsilon}\right] s^2, \tag{1}$$

wobei: $t(P)$ — eine in Abhängigkeit von dem vorgegebenen Vertrauenswert P tabellierte Grösse; ε — zulässige Abweichung bei der Abschätzung des Rauhigkeitswertes; s — Standardabweichung der Messungen des Rauhigkeitsparameters.

Da s vorher nicht bekannt ist, wurde die notwendige Anzahl von Messungen empirisch bestimmt. Bei einem Wert von $P=0{,}95$ und $q=1$ wurde anhand von [7] ein Wert von $n=7$ Messungen ermittelt. Es wurden $n=10$ Messungen gewählt, was $P=0{,}99$ entspricht. Damit die Versuchswerte durch die Methode der kleinsten Quadrate ausgewertet werden können und die mathematischen Berechnungen einfach sind, wurde die Unwucht mit einem Schritt von 0,0029 daN vergrössert, der konstant bei allen Versuchen eingehalten wurde.

Die arithmetischen Mittelwerte der zehn Messungen der mittleren arithmetischen Abweichung Ra, sind in Tabelle 1 eingetragen

In den Abbn. 2 bis 7 ist der Zusammenhang zwischen der Oberflächenrauhigkeit und der Zentrifugalkraft bei Unwucht dargestellt, wobei bekannt ist, dass $F_c=H\omega^2$.

Den Lauf der eingezeichneten Kurven analysierend, wurde festgestellt, dass der Zusammenhang zwischen der Oberflächenrauhigkeit, der Rundlaufabweichung und der Unwucht bzw. der als Folge der Unwucht aufgetretenen Zentrifugalkraft als Polynom geschrieben werden kann, ohne dass dessen Grad vorher bekannt ist. Im Falle der Anwendung der Polynome als empirische Formeln tritt das Problem der Festlegung des optimalen Polynomgrades auf, da ein zu kleiner Grad eine befriedigende Auswertung des empirischen Materials nicht gewährleistet und ein zu hoher Grad die Einzelmessfehler nicht ausgleicht.

Tabelle 1

Die arithmetischen Mittelwerte von Ra

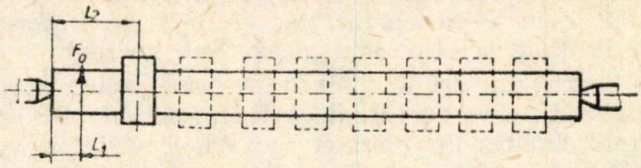

Länge L_2 mm	Drehzahl n Umdr./ Min.	Schnittgeschwindigkeit v m/s	P, daN						
			0	0,0029	0,0058	0,0089	0,0116	0,0145	0,0174
100	800	4,7	1,29	4,0	6,1	7,9	8,4	11,9	14,2
	1 250	6,8	5,09	2,0	1,4	1,2	1,2	1,6	1,1
	1 600	8,5	1,0	1,15	1,75	1,8	1,0	0,95	0,85
	2 500	14,3	0,59	1,0	6,0	6,2	6,4	7,2	8,2
150	800	4,7	11,0	13,0	15,8	18,5	22,0	26,3	29,7
	1 250	6,8	17,5	14,5	17,0	21,5	24,0	25,6	27,1
	1 600	8,5	1,5	1,8	2,8	4,9	10,0	12,0	14,0
	2 500	14,3	1,8	2,1	5,2	6,7	7,6	8,2	8,5
200	800	4,7	27,8	26,0	22,0	22,0	18,0	18,0	20,0
	1 250	6,8	11,1	11,2	12,0	12,2	15,5	20,0	24,3
	1 600	8,5	1,1	1,5	6,2	5,5	21,0	24,0	26,0
	2 500	14,3	1,8	2,1	5,2	6,7	7,6	8,2	8,5
250	800	4,7	27,8	26,0	22,0	22,0	18,0	18,0	20,0
	1 250	6,8	11,1	12,2	12,0	12,2	15,5	20,0	24,3
	1 600	8,5	1,1	1,5	6,2	5,5	21,0	24,0	26,0
	2 500	14,3	1,94	1,5	1,4	1,5	2,0	10,0	12,0
300	800	4,7	21,8	18,0	20,5	23,5	27,5	33,0	47,0
	1 250	6,8	22,65	12,7	13,2	16,95	25,2	25,5	29,8
	1 600	8,5	22,7	22,0	20,82	20,92	22,8	26,5	29,1
	2 500	14,3	2,75	3,6	4,08	11,5	16,1	23,3	30,5
350	800	4,7	16,5	17,0	17,2	20,2	23,5	24,2	26,2
	1 250	6,8	18,0	16,0	18,5	20,5	23,5	27,5	31,5
	1 600	8,5	18,9	19,2	20,2	21,5	23,4	24,8	27,5
	2 500	14,3	3,8	4,0	5,2	9,5	16,1	22,1	28,1
400	800	4,7	13,8	14,4	15,3	16,2	17,5	17,9	18,8
	1 250	6,8	13,0	13,86	18,4	20,3	15,2	14,1	15,3
	1 600	8,5	14,3	15,75	23,0	25,1	22,8	16,8	16,4
	2 500	14,3	3,1	13,1	19,7	23,3	28,5	17,95	18,0
450	800	4,7	14,5	16,0	15,4	16,8	18,0	19,5	20,8
	1 250	6,8	15,2	15,4	16,2	16,0	17,8	18,2	19,0
	1 600	8,5	14,2	16,0	21,5	24,6	22,2	18,0	17,2
	2 500	14,3	4,2	12,0	19,2	23,5	27,5	23,4	25,0

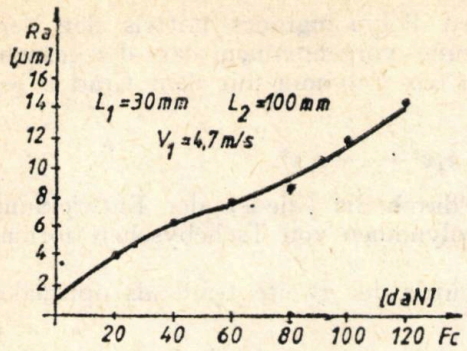

Abb. 2

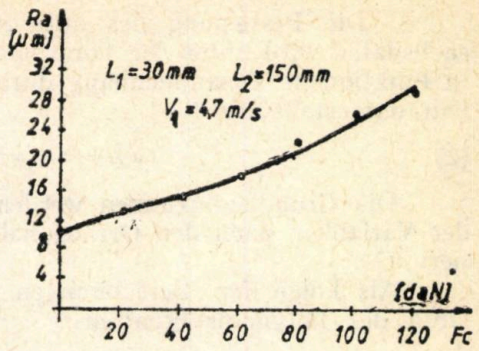

Abb. 3

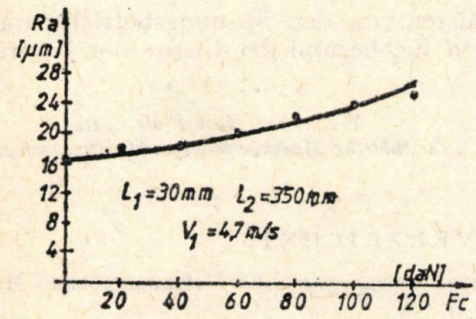

Abb. 4

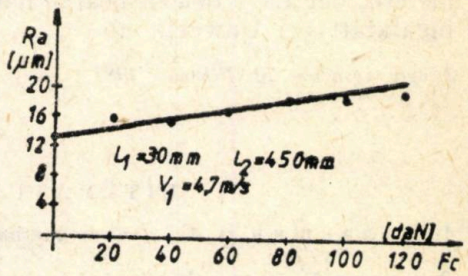

Abb. 5

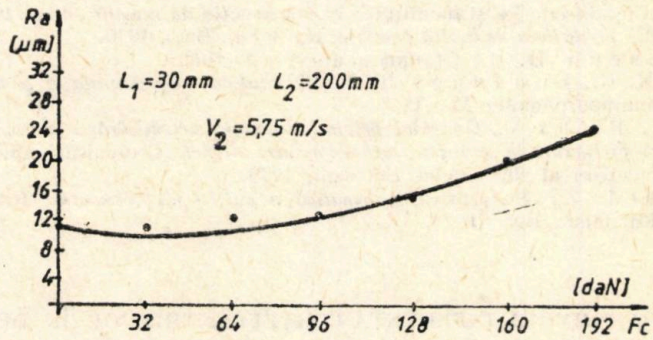

Abb. 6

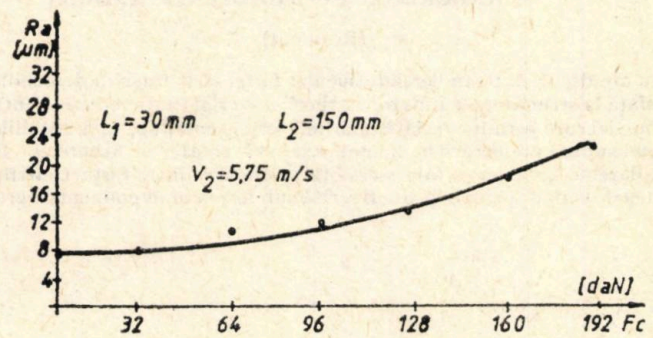

Abb. 7

Die Festlegung des optimalen Polynomgrades mittels der Versuchsdaten wird unter der Voraussetzung vorgenommen, dass der gesuchte funktionelle Zusammenhang durch das Polynom mit dem Grad n genau dargestellt ist

$$y=a_0+a_1x+a_2x^2+\ldots+a_nx^n. \tag{2}$$

Die Grundbedingungen werden durch die Glieder der Entwicklung der Variablen nach den Orthogonalpolynomen von Tschebyscheff formuliert [7].

Als Folge der Berechnungen wurde der zweite Grad als optimaler Grad des Polynoms erhalten

$$\mathrm{Ra}=AF_c^2+BF_c+C.$$

Die Konstanten A, B und C hängen von den Spanungsbetriebsparametern, der Lage der zu bearbeitenden Fläche und der Grösse der Zentrifugalkraft bei Unwucht ab.

Eingegangen am 12. Februar, 1985

Technische Hochschule, Jassy,
Lehrstuhl für Maschinenkonstruktionstechnologie

LITERATURVERZEICHNIS

1. Балакшин В. С., *Основы технологий машиностроения*. Машиностроение, М., 1966.
2. Braha V., *Asupra determinării pe calculator a traiectoriei axei piesei sub acţiunea forţelor centrifuge în dezechilibru şi a forţelor de aşchiere P_y şi P_z la strunjirea între vîrfuri*. „Creaţia tehnică şi fiabilitatea în construcţia de maşini", Iaşi, 1978.
3. Dodoc P., *Strunjirea de înaltă precizie*. Ed. tehn., Buc., 1970.
4. Котелевски Н. В., Станки и инстр., 5 (1962).
5. Колев К. С., Гопчяков Л. М., *Точности обработки и режимы резания*. Машиностроение, М., 1976.
6. Picoş C., Braha V., *Cercetări privind influenţa neechilibrării piesei asupra preciziei de prelucrare la strunjirea arborilor între vîrfuri*. „Comunicări ştiinţifice", Consiliul judeţean al sindicatelor Botoşani, 1978.
7. Rumşiski L. Z., *Prelucrarea matematică a datelor experimentale* (trad. din l. rusă). Ed. tehn., Buc., 1974.

CONTRIBUŢII PRIVIND INFLUENŢA FORŢEI CENTRIFUGE ÎN DEZECHILIBRU ASUPRA RUGOZITĂŢII DE SUPRAFAŢĂ LA STRUNJIREA DE FINISARE A ARBORILOR CU RIGIDITATE REDUSĂ

(Rezumat)

Lucrarea are drept scop studierea influenţei forţei centrifuge în dezechilibru asupra rugozităţii de suprafaţă la strunjirea de finisare a arborilor cu rigiditate redusă. Pentru experimentări s-a utilizat un model care permite variaţia mărimii forţei centrifuge în dezechilibru şi modificarea poziţiei epruvetei supuse prelucrării în lungul axei de rotaţie a arborelui. Prin prelucrarea matematică a datelor experiementale s-a obţinut o relaţie între forţa centrifugă în dezechilibru şi rugozitatea de suprafaţă, care poate fi scrisă sub forma unui polinom de gradul II.

BULETINUL INSTITUTULUI POLITEHNIC DIN IAŞI
Tomul XXXI (XXXV), Fasc. 1—4, 1985
Secţia IV
CONSTRUCŢII DE MAŞINI

C.D. 621.9.015

CONSIDÉRATIONS SUR L'INFLUENCE DES RÉGIMES DE COUPE SUR LA RUGOSITÉ DE SURFACE Ra PENDANT LA RECTIFICATION FRONTALE

PAR

DRAGOŞ PARASCHIV, OCTAVIAN PRUTEANU, GH. TEŞU et NINA AFRĂSINEI

1. **Considérations théoriques.** Afin de connaître les propriétés physiques de la couche superficielle il faut que l'on connaisse l'influence des facteurs qui concourent à l'usinage de surface. On sait bien que la couche superficielle se distingue par rapport au coeur du métal au niveau de la structure et des propriétés physiques.

La connaissance du mécanisme de formation de la couche superficielle aux usinages à abrasifs a une grande importance puisque ces opérations sont utilisées sur toutes les surfaces de précision à partir d'un usinage mécanique.

2. **Régimes de travail.** Pour mettre en vedette l'influence des facteurs technologiques sur la rugosité de surface, on a recours à une machine à rectifier frontale à segments abrasifs modèle 3756, produite en U.R.S.S. Les régimes de coupe utilisés sont donnés dans la fig. 1.

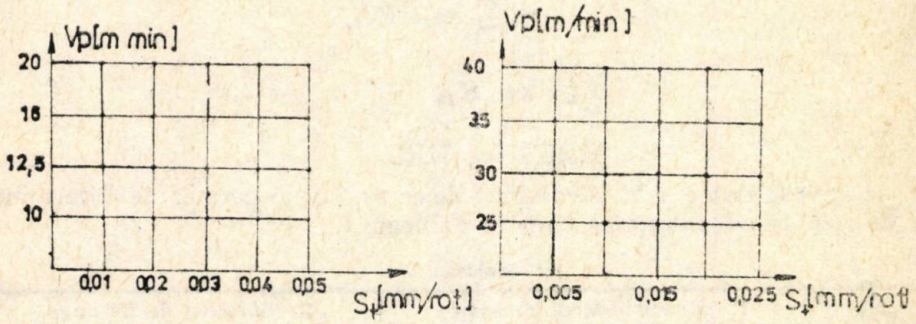

Fig. 1 — Régimes de coupe à la rectification : *a* — dégrossissage ; *b* — finition.

3. **Résultats expérimentaux.** En vue d'interpréter les résultats expérimentaux, on a utilisé le calcul statistique du coefficient empirique de corrélation r, gardant des valeurs différentes de l'unité, indigne de la dépendance des facteurs technologiques pris en considération, à savoir une dépendance linéaire.

Pour représenter graphiquement la rugosité, en fonction de la vitesse de la pièce v_p, de l'avance transversale S_t et de la dureté HRC à la rectientation, les valeurs moyennes de la rugosité Ra ont été soumises à l'alignetic conformément aux relations

$$X_0=\tfrac{1}{3}(X_{-1}+X_0+X_1),$$
$$X_{-1}=\tfrac{1}{6}(5X_{-1}+2X_0-X_1), \tag{1}$$
$$X_{+1}=\tfrac{1}{6}(-X_{-1}+2X_0+5X_1).$$

Dans le cas de la rectification, la rugosité Ra relève des facteurs technologiques ci dessus conformément à la relation

$$\mathrm{Ra}=K_R v_p^{X_R} S_t^{Y_R} \mathrm{HRC}^N. \tag{2}$$

Pour déterminer les valeurs du coefficient K_R et des exposants X_R, Y_R et N, on applique la méthode des moindres carrés; il en résulte un systhème de 4 équations à 4 inconnues :

$$mK'_R+\left(\sum_1^m v'_i\right)X_R+\left(\sum_{i=1}^m S'_{ti}\right)Y_R+\left(\sum_{j=1}^m \mathrm{HRC}'_i\right)N=\sum_{i=1}^m \mathrm{Ra}_i,$$

$$\left(\sum_{i=1}^m v'_i\right)K'_R+\left(\sum_{i=1}^m v'_i v'_i\right)X_R+\left(\sum_{i=1}^m S'_{ti}v'_i\right)Y_R+\left(\sum_{i=1}^m \mathrm{HRC}'_i v'_i\right)N=\sum_{i=1}^m \mathrm{Ra}'_i v'_i,$$

$$\left(\sum_{i=1}^m S'_{ti}\right)K'_R+\left(\sum_{i=1}^m v'_i S'_{ti}\right)X_R+\sum_{i=1}^m S'_{ti}S'_{ti}\Big)Y_R+\left(\sum_{i=1}^m \mathrm{HRC}'_i S'_{ti}\right)N=\sum_{i=1}^m \mathrm{Ra}'_i S'_{ti}, \tag{3}$$

$$\left(\sum_{i=1}^m \mathrm{HRC}'_i\right)K'_R+\left(\sum_{i=1}^m v'_i \mathrm{HRC}'_i\right)X_R+\left(\sum_{i=1}^m St'_i \mathrm{HRC}'_i\right)Y_R+\left(\sum_{i=1}^m \mathrm{HRC}'_i \mathrm{HRC}'_i\right)N=$$

$$=\sum_{i=1}^m \mathrm{Ra}'_i \mathrm{HRC}'_i,$$

où

$$K'_R=\log K_R,$$
$$\ldots\ldots\ldots$$
$$\mathrm{HRC}'=\log \mathrm{HRC}.$$

La résolution sur le calculateur de ce systhème permet de déterminer les valeurs désirées données dans le Tableau 1.

Tableau 1

Coefficients et exposants	Rectification de dégrossissage			Rectification de finissage		
	MoCN 15	RUL 2	VMoCN 17	MoCN 15	RUL 2	VMoCN 17
K_R	0,655	0,073	0,062	0,912	0,213	0,673
X_R	−0,339	0,089	0,278	−0,469	−0,227	−0,420
Y_R	0,216	0,078	0,204	0,037	0,029	−0,020
N	0,146	0,398	0,192	−0,047	0,045	−0,145

En utilisant la représentation graphique en coordonnées logarithmiques, on a tracé les nomogrammes de la fig. 2 qui permettent le choix juste des paramètres du régime de travail pour une certaine rugosité donnée.

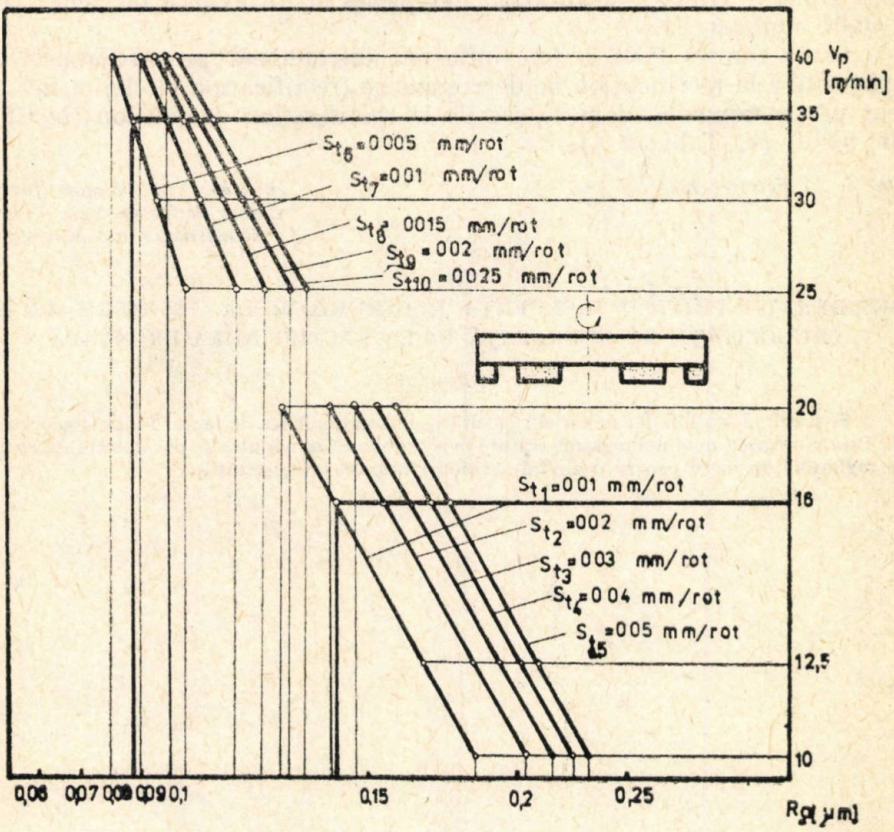

Fig. 2 — Nomograme : variation de la rugosité Ra en fonction des éléments du régime de coupe à la rectification frontale, à segments abrasifs.

4. Conclusions. Dans le cas de la rectification frontale à segments abrasifs sur une machine à rectifier à plateau tournant, la manière dont les paramètres des régimes de travail influence la rugosité de surface Ra, conduit aux conclusions suivantes.

1. La rugosité Ra a des valeurs différentes pour le dégrossissage et la finition, comprises entre 0,06 et 0,4 μm.

2. Le temps d'usinage modifie positivement la qualité de la surface mais diminue la productivité du processus. Les éprouvettes analysées ont été maintenues 15 minutes environ dans le processus d'usinage après le réglage de la profondeur de pénétration (avance transversale S_t).

3. L'usinage des éprouvettes a été aussi exécutée sous le liquide de graissage-refroidissement en émulsion, qui améliore la qualité des surfaces.

4. On a obtenu des valeurs élevées de la rugosité Ra (0,4 μm) au dégrossissage du matérial MoCH15 avec de faibles vitesses de rotation des pièces et des grandes avances de pénétration.

5. On a obtenu des faibles rugosités à la finition du matérial VMoCH17 à des grandes vitesses de rotation des pièces et un avance de pénétration S_t=0,01 mm/rot.

6. La dureté HRC a une influence directement proportionnelle sur la rugosité à la rectification de dégrossissage (rectification molle) et inversement proportionnelle, dans le cas de la rectification de finition (rectification forte) (v. Tableau 1).

Reçue le 11 Février, 1985

Institut Polytechnique, Jassy,
Chaire de Technologie de la
Construction des Machines

CONSIDERAŢII PRIVIND INFLUENŢA REGIMURILOR DE AŞCHIERE ASUPRA RUGOZITĂŢII DE SUPRAFAŢĂ Ra LA RECTIFICAREA FRONTALĂ

(Rezumat)

Se prezintă studiul dependenţei rugozităţii de suprafaţă Ra de factorii tehnologici principali. Prin realizarea unei nomograme trasate în coordonate logaritmice se pot determina elementele regimului de lucru pentru o anumită valoare impusă a rugozităţii.

BULETINUL INSTITUTULUI POLITEHNIC DIN IAŞI
Tomul XXXI (XXXV), Fasc. 1—4, 1985
Secţia IV
CONSTRUCŢII DE MAŞINI

D.K. 621.9.01

BETRACHTUNGEN HINSICHTLICH DER VERBINDUNG ZWISCHEN DEN PRÄZISIONSBEDINGUNGEN FÜR ZU BEARBEITENDE WERKSTÜCKE UND DEN FREIHEITSGRADEN, DIE DURCH AUSRICHTUNG DER WERKSTÜCKE BESEITIGT WERDEN MÜSSEN

VON

N. GHERGHEL

1. **Einführung.** Die Tatsache berücksichtigend, dass die Ausrichtung der Werkstücke die Beseitigung bestimmter Freiheitsgrade dieser voraussetzet, wird in der Konzepierung und Projektierung von Vorrichtungen die Festsetzung der Anzahl, der Natur (Verchiebung oder Drehung und die Zugehörigkeit zu einer bestimmten Achse des Orientierungssystems sowie die Bestimmung der Freiheitsgrade, die durch die Ausrichtung der Werkstücke beseitigt werden müssen, verlangt, unter Bedingungen von durch die Masszahl gesteuerten Systemen.

Die Freiheitsgrade, die durch Ausrichtung der Werkstücke beseitigt werden, müssen die Einhaltung aller bestimmenden Präzisionsbedingungen sowie auch einiger zusätzlicher Bedingungen, wie [6], [2]...[4]: Sicherung des Endes der Spankräfte, der zentrifugalen Trägheitskräfte und der Spannkräfte durch Orientierungs- oder Orientierungs-Spannelemente (Lager) und die Begrenzung der Arbeitszone der Spanwerkzeuge (des Vorschubs), gewährleisten, damit die Bearbeitungsproduktivität steigt.

Die vorliegende Arbeit enthält einige Beiträge hinsichtlich der Verbindung zwischen den Präzisionsbedingungen für die zu bearbeitenden Flächen und den Freiheitsgraden, die durch Ausrichtung der Werkstücke beseitigt werden müssen.

2. **Betrachtungen zur Verbindung zwischen den Präzisionsbedingungen und den durch Ausrichtung der Werkstücke zu beseitigenden Freiheitsgraden.** Ein Werkstück hat im dreidimensionalen Raum sechs Freiheitsgrade—g (drei Verschiebungen—t und drei Drehungen—r entlang der Achsen bzw. um die Achsen des Orientierungssystems).

Unter dem Begriff des Freiheitsgrades im Rahmen des Orientierungsprozesses versteht man die Möglichkeit der Placierung der Werkstücke im Verhältnis zu den Achsen des Orientierungssystems $O_0 X_0 Y_0 Z_0$.

Die Freiheisgrade, die durch Orientierung des Werkstückes beseitigt werden mussen, um die Einhaltung der ausschlaggebenden Präzisionsbedingungen (CD) zu gewährleisten entsprechen den Freiheitsgraden, die die Fläche oder die zu bearbeitende Flächengruppe im Bemassungssystem

$O_cX_cY_cZ_c$ hat. Zu erwähnen ist, dass man unter den bestimmenden Präzisionsbedingungen (*CD*) jene Präzisionsbedingungen versteht, die die relative Lage der Fläche oder die der zu bearbeitenden Flächengruppe angeben und die vom Ausrichtungsprozess des Werkstückes in der Vorrichtung beeinflusst werden bei durch Masszahlen gesteuerten technologischen Systemen.

Ihrerseits entsprechen die Freiheitsgrade, die die zu bearbeitende Fläche oder Flächengruppe hat, im Bemassungssystem den linearen Masszahlen oder Winkelmasszahlen, die von den bestimmenden Präzisionsbedingungen abgeleitet sind, unter Berücksichtigung der Tatsache, dass einige Präzisionsbedingungen der relativen Lage der Flächen äquivalent sind mit je zwei linearen Masszahlen oder Winkelmasszahlen. Zum Beispiel, eine Parallelitäts- oder Perpendikullaritätsbedingung ist äquivalent mit zwei Winkelmasszahlen, während eine Konzentrizitäts- oder Koaxialitätsbedingung äquivalent ist mit zwei linearen Masszahlen.

Die Verschiebungen entspreachen den linearen Masszahlen, und die Drehungen entsprechen den Winkelmasszahlen.

Manchmal verlangt die Einhaltung von zwei bestimmenden Präzisionsbedingungen die Beseitigung desselben Freiheitsgrades wegen der jeweiligen Lage, die die zu bearbeitenden Flächen im Bemassungssystem einnenhmen (z.B. eine ebene, perpendikuläre Fläche auf einer anderen ebenen Fläche, die simultan im Rahmen derselben Operation bearbeitet werden).

Die durch Ausrichtung entfernten Freiheitsgrade werden in der Regel dargestellet durch eine schräge Linie, die die doppelten rektangulären oder kreisförmigen Pfeile, plaziert an den Enden des Ausrichtungssystems, schneidet, und die die möglichen Freiheitsgrade des Werkstückes darstellen, Verschiebungen bzw. Drehungen.

Diese Freiheitsgrade können auch zusammengefasst werden in Tabellen der Form 1, 2 und 3 und komplettiert für die Operations- oder Phasenskizzen aus den Abbn. 1, 2, und 3.

In diesen Tabellen sind die Freiheitsgrade, die durch Ausrichtung beseitigt werden müssen, mit (—) notiert und jene, die nicht beseitigt werden müssen, mit (+).

3. **Methodologie zur Bestimmung der Freiheitsgrade, die durch Ausrichtung der Werkstücke beseitigt werden müssen,** Unter Berücksichtigung der direkten Verbindung, die zwischen den bestimmenden Präzisionsbedingungen (*CD*) für die zu bearbeitenden Oberflächen und den Freiheitsgraden, die durch Ausrichtung des Werkstückes beseitigt werden müssen, besteht, kann man, um diese Freiheitsgrade zu bestimmen, folgendermassen verfahren:

a) Ausgehend von jeder ausschlaggebenden Präzisionsbedingung (*CD*) für die zu bearbeitende Fläche oder Flachengruppe wird festgesetzt, welche Freiheitsgrade beseitigt werden müssen durch Ausrichtung des Werkstückes, um die entsprechenden Bedingungen zu gewährleisten, wobei der Einfluss der Freiheitsgrade auf die Einhaltung der Bedingungen berücksichtigt wird. Die entsprechenden Freiheitsgrade werden durch kleine schräge Striche mar-

kiert, die die Pfeile schneiden, die die möglichen Freiheitsgrade des Werkstückes auf der Operations- oder Phasenskizze darstellen. Diese Freiheitsgrade können in einer Tabelle der Tabellenformen 1, 2 und 3 zusammengefasst werden und ausgefüllt für die Operations- oder Phasenskizzen aus den Abbn. 1, 2 und 3. In diesen Tabellen werden die Freiheitsgrade, die durch Ausrichtung der Werkstücke beseitigt werden müssen, mit (—), aber jene, die nicht beseitigt werden müssen mit (+) gekennzeichnet. Auf diese Art und Weise kann man genau die Situationen festhalten, die einer vollständigen (statisch bestimmt) oder einer unvollständigen Ausrichtung (vereinfacht, statisch unbestimmt) bedurfen, und man kann Situationen der Beseitigung einer grösseren oder kleineren Anzahl von Freiheitsgraden vermeiden (Überorientierung ohne technisch-ökonomische Motivierung bzw. Unterorientierung) [6], [1], [3], [7], [4]. Wenn aus den bestimmenden Präzisionsbedingungen (CD) bervorgent, dass alle Freiheitsgrade des Werkstückes beseitigt werden müssen, dann ist die Fortführung einer Analyse der zusätzlichen Bedingungen nicht mehr notwendig [2], [4].

b) Im gegenteiligen Fall wird entschieden, welche Freiheitsgrade noch durch Ausrichtung des Werkstückes beseitigt werden müssen, um auch Einhaltung der Zusatzbedingungen zu gewährleisten, wie jene im §1 erwähnten ; ein Aspekt, der nicht Gegenstand der vorliegenden Arbeit ist.

c) Man fasst zusammen, welche Freiheitsgrade durch Ausrichtung der Werkstücke beseitigt werden müssen, um die Einhaltung der bestimmenden Präzisionsbedingungen und eventuell anderer, zusätzlicher Bedingungen abzusichern, sowie entscheidet man über den Typ des notwendigen Orientierungsschemas : komplet; inkomplet ; Überorientierung mit technisch-ökonomischer Motivierung.

Im weiteren werden einige Anwendungsbeispiele für die vorgestellte Methodologie dargelegt. Die Analyse beschränkt sich nur auf die bestimmenden Präzisionsbedingungen aus dem oben erwähnten Motiv.

Beispiel 1. Bei der Bearbeitungsoperation Fräsen, deren Skizze în Abb. 1 *a* dargestellt ist, wird die Einhaltung folgender bestimmender Präzisionsbedingungen verlangt:

CD_1—Einhaltung der Masszahl a (Ta);

CD_2—Einhaltung der Parallelität der Fläche A mit der Flache B.

Es muss die Tatsache berücksichtigt werden, dass die Einhaltung einer Parallelitätsbedingung zwischen zwei ebenen Flächen äquivalent ist mit Einhaltung der Winkelmasszahlen zwischen der Flächen A und B, sowohl in Richtung der Achse O_cX_c, als auch in Richtung der Achse O_cY_c.

Man kann erkennen, dass die Anzahl der aus den bestimmenden Präzisionsbedingungen für die zu bearbeitende Oberfläche obgeleiteten Masszahlen gleich ist der Anzahl der Freiheitsgrade, die die zu bearbeitende Fläche im Bemassungssystem hat, wobei die linearen Masszahlen den Verschiebungen und die Winkelmasszahlen den Drehungen entsprechen.

Um die beiden bestimmenden Präzisionsbedingungen einzuhalten, müssen die entsprechenden Freiheitsgrade durch Ausrichtung (Orientierung) des Werkstückes beseitigt werden (Abb. 1 *b* und 1 *c*).

Aus der Analyse über die Art und Weise, wie die Freiheitsgrade des Werkstückes die Einhaltung der bestimmenden Präzisionsbedingungen

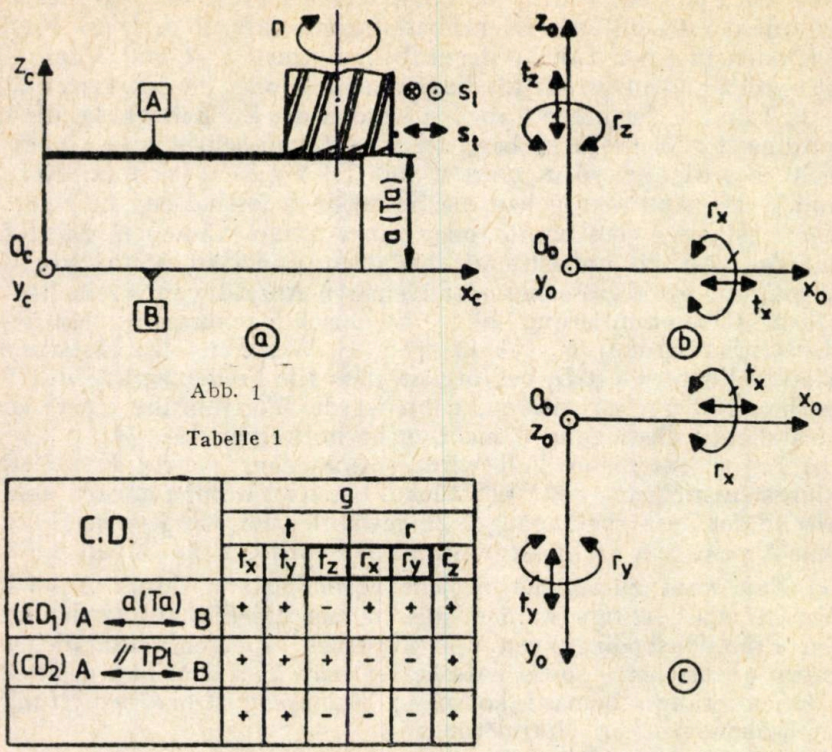

Abb. 1

Tabelle 1

C.D.	g					
	t			r		
	t_x	t_y	t_z	r_x	r_y	r_z
(CD_1) A —a(Ta)→ B	+	+	-	+	+	+
(CD_2) A —// TPl→ B	+	+	+	-	-	+
	+	+	-	-	-	+

beeinflussen, folgt, dass die Beseitigung folgender Freiheitsgrade notwendig wird:

a) die Einhaltung der Masszahl *a* (Ta) verlangt die Vermeidung einer Translation des Werkstückes entlang der O_0Z_0-Achse (t_z), weil unter den Bedingungen, unter denen das techonologische System durch die Masszahl *a* gesteuert wird, die Abweichung des Werkstückes vom Lot, mehr nach links oder mehr nach rechts verschoben in bestimmten Grenzen, zur Veränderung der Masszahl *a* führt, das heisst, man erhält einen Wert verschieden von dem, mit dem die Steuerung gemacht wurde ;

b) die Einhaltung der Parallelität der Fläche *A* zur Fläche *B* verlangt die Ausschaltung der Drehung um die Achsen O_0X_0 (r_x) und O_0Y_0 (r_y), weil unter den Bedingungen, unter denen das techonologische System mit der Masszahl *a* gesteuert wird, die Abweichung eines Werkstückes vom Lot, mehr nach links oder rechts gedreht gegenüber der Achse O_0X_0 oder O_0Y_0, in bestimmten Grenzen, zur Folge hat, dass die Fläche *A* nicht mehr parallel ist zur Fläche *B*.

Es folgt daraus, dass für die Einhaltung aller bestimmenden Präzisionsbedingungen die Beseitigung von drei Freiheitsgraden des Werkstückes notwending und ausreichend ist und zwar t_z, r_x und r_y, die in den Abbn. 1 *b* und 1 *c* sowie in der Tabelle 1 gekennzeichnet sind.

Beispiel 2. Bei der Bearbeitungsoperation (Phase) Fräsen, deren Skizze in Abb. 2 *a* dargestellt ist, wird die Einhaltung folgender bestimmender Präzisionsbedingungen verlangt:

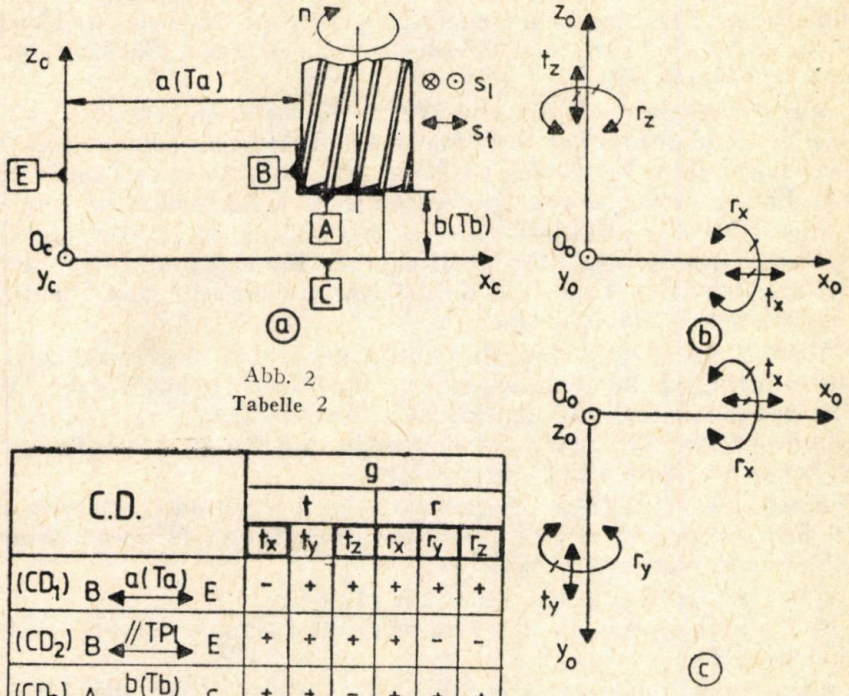

Abb. 2

Tabelle 2

C.D.	g					
	t			r		
	t_x	t_y	t_z	r_x	r_y	r_z
(CD_1) B a(Ta) E	-	+	+	+	+	+
(CD_2) B //TPl E	+	+	+	+	-	-
(CD_3) A b(Tb) C	+	+	-	+	+	+
(CD_4) A //TPl C	+	+	+	-	-	+
	-	+	-	-	-	-

CD_1—Einhaltung der Masszahl *a* (Ta);

CD_2—Einhaltung der Parallelität der Fläche *B* mit der Fläche *E*;

CD_3—Einhaltung der Masszahl *b* (Tb);

CD_4—Einhaltung der Parallelität zwischen der Fläche *A* und der Fläche *C*.

Die Einhaltung der Parallelität zwischen der Fläche *B* und der Fläche *E* ist äquivalent mit der Einhaltung der Winkelmasszahlen zwischen den Flächen *B* und *E*, sowohl in Richtung der Achse O_cY_c, als auch in Richtung der Achse O_cZ_c. Gleichfalls ist die Einhaltung der Parallelität zwischen den Flächen *A* und *C* äquivalent der Einhaltung der Winkelmasszahlen zwischen den Flächen *A* und *C*, sowohl in Richtung der Achse O_cX_c, als auch in Richtung der Achse O_cY_c.

Man kann feststellen, dass die Bedingungen CD_2 und CD_4 die Einhaltung einer gemeinsamen Winkelmasszahl einschliessen, und zwar der jeweiligen Lage, die die eine zu bearbeitende Fläche im Verhältnis zur anderen Fläche einnimmt (Fläche A ist perpendikulär zur Fläche B).

Es erweist sich also auch in diesem Fall, dass die Anzahl der aus den bestimmenden Präzisionsbedingungen abgeleiteten Masszahlen gleich ist der Anzahl der Freiheitsgrade, die die zu bearbeitende Flächengruppe im Bemassungssystem hat.

Aus der Analyse der Art und Weise, wie die Freiheitsgrade des Werkstückes dei Einhaltung der bestimmenden Präzisionsbedingungen beeinflussen, folgt, dass notwendig ist die in Abb. 2 *b*, 2 *c* und Tabelle 2 markierten Freiheitsgrade durch Ausrichtung des Werkstückes zu beseitigen.

Aus Tabelle 2 resultiert dass die Einhaltung der Bedingungen CD_2 und CD_4 die Beseitigung eines gemeinsamen Freiheitsgrades (r_y) verlangt wegen der jeweiligen Lage, die die beiden zu bearbeitenden Oberflächen im Bemassungssystem einnehmen.

Weiter folgt, dass für die Einhaltung aller bestimmenden Präzisionsbedingungen die Beseitigung von fünf Freiheitsgraden des Werkstückes norwendig und ausreichend ist und zwar: t_x, t_z, r_x, r_y, r_z. Diese Freiheitsgrade entsprechen den Freiheitsgraden, die die zu bearbeitende Flächengruppe im Bemassungssystem hat.

Beispiel 3. Bei der Bearbeitungsoperation Drehen oder Schleifen, deren Skizze in Abb. 3*a* dargestellt ist, wird die Einhaltung folgender bestimmender Präzisionsbedingungen verlangt:

CD_1—Einhaltung der Masszahl a (Ta);

CD_2—Einhaltung der Perpendikularität zwischen der Fläche A und der Fläche B;

CD_3—Einhaltung der Koaxialität der Fläche B mit der Fläche E.

Einhaltung der Perpendikularität der Fläche A auf der Fläche B ist äquivalent mit der Einhaltung der Winkelmasszahlen zwischen den Flächen A und B, sowohl in Richtung der Achse O_cY_c, als auch in Richtung der Achse O_cZ_c. Gleichfalls ist die Einhaltung der Koaxialität der Fläche B mit der Fläche E äquivalent mit der Einhaltung der linearen Masszahlen der Flächen B und E, sowohl in Richtung der Achse O_cY_c, als auch in Richtung der Achse O_cZ_c.

Es erweist sich also auch in diesem Falle, dass die Anzahl der aus den bestimmenden Präzisionsbedingungen für die zu bearbeitenden Flächen abgeleiteten Masszahlen gleich der Anzahl der Freiheitsgrade ist, die die Flächengruppe im Bemassungssystem hat.

Aus der Analyse der Art und Weise, wie die Freiheitsgrade des Werkstückes, die Einhaltung der bestimmenden Präzisionsbedingungen beeinflussen, resultiert, dass durch Ausrichtung die in den Abbn. 3 *b*, 3 *c*, und Tabelle 3 markierten Freiheitsgrade beseitigt werden müssen.

Es folgt, dass für die Einhaltung aller bestimmenden Präzisionsbedingungen die Beseitung von fünf Freiheitsgraden notwendig und ausreichend ist, und zwar: t_x, t_y, t_z, r_y, r_z. Diese entsprechen den Freiheitsgraden, die die zu bearbeitende Flächengruppe im Bemassungssystem hat.

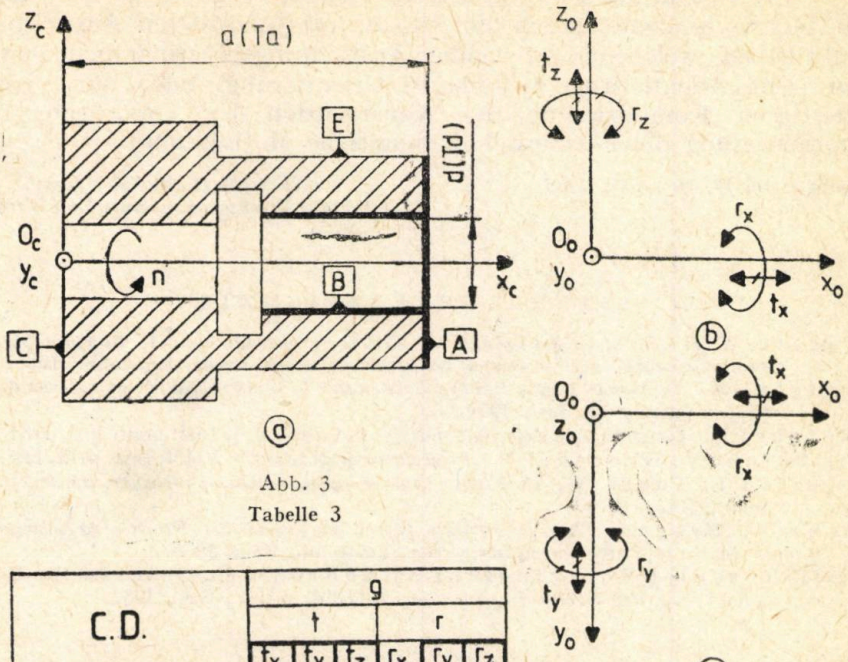

Abb. 3

Tabelle 3

C.D.	g					
	t			r		
	t_x	t_y	t_z	r_x	r_y	r_z
(CD_1) A ⟵ a(Ta) ⟶ C	-	+	+	+	+	+
(CD_2) A ⟵ ⊥TPd ⟶ B	+	+	+	+	-	+
(CD_3) B ⟵ ◎TPc ⟶ E	+	-	-	+	+	+
	-	-	-	+	-	-

4. Schlussfolgerungen. 1. Um inkorrekte Orientierungsschemas zu vermeiden, wie Überorientierung ohne technisch-ökonomische Motivierung, Unterorientierung und fehlerhafte Orientierung [5], [1], [4], [3], [6],[7], ist die exakte Festsetzung der Freiheitsgrade, die durch Ausrichtung des Werkstückes beseitigt werden müssen, notwendig.

2. Die im Rahmen der Arbeit vorgestellte Methodologie, die als Grundlage die direkte Verbindung, die zwischen den bestimmenden Präzisionsbedingungen (*CD*) für die zu bearbeitenden Flächen und den durch Ausrichtung zu beseitigenden Freiheitsgraden existiert, hat, entspricht den erwähnten Anforderungen.

3. Die dargelegten Betrachtungen tragen gleichzeitig zur wissenschaftlichen Fundierung der Ausrichtung der Werkstücke in den Vorrichtungen bei, also auch die Stellung der Konzepierung und Projektierung bei, also auch die Stellung der Konzepierung und Projektierung von Vorrichtungen auf eine wissenschaftlich Grundlage.

4. Die Bedeutung der vorgestellten Aspekte besteht in den ungünstigen technisch-ökonomischen Folgen, die die inkorrekten Ausrichtungsschemas haben, welche die notwendige Ausrichtungspräzision nicht gewährleisten (Unterorientierung, fehlerhafte Orientierung) oder zur nichtgerechtfertigten Komplizierung der Konstruktion der Vorrichtung führt (Überorientierung ohne technisch-ökonomische Motivierung).

Eingegangen am 19. Dezember, 1985

Technische Hochschule, Jassy,
Lehrstuhl für Werkzeugmaschinen und Werkzeuge

LITERATURVERZEICHNIS

1. Brăgaru A. și colab., *SEFA-DISROM. Sistem și metodă.* Vol. 1, *Teoria și practica proiectării dispozitivelor pentru prelucrări pe mașini-unelte.* Ed. tehn., Buc., 1982.
2. Gherghel N., *Îndrumar pentru lucrări de laborator la Construcția și exploatarea dispozitivelor.* Inst. polit. Iași, 1979.
3. Gherghel N., *Construcția și exploatarea dispozitivelor.* Vol. I, Inst. polit. Iași, 1981.
4. Gojineţchi N., Gherghel N., *Proiectarea dispozitivelor.* Vol. I, Inst. polit. Iași, 1983.
5. Stănescu I., Tache V., *Dispozitive pentru mașini-unelte. Proiectare, construcție.* Ed. tehn., Buc., 1979.
6. Tache V., Brăgaru A., *Dispozitive pentru mașini-unelte. Proiectarea schemelor de orientare și fixare a semifabricatelor.* Ed. tehn., Buc., 1976.
7. Vasii-Roşculeţ S., Gojineţchi N., Andronic C., Şelariu M., Gherghel N., *Proiectarea dispozitivelor.* Ed. did. și ped., Buc., 1982.

CONSIDERAȚII PRIVIND LEGĂTURA DINTRE CONDIȚIILE DE PRECIZIE DETERMINANTE ȘI GRADELE DE LIBERTATE CE TREBUIE ÎNLĂTURATE PIESELOR PRIN ORIENTARE

(Rezumat)

Se prezintă unele contribuții privind legătura dintre condițiile de precizie determinante impuse suprafețelor de prelucrat și gradele de libertate ce trebuie înlăturate pieselor prin orientare. Se expune, de asemenea, o metodologie de stabilire corectă a gradelor de libertate respective, ce are la bază legătura menționată.

Considerațiile din lucrare contribuie, în același timp, la fundamentarea științifică a orientării pieselor în dispozitive.

FABRICA DE RULMENȚI BÎRLAD

Str. Republicii nr. 320, Bîrlad 6400
Telefon : 1150

La Fabrique de Roulements de Bîrlad — Roumanie

vous offre

ROULEMENTS POUR WAGONS DE CHEMIN DE FER

Les roulements pour wagons de chemin de fer sont fabriqués avec une précision très élevée, les tolérances et écarts aux prescriptions étant réduites. Les conditions d'exécution de ces roulements les rendent interchangeables, c'est-à-dire que chaque anneau intérieur peut être monté dans n'importe quel ensemble : anneau extérieur — galet — cage.

Le superfinissage des galets ainsi que l'utilisation du contact liniaire modifié entre les galets et les voies de roulement des anneaux, assure à ces roulements une durée et une capacité de charge dynamique élevé.

En appliquant sur une vaste échelle des procédés avancés de travail à chaud des anneaux de roulements, par déformation plastique, ceux-ci acquièrent une structure homogène.

Les opérations de finissage et de superfinissage ainsi que les procédés technologiques utilisés, et l'outillage qui assure ces exécutions donnent aux éléments des roulements un degré de précision très élevé.

Les roulements pour wagons de chemin de fer sont construits en vue de permettre un fonctionnement normal jusqu'à une vitesse de 140 km/h, pour les wagons de voyageurs et de 120 km/h, pour les wagons de marchandises, conformément aux normes de l'Union Internationale des Chemins de Fer.

Pour que les roulements fonctionnent dans de bonnes conditions il faut respecter rigoureusement les conditions de montage, parmi lesquelles nous rappelons :

— quand ils seront montés, les anneaux intérieurs devront être chauffés dans des bains d'huile à la température de 90—120°C ;

— la quantité de graisse introduite dans la boîte devra assurer le graissage des roulements pendant 2 ans ;

— il n'est pas permis de heurter les anneaux avec des objets durs quand ils sont montés sur l'essieu ;

— avant de démonter, après avoir enlevé la boîte et l'anneau extérieur, les anneaux intérieurs seront chauffés avec des dispositifs spéciaux, en protégeant la voie de roulement.

IMPORTANT !

Les roulements de wagons produits par la F.R.B. correspondent intégralement aux normes internationales des U.I.C., I.S.O., D.I.N.

La production intérieure et d'exportation de nos wagons, connus et appréciés sur le marché mondial, est équipée de roulements fabriqués en Roumanie.

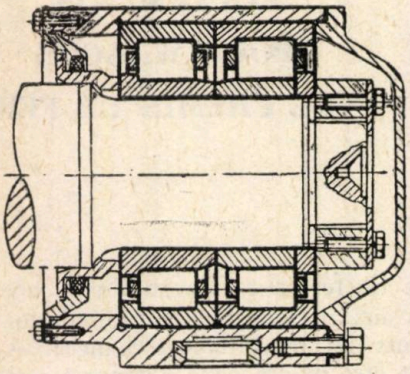

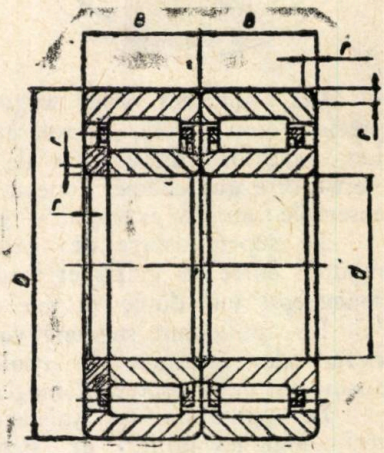

Type de roulement	Dimension en mm d	D	B	r	Jeu radial C_4 en m	Capacité de chargement dynamique C kgf	Capacité de chargement statique C_0 kgf
WJ 120	120	240	80	4	105	50.000	50.000
WJP 120	120	240	80	4	160	50.000	50.000
WJ 130	130	250	80	4	115	56.000	52.000
WJP 130	130	250	80	4	180	56.000	52.000
WJ 140	140	300	120	5	115	61.000	70.000
WJP 140	140	300	120	5	180	61.000	70.000

M.I.C.M. - C.I.E.A.

PNEUMATIC ELEMENTS AND MEASURING INSTRUMENTS ENTERPRISE

316 , Republicii Street Telephone: 15990, 14660 - Telex: 021723-iepamr - Code 6400

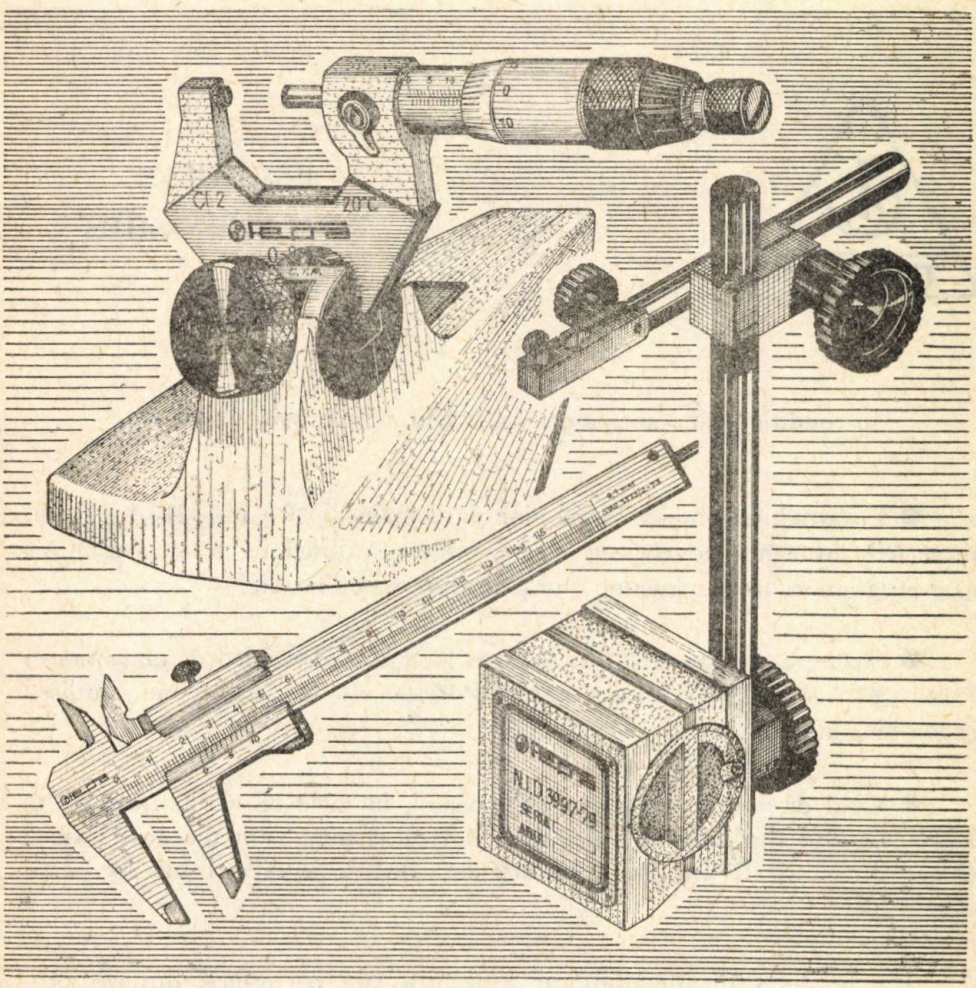

I E.P.A.M PRODUCES:

1. Micrometers
2. Slide gauges
3. Diverse control and measuring instruments

ÎNTREPRINDEREA METALURGICĂ IAŞI

Şoseaua Ţuţora Nr. 132
Tel 981/36320 ; Tlx.: 22297 TEPRO R

METALLURGICAL ENTERPRISE JASSY

TEPRO

PRODUCES
AND FURNISHES

in conditions of romanian, foreign and international standards

● Longitudinally welded steel pipes in domaine ∅10×1 — 213.1×8 mm, protected through zinc coating or warnishing, utilised in water, steam or gase-installation, in construction and petroleum pipe-line, etc.

● Square and rectangular steel pipes longitudinal welded of dimensions : 15×15×1 — 50×50×3 mm and 20×10×1 — 70×40×3 mm, utilised in machine-building industry.

● Cold drawing profilles of steel baand, in sacle of width from 50 to 1.000 mm and thickness of walls from 0.75 at 5 mm, with the next forms : omega, L, U, Z, T, metalurgic joinery and other especeally forms by particular order.

The products of Metallurgical Enterprise are performed through processing methods of high productivity from calm and incalms steels ensuring a high quality at a level of national and international requirements.

38

40822